AD-A062 262 DELAWARE UNIV NEWARK DEPT OF MECHANICAL AND AEROSPA--ETC F/G 11/4
THE BEHAVIOR OF RECTANGULAR COMPOSITE MATERIAL PLATES UNDER LAT--ETC(U)
JUL 78 J G SLOAN, J R VINSON AFOSR-74-2739

UNCLASSIFIED MAE-TR-216 AFOSR-TR-78-1477 NL

1 OF 2
AD
A062262

62

AD A062262

DDC FILE COPY

AFOSR-TR- 78-1477

AFOSR SCIENTIFIC REPORT

LEVE

THE BEHAVIOR OF RECTANGULA
MATERIAL PLATES UNDER
AND HYGROTHERMAL LO

JAMES G. SLOAN

AND

JACK R. VINSON

DEPARTMENT OF MECHANICAL AND AE
UNIVERSITY OF DEL
NEWARK, DELAWARE

JULY 1978

AIR FORCE OFFICE OF SCIENT
UNITED STATES AIR
CONTRACT NUMBER AFOSR

APPROVED FOR PUBLIC RELEASE; DIS

78 12 0

SECURITY CLASSIFICATION OF THIS PAGE (When Data Entered) UNCLASSIFIED

REPORT DOCUMENTATION PAGE

READ INSTRUCTIONS BEFORE COMPLETING FORM

1. REPORT NUMBER: AFOSR-TR- 78-1477

2. GOVT ACCESSION NO.

3. RECIPIENT'S CATALOG NUMBER

4. TITLE (and Subtitle): The Behavior of Rectangular Composite Material Plates under Lateral and Hygrothermal Loads.

5. TYPE OF REPORT & PERIOD COVERED: INTERIM

6. PERFORMING ORG. REPORT NUMBER

7. AUTHOR(s): James G. Sloan, Jack R. Vinson

8. CONTRACT OR GRANT NUMBER(s): AFOSR 74-2739

9. PERFORMING ORGANIZATION NAME AND ADDRESS: University of Delaware, Mechanical and Aerospace Engineering Dept., Newark, Delaware 19711

10. PROGRAM ELEMENT, PROJECT, TASK AREA & WORK UNIT NUMBERS: 2307B1, 61102F

11. CONTROLLING OFFICE NAME AND ADDRESS: Air Force Office of Scientific Research/NA, BLDG 410, Bolling Air Force Base, D.C. 20332

12. REPORT DATE: July 1978

13. NUMBER OF PAGES: 117

14. MONITORING AGENCY NAME & ADDRESS (if different from Controlling Office)

15. SECURITY CLASS. (of this report): Unclassified

15a. DECLASSIFICATION/DOWNGRADING SCHEDULE

16. DISTRIBUTION STATEMENT (of this Report)

Approved for public release; distribution unlimited.

17. DISTRIBUTION STATEMENT (of the abstract entered in Block 20, if different from Report)

18. SUPPLEMENTARY NOTES

19. KEY WORDS (Continue on reverse side if necessary and identify by block number)

COMPOSITE MATERIAL
HYGROTHERMAL LOADS

20. ABSTRACT (Continue on reverse side if necessary and identify by block number)

An analysis of generally laminated rectangular composite plates subject to lateral pressure and hygrothermal loads is presented. Included in the analysis are the effects of transverse shear and transverse normal deformations. The latter effect being included to determine the importance of through the thickness hygroscopic expansions of the polymetric matrix. Solutions are obtained using the theorem of minium potential energy for both clamped and simply-supported boundary conditions. In addition various in-plane

DD FORM 1 JAN 73 1473 EDITION OF 1 NOV 65 IS OBSOLETE

UNCLASSIFIED

SECURITY CLASSIFICATION OF THIS PAGE (When Data Entered)

boundary conditions are studied to demonstrate the behavior of unsymmetric laminates subjected to a hygrothermal environment.

Numerical results of plate deflections and rotations for various width to thickness and length to width aspect ratios show that, while transverse shear deformations are important, transverse normal deformations have no appreciable influence on the solution. Results presented display the magnitude and distribution of lamina stresses under lateral pressure and hygrothermal loads for different inplane restraint conditions and laminate lay-up patterns.

LEVEL II

AFOSR SCIENTIFIC REPORT

(14) MAE-TR-216

(18) AFOSR (19) TR-78-1477

(6) THE BEHAVIOR OF RECTANGULAR COMPOSITE MATERIAL PLATES UNDER LATERAL AND HYGROTHERMAL LOADS.

(9) Interim rept.,

(10) JAMES G. SLOAN

[redacted]

JACK R. VINSON

DEPARTMENT OF MECHANICAL AND AEROSPACE ENGINEERING
UNIVERSITY OF DELAWARE
NEWARK, DELAWARE 19711

(11) JUL [redacted]78

(12) 27p.

AIR FORCE OFFICE OF SCIENTIFIC RESEARCH
UNITED STATES AIR FORCE
CONTRACT NUMBER (15) AFOSR-74-2739

(16) 2307

(17) B1

405 927

TABLE OF CONTENTS

ABSTRACT

An analysis of generally laminated rectangular composite plates subject to lateral pressure and hygrothermal loads is presented. Included in the analysis are the effects of transverse shear and transverse normal deformations -- the latter effect being included to determine the importance of through the thickness hygroscopic expansions of the polymeric matrix. Solutions are obtained using the theorem of minimum potential energy for both clamped and simply-supported boundary conditions. In addition various in-plane boundary conditions are studied to demonstrate the behavior of unsymmetric laminates subjected to a hygrothermal environment.

Numerical results of plate deflections and rotations for various width to thickness and length to width aspect ratios show that, while transverse shear deformations are important, transverse normal deformations have no appreciable influence on the solution. Results presented display the magnitude and distribution of lamina stresses under lateral pressure and hygrothermal loads for different in-plane restraint conditions and laminate lay-up patterns.

NOMENCLATURE

a_n	parameter in moisture diffusion solution
A	plate length in x-direction
A^*	area of plate
A_{ij}	extensional stiffnesses of laminated plate
B	plate length in y-direction
B_{ij}	bending-extensional coupling stiffnesses of laminated plate
$C(x,y)$	integration constant
D	hygroscopic diffusivity
D_{ij}	bending stiffnesses of laminated plate
E_i	elastic modulus of lamina
f	tracing constant for TNS
F_i^*	body forces
F_{ij}	stiffness parameter from TNS
G_{ij}	shear modulus of lamina

h_o	lamina thickness
h_K	vectorial distance from the mid-plane, z = 0, to the upper surface of the K^{th} lamina
H	total laminate thickness
H_{ij}	stiffness parameter from TNS
$I_i^T, I_i^H, J_i^T, J_i^H, K_i^T, K_i^H, K_i^{TH}$	parameters defined in eqn. (2.32, 2.33, 2.34)
m_n	parameter in moisture diffusion solution
$\bar{M}(z,t), \bar{M}(z), \bar{M}$	moisture distribution within plate
M_i^T, M_i^H	thermal and hygroscopic moment resultants, respectively
M^*, MT^*	parameters defined in equation (2.27)
M_n	moment resultant normal to plate edge
$\bar{M}_o$	moisture concentration at upper or lower plate surface
$\bar{M}_u, \bar{M}_L$	moisture concentration at upper and lower plate surface, respectively
N	number of lamina
N_n, N_{nt}	in-plane stress resultant at plate edge
N_i^T, N_i^H	in-plane thermal and hygroscopic stress resultant, respectively
P_n	parameter in diffusion solution

$P(x,y)$, P	pressure distribution
q_n	parameter in diffusion solution
Q_{ij}	lamina stiffnesses in material (1,2,3) coordinate system
$\bar{Q}_{ij}$	transformed lamina stiffnesses in the plate (x,y,z) coordinate system
R	volume of elastic body
S_t	surface over which traction force acts
S_i	stress component in plate coordinate system (i=x,y,xy)
t	time
$T(z,t)$, T	temperature distribution
T_u, T_L	temperature at the upper and lower plate surface, respectively
T^*	parameter defined in equation (2.27)
u,v,w	displacements in the x,y,z directions, respectively
u_0,v_0,w_0	middle surface displacements in the x,y,z directions, respectively
U_{mn},V_{mn},W_{mn}, Γ_{mn},Λ_{mn}	coefficients of assumed displacement and rotation functions
V	total potential energy of a body

W	strain energy density function
x, y, z	plate coordinate directions
α, β	in-plane rotations in the x and y directions, respectively
$\gamma_i^T, \gamma_{ij}^T$	coefficients of thermal expansion
$\gamma_i^H, \gamma_{ij}^H$	coefficients of hygroscopic expansion
$\bar{\gamma}_i^T, \bar{\gamma}_i^H$	transformed coefficients of the thermal and hygroscopic expansions in the plate coordinates, respectively
ρ_{mn}	convergence test parameter
$\epsilon_i, \epsilon_{ij}$	strain components
ϵ_i^o	mid-surface extensional strains
$\eta(z), \eta$	transverse normal deformation
η_m, μ_m	constants based upon the boundary conditions
θ	angle from the x^+ to the 1^+ coordinate axis for each lamina
κ_i	plate curvature strains
ν_{ij}	Poisson's ratio
σ_i, σ_{ij}	stress components
ϕ	characteristic beam functions

CHAPTER ONE

INTRODUCTION

Investigations into the use of reinforced composite materials with polymeric matrices for structural applications have documented the deleterious effects of hygrothermal environments on structural performance [Ref. 15, 16, 17, 18, 19, 20, 21, 22]. The deleterious effects consists of degradation of the matrix dominated mechanical properties and hygroscopic expansions in the matrix [16]. As indicated during the AFOSR workshop at the University of Delaware [16], a need exists for a comprehensive analysis method including the effects of a hygrothermal environment.

In an effort to partially satisfy this need, an analysis of generally laminated rectangular composite plates subject to lateral pressure and hygrothermal loads is presented. Included in the analysis are the effects of transverse shear and transverse normal deformations. The latter effect being included to determine the importance of through the thickness hygroscopic expansions of the polymeric matrix. Solutions are obtained using the theorem of minimum potential energy for both clamped and simply-supported boundary conditions.

In addition various in-plane boundary conditions are studied to demonstrate the behavior of symmetric and unsymmetric laminates subjected to a hygrothermal environment.

The analysis of laminated composite material plates with various boundary conditions has been developed by many researchers, [2, 3, 5, 11, 12, 13, 23, 24, 25, 26, 33, 34, 35]. Of these [3, 5, 26] have shown the importance of transverse shear deformation, particularly for highly anisotropic materials. Also [24, 25] include thermal expansion loads in their analysis. Only [25] addresses the problem of moisture expansion, but considers moisture and thermal expansions separately and omits the effects of transverse shear and transverse normal deformations.

In regard to transverse normal strains (TNS), references [27, 28, 29] have included TNS to investigate the normal stresses generated near a free laminate edge. Flaggs [6] is the only researcher including TNS with moisture swelling in an investigation of the stability of generally laminated plates.

The analysis of hygroscopic residual stresses generated in rectangular plate elements without boundary conditions was presented by Pipes, Vinson and Chou [1]. The treatment of the hygroscopic expansions and moisture diffusion in [1] is used in this work. However, the diffusion

solutions of others [14, 32] could also be applied.

CHAPTER TWO

DERIVATION OF THE GOVERNING EQUATIONS

The governing equations necessary to obtain the solution for a rectangular laminated composite plate subject to lateral and hygrothermal loads will be derived. The Minimum Potential Energy Theorem will be used in conjunction with the generalized stress-strain and strain-displacement relations. The derivation will include the effects of transverse shear deformation and transverse normal strains. The inclusion of the latter is to determine the importance of the lateral expansions of a plate arising from moisture absorption.

The method used to introduce the hygroscopic effects will be that presented by Pipes, Vinson, and Chou [1].

Stress-Strain Relations

The constitutive relations for the Kth lamina of a laminated plate, which has one plane of symmetry and subject to dilatational deformations induced by a hygrothermal environment, is for the material (1,2,3) coordinate system,

$$\sigma_j^k = Q_{ij}^k\left[\epsilon_i^k - \gamma_i^{T^k} T(z,t) - \gamma_i^{M^k}\bar{M}(z,t)\right] \quad i,j=1,2..6 \tag{2.1}$$

where σ_j^k = lamina stresses in the j direction,

ϵ_i^k = lamina strains,

$\gamma_i^{T^k}$ = coefficient of thermal expansion,

$\gamma_i^{M^k}$ = coefficient of hygroscopic expansion,

$T(z,t)$ = temperature distribution through the thickness of the plate at time, t, defined as the difference between the temperature at that point at time, t, and the stress free temperature of the plate,

$\bar{M}(z,t)$ = moisture concentration distribution through the thickness of the plate at time, t, defined as the difference between the moisture concentration at that point at time, t, and the stress free moisture concentration.

Using the following contracted notation,

$$\left.\begin{aligned}\sigma_{ii} &= \sigma_i\\ \epsilon_{ii} &= \epsilon_i\end{aligned}\right\} \quad i = 1,2,3$$

$$\begin{aligned}\sigma_{23} &= \sigma_4 \qquad & \epsilon_{23} &= \epsilon_4\\ \sigma_{13} &= \sigma_5 \qquad & \epsilon_{13} &= \epsilon_5\\ \sigma_{12} &= \sigma_6 \qquad & \epsilon_{12} &= \epsilon_6\end{aligned} \tag{2.2}$$

equation (2.1) can be expanded, i.e.,

$$\begin{Bmatrix} \sigma_1 \\ \sigma_2 \\ \sigma_3 \\ \sigma_4 \\ \sigma_5 \\ \sigma_6 \end{Bmatrix}^K = \begin{bmatrix} Q_{11} & Q_{12} & Q_{13} & & & \\ Q_{12} & Q_{22} & Q_{23} & & & \\ Q_{13} & Q_{23} & Q_{33} & & & \\ & & & 2Q_{44} & & \\ & & & & 2Q_{55} & \\ & & & & & 2Q_{66} \end{bmatrix}^K \begin{Bmatrix} \epsilon_1 - \gamma_1^T T(z,t) - \gamma_1^H \bar{M}(z,t) \\ \epsilon_2 - \gamma_2^T T(z,t) - \gamma_2^H \bar{M}(z,t) \\ \epsilon_3 - \gamma_3^T T(z,t) - \gamma_3^H \bar{M}(z,t) \\ \epsilon_4 \\ \epsilon_5 \\ \epsilon_6 \end{Bmatrix}^K \tag{2.3}$$

The Q_{ij} are the elastic stiffness matrix components in the material coordinate system. These are given in Ref. [2] for the three dimensional case as,

$$Q_{11} = \frac{(1 - \nu_{23}\nu_{32})E_1}{\Delta}$$

$$Q_{12} = \frac{(\nu_{21} + \nu_{31}\nu_{23})E_1}{\Delta} = \frac{(\nu_{12} + \nu_{32}\nu_{13})E_2}{\Delta}$$

$$Q_{13} = \frac{(\nu_{31} + \nu_{21}\nu_{32})E_1}{\Delta} = \frac{(\nu_{13} + \nu_{12}\nu_{23})E_3}{\Delta} \tag{2.4}$$

$$Q_{22} = \frac{(1 - \nu_{13}\nu_{31})E_2}{\Delta}$$

$$Q_{23} = \frac{(\nu_{32} + \nu_{12}\nu_{31})E_2}{\Delta} = \frac{(\nu_{23} + \nu_{21}\nu_{13})E_3}{\Delta}$$

$$Q_{33} = \frac{(1 - \nu_{12}\nu_{21})E_3}{\Delta}$$

$$Q_{44} = G_{23}$$

$$Q_{55} = G_{13}$$

$$Q_{66} = G_{12}$$

where $\Delta = 1 - \nu_{12}\nu_{21} - \nu_{23}\nu_{32} - \nu_{31}\nu_{13} - 2\nu_{21}\nu_{32}\nu_{13}$

It is necessary to transform the material coordinate system stresses and strains to the plate (x,y,z) coordinate system as follows,

$$\begin{Bmatrix} \sigma_x \\ \sigma_y \\ \sigma_z \\ \sigma_{yz} \\ \sigma_{xz} \\ \sigma_{xy} \end{Bmatrix}^K = \left[T\right]^{-1} \begin{Bmatrix} \sigma_1 \\ \sigma_2 \\ \sigma_3 \\ \sigma_4 \\ \sigma_5 \\ \sigma_6 \end{Bmatrix}^K \tag{2.5}$$

and

$$\begin{Bmatrix} \epsilon_1 \\ \epsilon_2 \\ \epsilon_3 \\ \epsilon_4 \\ \epsilon_5 \\ \epsilon_6 \end{Bmatrix}^K = \left[T\right] \begin{Bmatrix} \epsilon_x \\ \epsilon_y \\ \epsilon_z \\ \epsilon_{yz} \\ \epsilon_{xz} \\ \epsilon_{xy} \end{Bmatrix}^K \tag{2.6}$$

where the transformation matrices for the angle, θ, defined

in Figure 2.1 are

$$[T] = \begin{bmatrix} m^2 & n^2 & 0 & 0 & 0 & 2mn \\ n^2 & m^2 & 0 & 0 & 0 & -2mn \\ 0 & 0 & 1 & 0 & 0 & 0 \\ 0 & 0 & 0 & m & -n & 0 \\ 0 & 0 & 0 & n & m & 0 \\ -mn & mn & 0 & 0 & 0 & m^2-n^2 \end{bmatrix} \tag{2.7}$$

and

$$[T]^{-1} = \begin{bmatrix} m^2 & n^2 & 0 & 0 & 0 & mn \\ n^2 & m^2 & 0 & 0 & 0 & -mn \\ 0 & 0 & 1 & 0 & 0 & 0 \\ 0 & 0 & 0 & m & -n & 0 \\ 0 & 0 & 0 & n & m & 0 \\ -2mn & 2mn & 0 & 0 & 0 & m^2-n^2 \end{bmatrix} \tag{2.8}$$

where $m = \cos\theta$, $n = \sin\theta$.

Using these transformations, the generalized stress-strain relation for the Kth lamina becomes,

$$\begin{Bmatrix} \sigma_x \\ \sigma_y \\ \sigma_z \\ \sigma_{yz} \\ \sigma_{xz} \\ \sigma_{xy} \end{Bmatrix}^K = \begin{bmatrix} \bar{Q}_{11} & \bar{Q}_{12} & \bar{Q}_{13} & 0 & 0 & 2\bar{Q}_{16} \\ \bar{Q}_{12} & \bar{Q}_{22} & \bar{Q}_{23} & 0 & 0 & 2\bar{Q}_{26} \\ \bar{Q}_{13} & \bar{Q}_{23} & \bar{Q}_{33} & 0 & 0 & 2\bar{Q}_{36} \\ 0 & 0 & 0 & 2\bar{Q}_{44} & 2\bar{Q}_{45} & 0 \\ 0 & 0 & 0 & 2\bar{Q}_{45} & 2\bar{Q}_{55} & 0 \\ \bar{Q}_{16} & \bar{Q}_{26} & \bar{Q}_{36} & 0 & 0 & 2\bar{Q}_{66} \end{bmatrix}^K \begin{Bmatrix} \epsilon_x - \bar{\gamma}_x^T T(z,t) - \bar{\gamma}_x^H \bar{m}(z,t) \\ \epsilon_y - \bar{\gamma}_y^T T(z,t) - \bar{\gamma}_y^H \bar{m}(z,t) \\ \epsilon_z - \bar{\gamma}_z^T T(z,t) - \bar{\gamma}_z^H \bar{m}(z,t) \\ \epsilon_{yz} \\ \epsilon_{xz} \\ \epsilon_{xy} - \frac{1}{2}\bar{\gamma}_{xy}^T T(z,t) - \frac{1}{2}\bar{\gamma}_{xy}^H \bar{m}(z,t) \end{Bmatrix}^K \tag{2.9}$$

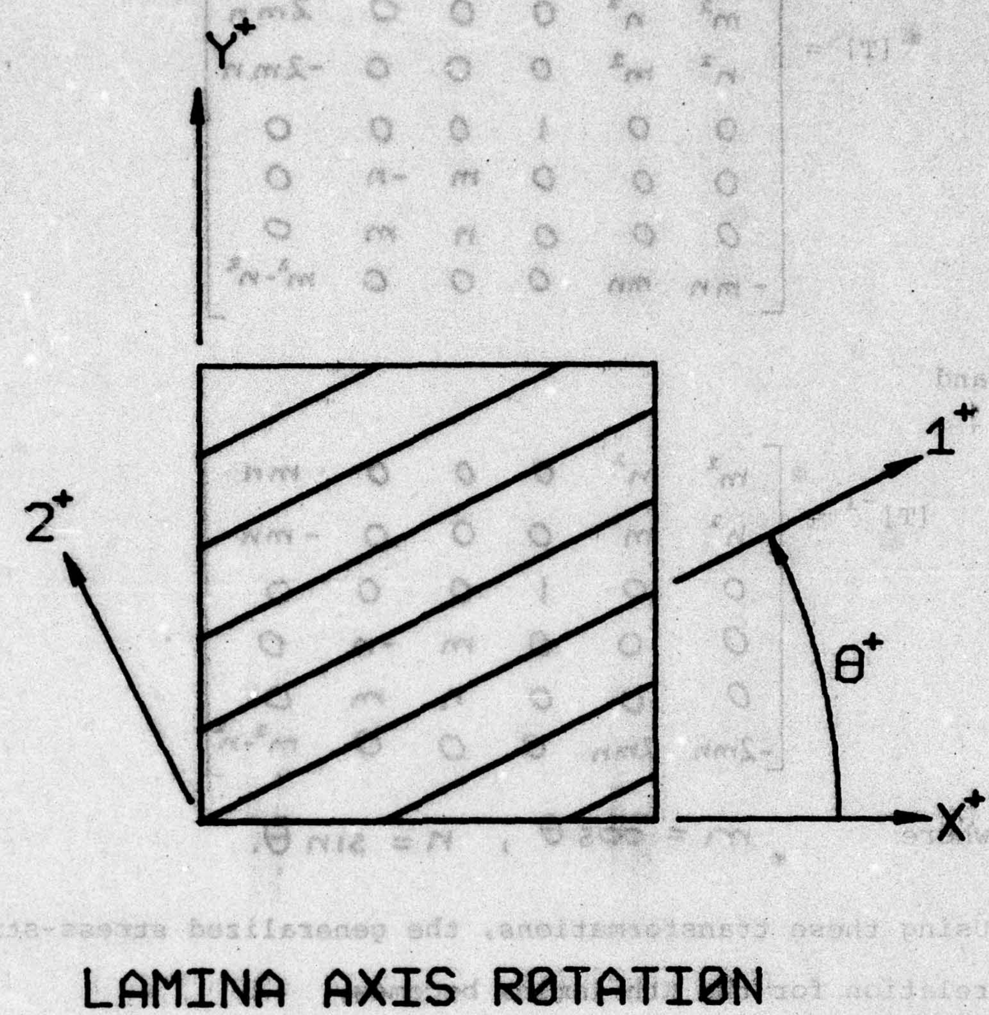

Figure 2.1

The transformed stiffness matrix components are defined as,

$$
\begin{aligned}
\bar{Q}_{11} &= Q_{11} m^4 + 2m^2n^2(Q_{12} + 2Q_{66}) + n^4 Q_{22} \\
\bar{Q}_{12} &= m^2n^2(Q_{11} + Q_{22} - 4Q_{66}) + (m^4+n^4)Q_{12} \\
\bar{Q}_{13} &= m^2 Q_{13} + n^2 Q_{23} \\
\bar{Q}_{16} &= -mn^3Q_{22} + m^3nQ_{11} - mn(m^2-n^2)(Q_{12} + 2Q_{66}) \\
\bar{Q}_{22} &= n^4Q_{11} + 2m^2n^2(Q_{12} + 2Q_{66}) + m^4 Q_{22} \\
\bar{Q}_{23} &= n^2Q_{13} + m^2 Q_{23} \\
\bar{Q}_{33} &= Q_{33} \\
\bar{Q}_{26} &= -m^3nQ_{22} + mn^3Q_{11} + mn(m^2-n^2)(Q_{12} + 2Q_{66}) \\
\bar{Q}_{36} &= -mn(Q_{23} - Q_{13}) \\
\bar{Q}_{44} &= m^2 Q_{44} + n^2 Q_{55} \\
\bar{Q}_{45} &= -mn(Q_{44} - Q_{55}) \\
\bar{Q}_{55} &= m^2 Q_{55} + n^2 Q_{44} \\
\bar{Q}_{66} &= m^2n^2(Q_{11} + Q_{22} - 2Q_{12}) + (m^2-n^2)^2 Q_{66}.
\end{aligned}
\tag{2.10}
$$

The transformed coefficients of expansion are,

$$
\begin{aligned}
\bar{\gamma}_x^T &= \gamma_{11}^T m^2 + \gamma_{22}^T n^2 & \bar{\gamma}_x^H &= \gamma_{11}^H m^2 + \gamma_{22}^H n^2 \\
\bar{\gamma}_y^T &= \gamma_{11}^T n^2 + \gamma_{22}^T m^2 & \bar{\gamma}_y^H &= \gamma_{11}^H n^2 + \gamma_{22}^H m^2 \\
\bar{\gamma}_z^T &= \gamma_{33}^T & \bar{\gamma}_z^H &= \gamma_{33}^H \\
\bar{\gamma}_{xy}^T &= 2(\gamma_{11}^T - \gamma_{22}^T)mn & \bar{\gamma}_{xy}^H &= 2(\gamma_{11}^H - \gamma_{22}^H)mn.
\end{aligned}
\tag{2.11}
$$

Note that while the hygrothermal expansion coefficients are dilatational in the material coordinate system, when transformed into the plate coordinate system, coefficients involving the in-plane shear strains are introduced.

Strain-Displacement Relations

The linear strain-displacement relations in the cartesian coordinate system are,

$$\begin{aligned}
\epsilon_x &= \frac{\partial u}{\partial x} & \epsilon_{xy} &= \frac{1}{2}\left(\frac{\partial u}{\partial y} + \frac{\partial v}{\partial x}\right) \\
\epsilon_y &= \frac{\partial v}{\partial y} & \epsilon_{yz} &= \frac{1}{2}\left(\frac{\partial w}{\partial y} + \frac{\partial v}{\partial z}\right) \qquad (2.12) \\
\epsilon_z &= \frac{\partial w}{\partial z} & \epsilon_{xz} &= \frac{1}{2}\left(\frac{\partial w}{\partial x} + \frac{\partial u}{\partial z}\right)
\end{aligned}$$

Only the linear order terms are included in equation (2.12) in that only small deflections relative to the plate thickness are being considered.

The assumed form of the u, v, w displacements in the x, y, z directions, respectively, are

$$\begin{aligned}
u(x,y,z) &= u_o(x,y) + z\,\alpha(x,y) \\
v(x,y,z) &= v_o(x,y) + z\,\beta(x,y) \qquad (2.13) \\
w(x,y,z) &= w_o(x,y) + f\,\eta(z)
\end{aligned}$$

where the subscript "o" denotes the mid-plane displacements. The, f, in the w(x,y,z) equation is a tracing constant for the transverse normal deformation function, $\eta(z)$. Substitution of equation (2.13) into equation (2.12) gives,

$$\epsilon_x = \frac{\partial u_0}{\partial x} + z\frac{\partial \alpha}{\partial x} \qquad \epsilon_{xz} = \frac{1}{2}\left(\frac{\partial u_0}{\partial z} + \alpha + \frac{\partial w_0}{\partial x}\right)$$

$$\epsilon_y = \frac{\partial v_0}{\partial y} + z\frac{\partial \beta}{\partial y} \qquad \epsilon_{yz} = \frac{1}{2}\left(\frac{\partial v_0}{\partial z} + \beta + \frac{\partial w_0}{\partial y}\right) \tag{2.14}$$

$$\epsilon_z = f\frac{\partial \eta}{\partial z} \qquad \epsilon_{xy} = \frac{1}{2}\left(\frac{\partial u_0}{\partial y} + \frac{\partial v_0}{\partial x}\right) + \frac{1}{2}\left(\frac{\partial \alpha}{\partial y} + \frac{\partial \beta}{\partial x}\right)z$$

In this analysis the variation of u_o and v_o with respect to the z direction will be assumed zero, therefore,

$$\frac{\partial u_0}{\partial z} = \frac{\partial v_0}{\partial z} = 0 \tag{2.15}$$

The strain-displacement relations from equation (2.14) are,

$$\epsilon_x = \frac{\partial u_0}{\partial x} + z\frac{\partial \alpha}{\partial x} \qquad \epsilon_{xz} = \frac{1}{2}\left(\alpha + \frac{\partial w_0}{\partial x}\right)$$

$$\epsilon_y = \frac{\partial v_0}{\partial y} + z\frac{\partial \beta}{\partial y} \qquad \epsilon_{yz} = \frac{1}{2}\left(\beta + \frac{\partial w_0}{\partial y}\right) \tag{2.16}$$

$$\epsilon_z = f\frac{\partial \eta}{\partial z} \qquad \epsilon_{xy} = \frac{1}{2}\left(\frac{\partial u_0}{\partial y} + \frac{\partial v_0}{\partial x}\right) + \frac{z}{2}\left(\frac{\partial \alpha}{\partial y} + \frac{\partial \beta}{\partial x}\right)$$

Application of the Theorem of Minimum Potential Energy

The solution of genera[illegible]ated composite plates under uniform pressure and hygrothermal loads will be obtained using the Theorem of Minimum Potential Energy.

The total potential energy of a body, V, can be expressed as, (Ref. [3]),

$$V = \int_R W\,dR - \int_{S_t} T_i u_i \,dS_t - \int_R F_i u_i \,dR \tag{2.17}$$

where W = strain energy density function,

R = volume of the elastic body,

T_i = ith component of the surface traction,

u_i = ith component of the deformation,

F_i = ith component of the body force,

S_t = portion of the surface over which the tractions are prescribed.

The mathematical statement of the minimum potential energy theorem is,

$$\delta V = 0 \tag{2.18}$$

where $\delta(\;)$ represents the variation operation. In the present work, body forces will be neglected. The strain energy density function can be defined as,

$$W \equiv \frac{1}{2}\sigma_{ij}\epsilon_{ij} \qquad i, j, = 1,2,3 \tag{2.19}$$

or, in the cartesian coordinate system,

$$W = \frac{1}{2}\sigma_x\epsilon_x + \frac{1}{2}\sigma_y\epsilon_y + \frac{1}{2}\sigma_z\epsilon_z + \sigma_{yz}\epsilon_{yz} + \sigma_{xz}\epsilon_{xz} + \sigma_{xy}\epsilon_{xy} \tag{2.20}$$

The surface tractions considered in the analysis will be those normal to the surface of the plate, specified as $P(x,y)$. Then,

$$\int_{S_*} T_i u_i \, dS_* = \iint_{A^*} P(x,y)\, w_o(x,y)\, dA^* \tag{2.21}$$

In addition, the plate theory assumptions on the normal stresses and strains will not be used. The transverse shear stresses will be included because of their importance in the analysis of highly anisotropic plates.

The strain energy density function, W, including the hygrothermal strains, will be

$$\begin{aligned} W = \frac{1}{2}\Big\{ & \sigma_x\left[\epsilon_x - \bar{\gamma}_x^T T - \bar{\gamma}_x^H \bar{m}\right] + \sigma_y\left[\epsilon_y - \bar{\gamma}_y^T T - \bar{\gamma}_y^H \bar{m}\right] \\ & + \sigma_z\left[\epsilon_z - \bar{\gamma}_z^T T - \bar{\gamma}_z^H \bar{m}\right] + 2\left[\sigma_{xz}\epsilon_{xz}\right] + 2\left[\sigma_{yz}\epsilon_{yz}\right] \\ & + 2\sigma_{xy}\left[\epsilon_{xy} - \frac{1}{2}\bar{\gamma}_{xy}^T T - \frac{1}{2}\bar{\gamma}_{xy}^H \bar{m}\right]\Big\} \end{aligned} \tag{2.22}$$

Thus, the potential energy of a generally laminated plate will be,

$$\begin{aligned} V = \frac{1}{2}\sum_{K=1}^{N} \iint_{A^*} \int_{h_{K-1}}^{h_K} \Big\{ & \sigma_x\left[\epsilon_x - \bar{\gamma}_x^T T - \bar{\gamma}_x^H \bar{m}\right] + \sigma_y\left[\epsilon_y - \bar{\gamma}_y^T T - \bar{\gamma}_y^H \bar{m}\right] \\ & + \sigma_z\left[\epsilon_z - \bar{\gamma}_z^T T - \bar{\gamma}_z^H \bar{m}\right] + \sigma_{xz}\left[2\epsilon_{xz}\right] + \sigma_{yz}\left[2\epsilon_{yz}\right] \\ & + \sigma_{xy}\left[2\epsilon_{xy} - \bar{\gamma}_{xy}^T T - \bar{\gamma}_{xy}^H \bar{m}\right]\Big\}\, dz\, dA^* \\ & - \iint_{A^*} P\, w_o\, dA^* \end{aligned} \tag{2.23}$$

Substitution of the stress-strain relations, equation (2.9), and the strain-displacement relations, equation (2.16), into equation (2.23), and integrating across the thickness for all terms except those involving η (z), gives,

$$
\begin{aligned}
V = \iint_{A^*} \Bigg\{ & \frac{A_{11}}{2}\left(\frac{\partial u_0}{\partial x}\right)^2 + B_{11}\frac{\partial u_0}{\partial x}\frac{\partial \alpha}{\partial x} + \frac{D_{11}}{2}\left(\frac{\partial \alpha}{\partial x}\right)^2 + A_{12}\frac{\partial u_0}{\partial x}\frac{\partial v_0}{\partial y} \\
& + B_{12}\frac{\partial u_0}{\partial x}\frac{\partial \beta}{\partial y} + B_{12}\frac{\partial v_0}{\partial y}\frac{\partial \alpha}{\partial x} + D_{12}\frac{\partial \beta}{\partial y}\frac{\partial \alpha}{\partial x} + A_{16}\frac{\partial u_0}{\partial x}\frac{\partial u_0}{\partial y} \\
& + A_{16}\frac{\partial u_0}{\partial x}\frac{\partial v_0}{\partial x} + B_{16}\frac{\partial u_0}{\partial x}\frac{\partial \alpha}{\partial y} + B_{16}\frac{\partial u_0}{\partial x}\frac{\partial \beta}{\partial x} + B_{16}\frac{\partial u_0}{\partial y}\frac{\partial \alpha}{\partial x} \\
& + B_{16}\frac{\partial v_0}{\partial x}\frac{\partial \alpha}{\partial x} + D_{16}\frac{\partial \alpha}{\partial x}\frac{\partial \beta}{\partial x} + D_{16}\frac{\partial \alpha}{\partial x}\frac{\partial \alpha}{\partial y} + \frac{A_{22}}{2}\left(\frac{\partial v_0}{\partial y}\right)^2 \\
& + B_{22}\frac{\partial v_0}{\partial y}\frac{\partial \beta}{\partial y} + \frac{D_{22}}{2}\left(\frac{\partial \beta}{\partial y}\right)^2 + A_{26}\frac{\partial v_0}{\partial y}\frac{\partial u_0}{\partial y} + A_{26}\frac{\partial v_0}{\partial y}\frac{\partial v_0}{\partial x} \\
& + B_{26}\frac{\partial v_0}{\partial y}\frac{\partial \alpha}{\partial y} + B_{26}\frac{\partial v_0}{\partial y}\frac{\partial \beta}{\partial x} + B_{26}\frac{\partial u_0}{\partial y}\frac{\partial \beta}{\partial y} + B_{26}\frac{\partial v_0}{\partial x}\frac{\partial \beta}{\partial y} \\
& + D_{26}\frac{\partial \alpha}{\partial y}\frac{\partial \beta}{\partial y} + D_{26}\frac{\partial \beta}{\partial x}\frac{\partial \beta}{\partial y} + A_{45}\alpha\beta + A_{45}\alpha\frac{\partial w_0}{\partial y} \\
& + A_{45}\beta\frac{\partial w_0}{\partial x} + A_{45}\frac{\partial w_0}{\partial x}\frac{\partial w_0}{\partial y} + \frac{A_{55}}{2}\alpha^2 + A_{55}\alpha\frac{\partial w_0}{\partial x} \\
& + \frac{A_{55}}{2}\left(\frac{\partial w_0}{\partial x}\right)^2 + \frac{A_{44}}{2}\beta^2 + A_{44}\beta\frac{\partial w_0}{\partial y} + \frac{A_{44}}{2}\left(\frac{\partial w_0}{\partial y}\right)^2
\end{aligned}
$$

$$
\begin{aligned}
&+\frac{A_{66}}{2}\left(\frac{\partial u_0}{\partial y}\right)^2 + A_{66}\frac{\partial u_0}{\partial y}\frac{\partial v_0}{\partial x} + \frac{A_{66}}{2}\left(\frac{\partial v_0}{\partial x}\right)^2 + B_{66}\frac{\partial u_0}{\partial y}\frac{\partial \alpha}{\partial y} \\
&+B_{66}\frac{\partial u_0}{\partial y}\frac{\partial \beta}{\partial x} + B_{66}\frac{\partial v_0}{\partial x}\frac{\partial \alpha}{\partial y} + B_{66}\frac{\partial v_0}{\partial x}\frac{\partial \beta}{\partial x} + \frac{D_{66}}{2}\left(\frac{\partial \alpha}{\partial y}\right)^2 \\
&+D_{66}\frac{\partial \alpha}{\partial y}\frac{\partial \beta}{\partial x} + \frac{D_{66}}{2}\left(\frac{\partial \beta}{\partial x}\right)^2 - \left(\frac{\partial u_0}{\partial x}\right)\left(N_1^T + N_1^H\right) - \left(\frac{\partial v_0}{\partial y}\right)\left(N_2^T + N_2^H\right) \\
&-\left(\frac{\partial u_0}{\partial y} + \frac{\partial v_0}{\partial x}\right)\left(N_6^T + N_6^H\right) - \left(\frac{\partial \alpha}{\partial x}\right)\left(M_1^T + M_1^H\right) - \left(\frac{\partial \beta}{\partial y}\right)\left(M_2^T + M_2^H\right) \\
&-\left(\frac{\partial \alpha}{\partial y} + \frac{\partial \beta}{\partial x}\right)\left(M_6^T + M_6^H\right) + T^* + M^* + MT^*\Big\}\, dA^* \qquad (2.24) \\
&+\sum_{K=1}^{N}\iint_{A^*}\int_{h_{K-1}}^{h_K} f\Big\{\Big[\Big[\bar{Q}_{13}^K\frac{\partial u_0}{\partial x} + \bar{Q}_{23}^K\frac{\partial v_0}{\partial y} + \bar{Q}_{36}^K\left(\frac{\partial u_0}{\partial y} + \frac{\partial v_0}{\partial x}\right)\Big]\Big]\frac{\partial \eta}{\partial z} \\
&+\left[\bar{Q}_{13}^K\frac{\partial \alpha}{\partial x} + \bar{Q}_{23}^K\frac{\partial \beta}{\partial y} + \bar{Q}_{36}^K\left(\frac{\partial \alpha}{\partial y} + \frac{\partial \beta}{\partial x}\right)\right] z\,\frac{\partial \eta}{\partial z} + \left[\frac{\bar{Q}_{33}^K}{2}\right]\left(\frac{\partial \eta}{\partial z}\right)^2 \\
&-\left[\bar{Q}_{13}^K\bar{\gamma}_x^T + \bar{Q}_{23}^K\bar{\gamma}_y^T + \bar{Q}_{33}^K\bar{\gamma}_z^T + \bar{Q}_{36}^K\bar{\gamma}_{xy}^T\right] T\,\frac{\partial \eta}{\partial z} \\
&-\left[\bar{Q}_{13}^K\bar{\gamma}_x^H + \bar{Q}_{23}^K\bar{\gamma}_y^H + \bar{Q}_{33}^K\bar{\gamma}_z^H + \bar{Q}_{36}^K\bar{\gamma}_{xy}^H\right]\bar{M}\,\frac{\partial \eta}{\partial z}\Big\}\, dz\, dA^* \\
&-\iint_{A^*} P\, w_0\, dA^*
\end{aligned}
$$

where from [3]

$$A_{ij} = \sum_{K=1}^{N} [\bar{Q}_{ij}]^K (h_K - h_{K-1}) \qquad ij = 1,2,6$$
$$\qquad ij = 4,5$$

$$B_{ij} = \frac{1}{2} \sum_{K=1}^{N} [\bar{Q}_{ij}]^K (h_K^2 - h_{K-1}^2) \qquad ij = 1,2,6 \qquad (2.25)$$

$$D_{ij} = \frac{1}{3} \sum_{K=1}^{N} [\bar{Q}_{ij}]^K (h_K^3 - h_{K-1}^3) \qquad ij = 1,2,6$$

and,

$$\left.\begin{aligned} N_i^T &= \sum_{K=1}^{N} \int_{h_{K-1}}^{h_K} [\bar{Q}_{ij}]^K \bar{\gamma}_j^T T \, dz \\ N_i^H &= \sum_{K=1}^{N} \int_{h_{K-1}}^{h_K} [\bar{Q}_{ij}]^K \bar{\gamma}_j^H \bar{M} \, dz \\ M_i^T &= \sum_{K=1}^{N} \int_{h_{K-1}}^{h_K} [\bar{Q}_{ij}]^K \bar{\gamma}_j^T T z \, dz \\ M_i^H &= \sum_{K=1}^{N} \int_{h_{K-1}}^{h_K} [\bar{Q}_{ij}]^K \bar{\gamma}_j^H \bar{M} z \, dz \end{aligned}\right\} \quad \begin{aligned} i &= 1,2,6 \\ j &= 1,2,3,6 \end{aligned} \qquad (2.26)$$

and,

$$\left.\begin{aligned} T^* &= \frac{1}{2}\sum_{K=1}^{N}\int_{h_{K-1}}^{h_K}\left[\bar{Q}_{ij}\right]^K\left[\bar{\gamma}_i^T\right]\left[\bar{\gamma}_j^T\right]T^2\,dz \\ M^* &= \frac{1}{2}\sum_{K=1}^{N}\int_{h_{K-1}}^{h_{K=1}}\left[\bar{Q}_{ij}\right]^K\left[\bar{\gamma}_i^M\right]\left[\bar{\gamma}_j^M\right]\bar{M}^2\,dz \\ MT^* &= \sum_{K=1}^{N}\int_{h_{K-1}}^{h_K}\left[\bar{Q}_{ij}\right]^K\left[\bar{\gamma}_i^T\right]\left[\bar{\gamma}_j^M\right]T\,\bar{M}\,dz \end{aligned}\right\}\quad ij = 1,2,3,6 \tag{2.27}$$

At this point one could obtain an approximate solution by using the Rayleigh-Ritz method. This is accomplished by assuming a functional form of the unknown displacement and rotation variables, substituting these into the potential energy equation, and taking variations with respect to the unknown amplitudes. However, problems arise, in that, while forms for the u_o, v_o, w_o, α, and β variables can be assumed for certain boundary conditions, the form of the transverse normal deformation function, η, is not intuitively known. In order to circumvent this problem, the Euler-Lagrange equation for the $\delta\eta$ term will be used to approximate η in terms of the other displacements and rotations. Thus, taking the variation of equation (2.24), and collecting all terms involving $\delta\eta$ gives, after integration by parts,

$$\delta V = -\sum_{K=1}^{N}\iint_{A^*}\int_{h_{K-1}}^{h_K} f\left\{\bar{Q}_{13}^K\frac{\partial\alpha}{\partial x} + \bar{Q}_{23}^K\frac{\partial\beta}{\partial y} + \bar{Q}_{36}^K\left(\frac{\partial\alpha}{\partial y} + \frac{\partial\beta}{\partial x}\right)\right.$$

$$+\bar{Q}_{33}^{K}\frac{\partial^{2}\eta}{\partial z^{2}}-\left[\bar{Q}_{13}^{K}\bar{\gamma}_{x}^{T}+\bar{Q}_{23}^{K}\bar{\gamma}_{y}^{T}+\bar{Q}_{33}^{K}\bar{\gamma}_{z}^{T}+\bar{Q}_{36}^{K}\bar{\gamma}_{xy}^{T}\right]\frac{\partial T}{\partial z}$$

$$-\left[\bar{Q}_{13}^{K}\bar{\gamma}_{x}^{H}+\bar{Q}_{23}^{K}\bar{\gamma}_{y}^{H}+\bar{Q}_{33}^{K}\bar{\gamma}_{z}^{H}+\bar{Q}_{36}^{K}\bar{\gamma}_{xy}^{H}\right]\frac{\partial \bar{M}}{\partial z}\Bigg\}\delta\eta\, dz\, dA^{*}$$

$$+\sum_{K=1}^{N}\iint_{A^{*}} f\Bigg\{\left[\bar{Q}_{13}^{K}\frac{\partial u_{0}}{\partial x}+\bar{Q}_{23}^{K}\frac{\partial v_{0}}{\partial y}+\bar{Q}_{36}^{K}\left(\frac{\partial u_{0}}{\partial y}+\frac{\partial v_{0}}{\partial x}\right)\right]\Bigg|_{h_{K-1}}^{h_{K}} \qquad (2.28)$$

$$+\left[\bar{Q}_{13}^{K}\frac{\partial \alpha}{\partial x}+\bar{Q}_{23}^{K}\frac{\partial \beta}{\partial y}+\bar{Q}_{36}^{K}\left(\frac{\partial \alpha}{\partial y}+\frac{\partial \beta}{\partial x}\right)\right]z\Bigg|_{h_{K-1}}^{h_{K}}$$

$$-\left[\bar{Q}_{13}^{K}\bar{\gamma}_{x}^{T}+\bar{Q}_{23}^{K}\bar{\gamma}_{y}^{T}+\bar{Q}_{33}^{K}\bar{\gamma}_{z}^{T}+\bar{Q}_{36}^{K}\bar{\gamma}_{xy}^{T}\right]T\Bigg|_{h_{K-1}}^{h_{K}}$$

$$-\left[\bar{Q}_{13}^{K}\bar{\gamma}_{x}^{H}+\bar{Q}_{23}^{K}\bar{\gamma}_{y}^{H}+\bar{Q}_{33}^{K}\bar{\gamma}_{z}^{H}+\bar{Q}_{36}^{K}\bar{\gamma}_{xy}^{H}\right]\bar{M}\,\Bigg|_{h_{K-1}}^{h_{K}}\Bigg\}\delta\eta\, dA^{*}$$

From the first half of equation (2.28) either $\delta\eta = o$ or,

$$f\Bigg\{\bar{Q}_{13}^{K}\frac{\partial \alpha}{\partial x}+\bar{Q}_{23}^{K}\frac{\partial \beta}{\partial y}+\bar{Q}_{36}^{K}\left(\frac{\partial \alpha}{\partial y}+\frac{\partial \beta}{\partial x}\right)+\bar{Q}_{33}^{K}\frac{\partial^{2}\eta}{\partial z^{2}} \qquad (2.29)$$

$$-\left[\bar{Q}_{13}^{K}\bar{\gamma}_{x}^{T}+\bar{Q}_{23}^{K}\bar{\gamma}_{y}^{T}+\bar{Q}_{33}^{K}\bar{\gamma}_{z}^{T}+\bar{Q}_{36}^{K}\bar{\gamma}_{xy}^{T}\right]\frac{\partial T}{\partial z}$$

$$-\left[\bar{Q}_{13}^{K}\bar{\gamma}_{x}^{H}+\bar{Q}_{23}^{K}\bar{\gamma}_{y}^{H}+\bar{Q}_{33}^{K}\bar{\gamma}_{z}^{H}+\bar{Q}_{36}^{K}\bar{\gamma}_{xy}^{H}\right]\frac{\partial \bar{M}}{\partial z}\Bigg\}=0$$

The second half of equation (2.28) represents the natural boundary conditions at the $h = h_{k-1}$ and h_k edges of the plate.

Equation (2.29) can now be used to obtain an approximate expression for the $\partial\eta/\partial_z$ terms in equation (2.24). Solving equation (2.29) for $\partial^2\eta/\partial_z{}^2$ and integrating with respect to z gives,

$$\begin{aligned}\frac{\partial\eta}{\partial z} = f\Big\{ & -\frac{1}{\bar{Q}^k_{33}}\left[\bar{Q}^k_{13}\frac{\partial\alpha}{\partial x} + \bar{Q}^k_{23}\frac{\partial\beta}{\partial y} + \bar{Q}^k_{36}\left(\frac{\partial\alpha}{\partial y} + \frac{\partial\beta}{\partial x}\right)\right]z \\ & + \frac{1}{\bar{Q}^k_{33}}\left[\bar{Q}^k_{13}\bar{\gamma}^T_x + \bar{Q}^k_{23}\bar{\gamma}^T_y + \bar{Q}^k_{33}\bar{\gamma}^T_z + \bar{Q}^k_{36}\bar{\gamma}^T_{xy}\right]T \\ & + \frac{1}{\bar{Q}^k_{33}}\left[\bar{Q}^k_{13}\bar{\gamma}^H_x + \bar{Q}^k_{23}\bar{\gamma}^H_y + \bar{Q}^k_{33}\bar{\gamma}^H_z + \bar{Q}^k_{36}\bar{\gamma}^H_{xy}\right]\bar{M} + C(x,y)\Big\}\end{aligned} \qquad (2.30)$$

The constant of integration, C(x,y), will be arbitrarily set equal to zero, making z = 0 the reference temperature or moisture concentration for the effects of the transverse normal strains. Substituting equation (2.30) into equation (2.24) gives,

$$V = \iiint_{A^*} \Big\{ \frac{A_{11}}{2}\left(\frac{\partial u_0}{\partial x}\right)^2 + B_{11}\frac{\partial u_0}{\partial x}\frac{\partial \alpha}{\partial x} + \frac{D_{11}}{2}\left(\frac{\partial \alpha}{\partial x}\right)^2 + A_{12}\frac{\partial u_0}{\partial x}\frac{\partial v_0}{\partial y}$$

$$+ B_{12}\left[\frac{\partial u_0}{\partial x}\frac{\partial \beta}{\partial y} + \frac{\partial v_0}{\partial y}\frac{\partial \alpha}{\partial x}\right] + D_{12}\frac{\partial \beta}{\partial y}\frac{\partial \alpha}{\partial x} + A_{16}\left[\frac{\partial u_0}{\partial x}\frac{\partial u_0}{\partial y} + \frac{\partial u_0}{\partial x}\frac{\partial v_0}{\partial x}\right]$$

$$+ B_{16}\left[\frac{\partial u_0}{\partial x}\frac{\partial \alpha}{\partial y} + \frac{\partial u_0}{\partial x}\frac{\partial \beta}{\partial x} + \frac{\partial u_0}{\partial y}\frac{\partial \alpha}{\partial x} + \frac{\partial v_0}{\partial x}\frac{\partial \alpha}{\partial x}\right] + D_{16}\left[\frac{\partial \alpha}{\partial x}\frac{\partial \alpha}{\partial y} + \frac{\partial \alpha}{\partial x}\frac{\partial \beta}{\partial x}\right]$$

$$+ \frac{A_{22}}{2}\left(\frac{\partial v_0}{\partial y}\right)^2 + B_{22}\frac{\partial v_0}{\partial y}\frac{\partial \beta}{\partial y} + \frac{D_{22}}{2}\left(\frac{\partial \beta}{\partial y}\right)^2 + A_{26}\left[\frac{\partial v_0}{\partial y}\frac{\partial u_0}{\partial y} + \frac{\partial v_0}{\partial y}\frac{\partial v_0}{\partial x}\right]$$

$$+ B_{26}\left[\frac{\partial v_0}{\partial y}\frac{\partial \alpha}{\partial y} + \frac{\partial v_0}{\partial y}\frac{\partial \beta}{\partial x} + \frac{\partial u_0}{\partial y}\frac{\partial \beta}{\partial y} + \frac{\partial v_0}{\partial x}\frac{\partial \beta}{\partial y}\right] + D_{26}\left[\frac{\partial \alpha}{\partial y}\frac{\partial \beta}{\partial y} + \frac{\partial \beta}{\partial x}\frac{\partial \beta}{\partial y}\right]$$

$$+ A_{45}\left[\alpha\beta + \alpha\frac{\partial w_0}{\partial y} + \beta\frac{\partial w_0}{\partial x} + \frac{\partial w_0}{\partial x}\frac{\partial w_0}{\partial y}\right] + A_{55}\left[\frac{\alpha^2}{2} + \alpha\frac{\partial w_0}{\partial x} + \frac{1}{2}\left(\frac{\partial w_0}{\partial x}\right)^2\right]$$

$$+ A_{44}\left[\frac{\beta^2}{2} + \beta\frac{\partial w_0}{\partial y} + \frac{1}{2}\left(\frac{\partial w_0}{\partial y}\right)^2\right] + A_{66}\left[\frac{1}{2}\left(\frac{\partial u_0}{\partial y}\right)^2 + \frac{\partial u_0}{\partial y}\frac{\partial v_0}{\partial x}\right.$$

$$\left. + \frac{1}{2}\left(\frac{\partial v_0}{\partial x}\right)^2\right] + B_{66}\left[\frac{\partial u_0}{\partial y}\frac{\partial \alpha}{\partial y} + \frac{\partial u_0}{\partial y}\frac{\partial \beta}{\partial x} + \frac{\partial v_0}{\partial x}\frac{\partial \alpha}{\partial y} + \frac{\partial v_0}{\partial x}\frac{\partial \beta}{\partial x}\right] + D_{66}\left[\frac{1}{2}\left(\frac{\partial \alpha}{\partial y}\right)^2\right.$$

$$\left. + \frac{\partial \alpha}{\partial y}\frac{\partial \beta}{\partial x} + \frac{1}{2}\left(\frac{\partial \beta}{\partial x}\right)^2\right] - \int \Big[F_{11}\frac{\partial u_0}{\partial x}\frac{\partial \alpha}{\partial x} + F_{12}\left[\frac{\partial u_0}{\partial x}\frac{\partial \beta}{\partial y} + \frac{\partial v_0}{\partial y}\frac{\partial \alpha}{\partial x}\right]$$

$$+F_{16}\left[\frac{\partial u_0}{\partial x}\left(\frac{\partial \alpha}{\partial y}+\frac{\partial \beta}{\partial x}\right)+\frac{\partial \alpha}{\partial x}\left(\frac{\partial u_0}{\partial y}+\frac{\partial v_0}{\partial x}\right)\right] + F_{22}\frac{\partial v_0}{\partial y}\frac{\partial \beta}{\partial y}$$

$$+F_{26}\left[\frac{\partial v_0}{\partial y}\left(\frac{\partial \alpha}{\partial y}+\frac{\partial \beta}{\partial x}\right)+\frac{\partial \beta}{\partial y}\left(\frac{\partial u_0}{\partial y}+\frac{\partial v_0}{\partial x}\right)\right]+F_{66}\left(\frac{\partial u_0}{\partial y}+\frac{\partial v_0}{\partial x}\right)\left(\frac{\partial \alpha}{\partial y}+\frac{\partial \beta}{\partial x}\right)$$

$$-\left(I_1^T+I_1^H\right)\frac{\partial u_0}{\partial x}-\left(I_2^T+I_2^H\right)\frac{\partial v_0}{\partial y}-\left(I_6^T+I_6^H\right)\left(\frac{\partial u_0}{\partial y}+\frac{\partial v_0}{\partial x}\right) \qquad (2.31)$$

$$+\frac{H_{11}}{2}\left(\frac{\partial \alpha}{\partial x}\right)^2+H_{12}\frac{\partial \beta}{\partial y}\frac{\partial \alpha}{\partial x}+H_{16}\frac{\partial \alpha}{\partial x}\left(\frac{\partial \alpha}{\partial y}+\frac{\partial \beta}{\partial x}\right)+\frac{H_{22}}{2}\left(\frac{\partial \beta}{\partial y}\right)^2$$

$$+H_{26}\frac{\partial \beta}{\partial y}\left(\frac{\partial \alpha}{\partial y}+\frac{\partial \beta}{\partial x}\right)+\frac{H_{66}}{2}\left(\frac{\partial \alpha}{\partial y}+\frac{\partial \beta}{\partial x}\right)^2-\left(J_1^T+J_1^H\right)\frac{\partial \alpha}{\partial x}$$

$$-\left(J_2^T+J_2^H\right)\frac{\partial \beta}{\partial y}-\left(J_6^T+J_6^H\right)\left(\frac{\partial \alpha}{\partial y}+\frac{\partial \beta}{\partial x}\right)+\frac{K^T}{2}+\frac{K^H}{2}+K^{TH}\Bigg]$$

$$-\left(\frac{\partial u_0}{\partial x}\right)\left(N_1^T+N_1^H\right)-\left(\frac{\partial v_0}{\partial y}\right)\left(N_2^T+N_2^H\right)-\left(\frac{\partial u_0}{\partial y}+\frac{\partial v_0}{\partial x}\right)\left(N_6^T+N_6^H\right)$$

$$-\left(\frac{\partial \alpha}{\partial x}\right)\left(M_1^T+M_1^H\right)-\left(\frac{\partial \beta}{\partial y}\right)\left(M_2^T+M_2^H\right)-\left(\frac{\partial \alpha}{\partial y}+\frac{\partial \beta}{\partial x}\right)\left(M_6^T+M_6^H\right)$$

$$+T^*+M^*+MT^*-Pw_0\Big\}\,dA^*$$

where

$$\left.\begin{aligned} F_{ij} &= \frac{1}{2}\sum_{K=1}^{N} \frac{\bar{Q}_{i3}^{K}\,\bar{Q}_{j3}^{K}}{\bar{Q}_{33}^{K}}\left(h_K^2 - h_{K-1}^2\right) \\ H_{ij} &= \frac{1}{3}\sum_{K=1}^{N} \frac{\bar{Q}_{i3}^{K}\,\bar{Q}_{j3}^{K}}{\bar{Q}_{33}^{K}}\left(h_K^3 - h_{K-1}^3\right) \end{aligned}\right\} \; ij = 1,2,6 \qquad (2.32)$$

$$\left.\begin{aligned} I_i^T &= \sum_{K=1}^{N} \frac{\bar{Q}_{i3}^{K}}{\bar{Q}_{33}^{K}}\,\bar{Q}_{3j}^{K}\,\bar{\gamma}_j^{T} \int_{h_{K-1}}^{h_K} T\,dz \\ I_i^H &= \sum_{K=1}^{N} \frac{\bar{Q}_{i3}^{K}}{\bar{Q}_{33}^{K}}\,\bar{Q}_{3j}^{K}\,\bar{\gamma}_j^{H} \int_{h_{K-1}}^{h_K} \bar{M}\,dz \\ J_i^T &= \sum_{K=1}^{N} \frac{\bar{Q}_{i3}^{K}}{\bar{Q}_{33}^{K}}\,\bar{Q}_{3j}^{K}\,\bar{\gamma}_j^{T} \int_{h_{K-1}}^{h_K} Tz\,dz \\ J_i^H &= \sum_{K=1}^{N} \frac{\bar{Q}_{i3}^{K}}{\bar{Q}_{33}^{K}}\,\bar{Q}_{3j}^{K}\,\bar{\gamma}_j^{H} \int_{h_{K-1}}^{h_K} \bar{M}z\,dz \end{aligned}\right\} \; \begin{aligned} i &= 1,2,6 \\ j &= 1,2,3,6 \end{aligned} \qquad (2.33)$$

$$\left.\begin{aligned} K_i^T &= \sum_{K=1}^{N} \frac{\left(\bar{Q}_{3j}^{K}\,\bar{\gamma}_j^{T}\right)^2}{\bar{Q}_{33}^{K}} \int_{h_{K-1}}^{h_K} T^2\,dz \\ K_i^H &= \sum_{K=1}^{N} \frac{\left(\bar{Q}_{3j}^{K}\,\bar{\gamma}_j^{H}\right)^2}{\bar{Q}_{33}^{K}} \int_{h_{K-1}}^{h_K} \bar{M}^2\,dz \\ K_i^{TH} &= \sum_{K=1}^{N} \frac{\left(\bar{Q}_{3j}^{K}\,\bar{\gamma}_j^{T}\right)\left(\bar{Q}_{3j}^{K}\,\bar{\gamma}_j^{H}\right)}{\bar{Q}_{33}^{K}} \int_{h_{K-1}}^{h_K} T\bar{M}\,dz \end{aligned}\right\} \; ij = 1,2,3,6 \qquad (2.34)$$

Equation (2.31) can now be used to obtain the solution for a generally laminated plate by the Rayleigh-Ritz method. The Rayleigh-Ritz method requires that admissible functions be chosen for the unknown displacements and rotations. These functions, which satisfy the geometric boundary conditions, can be substituted into the potential energy equation and variations taken with respect to the unknown amplitudes. This leaves a set of simultaneous equations to solve for the unknown amplitudes.

To study the effects of the transverse normal strain (TNS) a tracing constant, f, has been included in the derivation. To include TNS effects set f = 1. To exclude TNS effects set f = 0.

<u>Hygrothermal Effects</u>

The effects of a hygrothermal environment on a laminated composite plate are introduced into the analysis through dilatational strains in the constitutive relations. These strains are related to the thermal and moisture concentration distributions, $T(z,t)$ and $\bar{M}(z,t)$, by the coefficients of expansion, as expressed in equation (2.3). After integration through the thickness of the plate, the hygrothermal strains take the form of stress resultants and couples as defined in equation (2.26). To evaluate the stress resultants and couples, it is necessary to define distributions

which are integrable.

Transient Case: Pipes, Vinson and Chou [1] derived the moisture concentration distribution using the classical diffusion equation,

$$D\frac{\partial^2 \bar{M}}{\partial z^2} - \frac{\partial \bar{M}}{\partial t} = 0 , \tag{2.35}$$

where D is the diffusion constant of the material. For symmetric moisture absorption, the solution to equation (2.35), with the appropriate boundary conditions, is,

$$\bar{M}(z,t) = \bar{M}_o\left[1 - \sum_{n=0}^{\infty} m_n \cos a_n z\right] \tag{2.36}$$

where,
$$a_n = \frac{(2n+1)\pi}{h} \tag{2.37}$$

and
$$m_n = \frac{4}{\pi}\left\{\frac{(-1)^n}{2n+1}\, e^{-a_n^2 D t}\right\} \tag{2.38}$$

For symmetric moisture desorption,

$$\bar{M}(z,t) = \bar{M}_o \sum_{n=0}^{\infty} m_n \cos a_n z \tag{2.39}$$

For single surface moisture absorption,

$$\bar{M}(z,t) = \bar{M}_o\left\{1 - \sum_{n=0}^{\infty} p_n \cos q_n\left(z + \frac{h}{2}\right)\right\} \tag{2.40}$$

where
$$q_n = \frac{(2n+1)\pi}{2h} \tag{2.41}$$

$$P_n = \frac{4}{\pi}\left\{ \frac{(-1)^n}{2n+1} e^{-q_n^2 D t} \right\} \tag{2.42}$$

These solutions are also valid for the transient thermal distribution, by using the thermal diffusivity for D.

Steady-State Case: The steady-state distributions for the temperature and moisture concentration will be simply linear functions in the z direction,

$$\bar{M}(z) = \left(\frac{\bar{M}_u + \bar{M}_L}{2}\right) + \left(\frac{\bar{M}_u - \bar{M}_L}{h}\right) z \tag{2.43}$$

$$T(z) = \left(\frac{T_u + T_L}{2}\right) + \left(\frac{T_u - T_L}{h}\right) z \tag{2.44}$$

where the subscripts u and L signify the upper and lower surface respectively.

The given distribution functions $\bar{M}$ and T can be substituted into equation (2.26) and integrated to obtain the hygrothermal stress resultants and couples.

CHAPTER THREE

SOLUTION TECHNIQUE

The Rayleigh-Ritz Method is used to obtain the solution for the laminated plate in the form of displacements and rotations. This approximate method calls for an assumed functional form of the unknown variables to be substituted into the potential energy equation. Variations taken with respect to the undetermined coefficients give the conditions necessary to minimize the potential energy of the plate. These conditions are a set of linear simultaneous equations in the unknown coefficients introduced in the assumed functional form of the variables.

The requirements on the functional form of the displacements and rotations are that they be an admissible set of functions. That is to say, these functions only need to satisfy the geometric boundary conditions for a given support condition to insure convergence to the correct solution. This is the useful feature of the Rayleigh-Ritz Method, in that admissible functional forms are readily available in the literature for most common support conditions.

The Rayleigh-Ritz Method is not without its short-

comings, particularly for obtaining the stress solution for a problem. The convergence of the deflection solution is generally rapid, assuming that a reasonable displacement function is chosen. However, to obtain the same degree of convergence for derivatives of the displacement functions that are needed to obtain stresses, more terms of the admissible functions are needed.

Boundary Conditions

The solutions obtained herein were for plates with the following three support configurations.

1. All Edges Simply Supported
2. All Edges Clamped.
3. Two Opposite Edges Simply Supported, Two Opposite Edges Clamped.

In any analysis of unsymmetrically laminated plates, the in-plane displacements, u and v, must be included. These displacements are necessary to account for the bending-extensional coupling present in unsymmetric laminates.

The boundary conditions used in the analysis of generally laminated simply supported plates, as presented by Whitney [11], are

$$S1: \quad W_n = 0,\ M_n = 0,\ u_n = 0,\ N_{nt} = 0 \tag{3.1}$$

$$S2: \quad W_n = 0,\ M_n = 0,\ N_n = 0,\ u_t = 0, \tag{3.2}$$

where the subscripts n and t represent the normal and tangential direction to the plate edge, respectively.

For the clamped plate the following boundary conditions are used,

$$C1: \quad W_n = 0, \ \alpha_n = 0, \ u_n = 0, \ N_{nt} = 0 \tag{3.3}$$

$$C2: \quad W_n = 0, \ \alpha_n = 0, \ N_n = 0, \ u_t = 0 \tag{3.4}$$

For the simple-clamped plate the edges parallel to the x axis use the clamped boundary conditions. The edges parallel to the y axis use the simply-supported boundary conditions.

Assumed Displacement and Rotation Functions

Contrary to the approach of many researchers [6,7,8], which include transverse shear deformations, the reduced unit width beam approximation from the Euler-Lagrange equations will not be used to remove the rotational dependent variables, α and β. Instead, a functional form for these variables will be assumed as done by Wu and Vinson [9].

The assumed functional forms for the simply-supported boundary condition, S1, are,

$$w(x,y) = \sum_{m=1,3,5}^{\infty} \sum_{n=1,3,5}^{\infty} W_{mn} \sin\frac{m\pi x}{A} \sin\frac{n\pi y}{B}$$

$$\alpha(x,y) = \sum_{m=1,3,5}^{\infty} \sum_{n=1,3,5}^{\infty} \Gamma_{mn} \sin\frac{m\pi x}{A} \cos\frac{n\pi y}{B} \tag{3.5}$$

$$\beta(x,y) = \sum_{m=1,3,5}^{\infty} \sum_{n=1,3,5}^{\infty} \Lambda_{mn} \cos\frac{m\pi x}{A} \sin\frac{n\pi y}{B}$$

$$u(x,y) = \sum_{m=1,3,5}^{\infty} \sum_{n=1,3,5}^{\infty} U_{mn} \sin\frac{m\pi x}{A} \cos\frac{n\pi y}{B}$$

$$v(x,y) = \sum_{m=1,3,5} \sum_{n=1,3,5} V_{mn} \cos\frac{m\pi x}{A} \sin\frac{n\pi y}{B} \tag{3.6}$$

The form for the S2 boundary condition will be similar to S1, except that the following forms for u and v are used instead of equation (3.6).

$$u(x,y) = \sum_{m=1,3,5}^{\infty} \sum_{n=1,3,5}^{\infty} U_{mn} \cos\frac{m\pi x}{A} \sin\frac{n\pi y}{B} \tag{3.7}$$

$$v(x,y) = \sum_{m=1,3,5}^{\infty} \sum_{n=1,3,5}^{\infty} V_{mn} \sin\frac{m\pi x}{A} \cos\frac{n\pi y}{B}$$

The assumed form of the displacements and rotations for the C1 clamped boundary condition are the characteristic beam functions, originally presented by Warburton in [4]

and extended by Wu and Vinson in [9],

$$w(x,y) = \sum_{m=1,3,5}^{\infty} \sum_{n=1,3,5}^{\infty} W_{mn} \, \phi_{wm}(x) \, \phi_{wn}(y)$$

$$\alpha(x,y) = \sum_{m=1,3,5}^{\infty} \sum_{n=1,3,5}^{\infty} \Gamma_{mn} \, \phi_{\alpha m}(x) \, \phi_{\alpha n}(y) \qquad (3.8)$$

$$\beta(x,y) = \sum_{m=1,3,5}^{\infty} \sum_{n=1,3,5}^{\infty} \Lambda_{mn} \, \phi_{\beta m}(x) \, \phi_{\beta n}(y)$$

$$u(x,y) = \sum_{m=1,3,5}^{\infty} \sum_{n=1,3,5}^{\infty} U_{mn} \sin \frac{m\pi x}{A} \cos \frac{n\pi y}{B} \qquad (3.9)$$

$$v(x,y) = \sum_{m=1,3,5}^{\infty} \sum_{n=1,3,5}^{\infty} V_{mn} \cos \frac{m\pi x}{A} \sin \frac{n\pi y}{B},$$

where

$$\phi_{wm}(x) = \cos \mu_m \left(\frac{x}{A} - \frac{1}{2}\right) + \eta_m \cosh \mu_m \left(\frac{x}{A} - \frac{1}{2}\right)$$

$$\phi_{\alpha m}(x) = \sin \mu_m \left(\frac{x}{A} - \frac{1}{2}\right) - \eta_m \sinh \mu_m \left(\frac{x}{A} - \frac{1}{2}\right) \qquad (3.10)$$

$$\phi_{\beta m}(x) = \cos \mu_m \left(\frac{x}{A} - \frac{1}{2}\right) + \eta_m \cosh \mu_m \left(\frac{x}{A} - \frac{1}{2}\right)$$

and

$$\eta_m = \frac{\sin(\mu_m/2)}{\sinh(\mu_m/2)} \tag{3.11}$$

$$\tan\left(\frac{\mu_m}{2}\right) + \tanh\left(\frac{\mu_m}{2}\right) = 0. \tag{3.12}$$

By interchanging α and β and substituting y for x, n for m, and B for A, the equations given in (3.10) yield the proper functions for the y direction. The solution to the transcendental equation (3.12) gives the necessary values for the μ_m constant in equations (3.10). These solutions are,

$$\begin{aligned} &\mu_1 = 1.50562\pi, \quad \mu_2 = 2.49975\pi \\ &\mu_K \cong \left(K + \tfrac{1}{2}\right)\pi \qquad K \geq 3 \end{aligned} \tag{3.13}$$

Again for the C2 boundary conditions, u and v will be changed to the functions given in equation (3.7).

It should be noted that only the odd mode shapes of m and n are involved in the analysis. This occurs because only the odd terms will be non-zero for the loads and symmetric boundary conditions considered.

For the simple-clamped boundary conditions the following combinations of the previous functional forms are used.

$$w(x,y) = \sum_{m=1,3,5}^{\infty} \sum_{n=1,3,5}^{\infty} W_{mn}\, \phi_{wm}(x) \sin \frac{n\pi y}{B}$$

$$\alpha(x,y) = \sum_{m=1,3,5}^{\infty} \sum_{n=1,3,5}^{\infty} \Gamma_{mn}\, \phi_{\alpha m}(x) \cos \frac{n\pi y}{B} \qquad (3.14)$$

$$\beta(x,y) = \sum_{m=1,3,5}^{\infty} \sum_{n=1,3,5}^{\infty} \Lambda_{mn}\, \phi_{\beta m}(x) \sin \frac{n\pi y}{B}$$

The u and v variables have the same form as given by equations (3.6) or (3.7) depending on the desired in-plane boundary conditions.

Deflection and Stress Calculations

With the values of the unknown amplitude coefficients, W_{mn}, Γ_{mn}, Λ_{mn}, U_{mn}, and V_{mn}, the deflections and rotations of the plate can be easily calculated from the appropriate support condition given in equation (3.5) to (3.14).

The laminate strains can be calculated using the strain-displacement relationships in equation (2.16) along with the assumed form of the displacements and rotations. Separating the strains into mid-plane strains and curvatures gives,

$$\epsilon_j = \epsilon_j^{o} + z K_j \qquad j = 1,2,6 \qquad (3.15)$$

where,

$$\begin{aligned} \epsilon_1 &= \frac{\partial u_o}{\partial x} & K_1 &= \frac{\partial \alpha}{\partial x} \\ \epsilon_2 &= \frac{\partial v_o}{\partial y} & K_2 &= \frac{\partial \beta}{\partial y} \\ \epsilon_6 &= \frac{1}{2}\left(\frac{\partial u_o}{\partial y} + \frac{\partial v_o}{\partial x}\right) & K_6 &= \frac{1}{2}\left(\frac{\partial \alpha}{\partial y} + \frac{\partial \beta}{\partial x}\right) \end{aligned} \qquad (3.16)$$

These laminate strains are strains caused by the deformation of the plate only. The strains due to the hygrothermal stress resultants and couples can be included by using the A, B, D matrices, relating these quantities to strains. As presented in ref. [1],

$$\begin{aligned} N_i^T + N_i^H &= A_{ij} \epsilon_j^{o} + B_{ij} K_j \\ M_i^T + M_i^H &= B_{ij} \epsilon_j^{o} + D_{ij} K_j \end{aligned} \qquad ij = 1,2,6 \qquad (3.17)$$

By inverting equation (3.17), the strains due to the N_i^T, N_i^H and M_i^T, M_i^H can be calculated.

It should be noted that no attempt has been made to include the transverse normal strains in the stress calculations.

With the laminate strains determined, the stresses within each lamina are,

$$\sigma_j^K = \bar{Q}_{ij}^K\left[\epsilon_j^o + z\,\kappa_j - \bar{\gamma}_j^T T - \bar{\gamma}_j^H \bar{M}\right]^K$$

$$ij = 1,2,6 \quad (3.18)$$

The stresses in a laminated plate for varying degrees of edge restraint, can be determined by the exclusion of the appropriate terms in equation (3.18) as presented in [10]. For example, if the laminated plate is fully restrained, (i.e. clamped), the stress resultant and couple strains are not included in the stress calculation. For a plate with in-plane restraints only, the N_i^T and N_i^H terms are omitted. For a plate free of all edge restraints all terms are included in equation (3.17). This last case is essentially the rectangular plate element considered by Pipes, Vinson and Chou in [1].

Therefore, using the displacement solution along with the hygrothermal stress resultants and couples, lamina stresses can be determined for various support conditions.

CHAPTER FOUR

NUMERICAL ANALYSIS

In order to determine the importance of hygrothermal loads in analyzing a laminated composite plate, solutions are presented using the theory developed in the previous two chapters. The examples given indicate the importance of hygrothermal loads, as well as the complexity of the theory required to obtain satisfactory engineering solutions.

To efficiently obtain solutions using the solution technique given in Chapter 3, a computer program was developed. The program is listed in Appendix D, along with a brief description of the input data required and an example output. The program analyzes rectangular laminated plates, symmetric or unsymmetric, with clamped, simply-supported, or clamped-simple support boundary conditions. Loads included are through the thickness moisture and temperature gradients and uniform lateral pressures. The output gives the deflections, rotations, stress resultants, stress couples, strains and stresses in the plate coordinate system. Also included are options to perform the analysis based on linear plate theory (LPT), plate theory including transverse shear de-

formation (TSD), and plate theory including transverse shear deformation plus transverse normal strains (TSD+TNS).

In using the Rayleigh-Ritz procedure to obtain solutions to the governing equations, large systems of linear equations are generated. Only the digital computer can efficiently solve such systems. However, an important part of using the computer as an analysis tool for solving equations is verification of the program logic or code. The detailed results of the many example cases run to verify the program used are given in Appendix A. The examples analyzed include classical isotropic plate solutions as well as duplication of many of the results published by Whitney [5, 11, 12, 13] for both symmetric and unsymmetric laminated plates.

During program verification, a computational error was uncovered in the single surface moisture absorption example presented by Pipes et al in reference [1]. As an aid to those attempting to duplicate these particular results, the corrected stress plots and details are given in Appendix B.

In using an approximate solution procedure with a finite number of terms for the assumed displacements and rotations, it is important to determine the convergence to the solution. For the results presented, all odd terms up through m, n equal to seven were used. The convergence

of the solution was evaluated by calculating the percent change in the lateral defection solution, $\rho_{m,n}$, contributed by each term containing the highest index.

For the simply-supported results present, using terms through m,n = 7,

$$\rho_{m,n} < 0.1\%$$

For the clamped boundary conditions,

$$\rho_{m,n} < 0.7\%$$

The following material property data from reference [6] for the T300/5208 graphite epoxy composite were used in the analysis.

	70°F	350°F
E_1 (psi)	21.0×10^{6}	18.7×10^{6}
E_2 (psi)	1.7×10^{6}	0.87×10^{6}
G_{12} (psi)	0.65×10^{6}	0.65×10^{6}
ν_{12}	0.21	0.21
ν_{21}	0.017	0.010
ν_{23}	0.33	0.33
γ^T (in/in °F)	-0.21×10^{-6}	-0.005×10^{-6}
γ^T (in/in °F)	16.0×10^{-6}	21.8×10^{-6}

	70°F	350°F
γ_1^H(in/in %WT)	0	0
γ_2^H(in/in %WT)	6.67×10^{-3}	6.67×10^{-3}
h_o(in)	0.0055	0.0055

Temperature dependent material properties for each lamina were based on linear interpolation of the above data using the mean lamina temperature. Linear interpolation is sufficient for most problems encountered due to the much higher thermal diffusivity compared to moisture diffusivity [14].

Comparison of Theories

To assess the importance of the more complex plate theory including transverse shear deformation and transverse normal strain, the lateral deflections of several T300/5208 plates subjected only to a linear moisture gradient were evaluated. Figure 4.1 shows the center deflection of four layer symmetric and unsymmetric, angle ply, simply-supported laminates using the different plate theories for various A/B ratios. Figure 4.2 shows the deflections of the same plate for different A/H ratios. To determine if thickness had an effect, results for a 24 layer, symmetric, angle ply plate are shown in Figure 4.3 for A/B ratios and Figure 4.4 for A/H ratios.

Tables 4.1 through 4.6 tabulates the results used to plot the curves in Figures 4.1 through 4.4.

Effects of Hygrothermal Loads

To demonstrate the importance of hygrothermal loads, several examples of the stress distributions in T300/5208 laminated plates with different support conditions are given. The plate theory including only transverse shear deformation is used throughout these examples. The single surface absorption moisture distributions, as presented by Pipes et al [1], are used at various time intervals. The temperature conditions used are either a uniform temperature or a linear temperature gradient through the thickness of the plate. Temperature dependent material properties are used based on the mean lamina temperature.

Figures 4.5 and 4.6 show the moisture distributions for single surface absorption at the time intervals evaluated in the examples for the 6 and 4 layer laminates, respectively. These moisture distributions reflect the faster diffusion expected through the thinner 4 layer laminate.

The first example is a square six layer, $/0_1, 45_1, -45/_{2s}$, symmetric plate with clamped boundary conditions. The loads considered are a lateral pressure of 2 psi, a uniform temperature of 150°F, and a sudden moisture change

to $M_o = 1.0\%$ on the top surface at $Dt = 0$. The plate is assumed to be moisture free for $Dt < 0$. Figures 4.7, 4.8, and 4.9 show the stresses in the x,y and xy directions at various Dt's for a plate without in-plane restraints against the dilatational expansions. Figures 4.10, 4.11, and 4.12 show the stresses with in-plane restraints. As a basis of comparison, Figure 4.13 shows the stress distributions through the plate for the pressure and temperature conditions only.

The second example is a simply-supported 4 layer, $\theta = \pm 45°$, angle ply laminate. The loading is a uniform pressure of 1 psi, a linear temperature gradient of from 200°F on the top surface to 100°F on the bottom, and a single surface moisture absorption load for $M_o = 1.0\%$. The plate is again assumed to be moisture free at $Dt < 0$, and unrestrained in-plane. Figures 4.14 and 4.15 show the stress distributions for a symmetric, $/45_1, -45/_{2s}$, laminate. Figures 4.16 and 4.17 show the stress distributions for an unsymmetric, $/45_1, -45_1, 45_1, -45/$ laminate. Since the stress distribution in the x and y directions are identical, they are plotted together in one figure. For comparison, the pressure and temperature loads only stress distributions are included in the figures.

Figures 4.18 through 4.21 show the stresses for a 4 layer, $\theta = 0, 90°$, cross ply laminate under the same load

conditions as the previous example. In this case the shear stresses are zero and therefore not shown.

Finally, Figures 4.22 and 4.23 show the variation in center deflection with time for the symmetric angle and cross ply four layer laminate examples. The line labeled "P + T Only" represents the deflections caused by the pressure and temperature loads only, which do not vary with time. The straight lines drawn between data points do not represent the actual variation in deflections. These lines are included only as an aid to visualize the varying center deflection.

TABLE 4.1

T300/5208 GRAPHITE EPOXY PLATE

4-LAYER /45, -45, -45, 45/

A/H = 100 H = 0.022 IN

$\bar{M}(z) = 1.0 + 18.1818z$ (%WT)

A/B (A/H=100)	$W_{CENTER} \times 10^3$ (IN)		
	LPT	TSD	TSD+TNS
0.33	8.394	8.395	8.395
0.5	6.382	6.383	6.383
0.67	4.958	4.958	4.957
1.0	3.335	3.334	3.334
1.25	2.663	2.662	2.662
1.50	2.204	2.204	2.204
1.75	1.862	1.863	1.863
2.0	1.596	1.596	1.596
3.0	0.927	0.928	0.928
4.0	0.586	0.587	0.587

TABLE 4.2

T300/5208 GRAPHITE EPOXY PLATE

SIMPLY-SUPPORTED ALL EDGES

4-LAYER /45, -45, -45, 45/

A/B = 1 H = 0.022 IN

$\bar{M}(z) = 1.0 + 18.1818z$ (%WT)

A/H (A=B)	$W_{CENTER} \times 10^3$ (IN)		
	LPT	TSP	TSD+TNS
5.0	0.00834	0.00810	0.00810
10.0	0.0335	0.0329	0.0329
15.0	0.0750	0.0745	0.0745
25.0	0.2084	0.2079	0.2079
35.0	0.4085	0.4080	0.4080
50.0	0.8337	0.8332	0.8331
75.0	1.876	1.875	1.875
100.0	3.335	3.334	3.334
200.0	13.34	13.34	13.34
300.0	30.01	30.01	30.01
500.0	83.37	83.37	83.37

TABLE 4.3

T300/5208 GRAPHITE EPOXY PLATE

SIMPLY-SUPPORTED ALL EDGES

4-LAYER /45, -45, 45, -45/

A/H = 100 H = 0.022 IN

$\bar{M}(z) = 1.0 + 18.1818z$ (%WT)

A/B (A/H=100)	$W_{CENTER} \times 10^3$ (IN)		
	LPT	TSD	TSD+TNS
0.33	10.75	10.75	10.74
0.5	8.207	8.207	8.190
0.67	6.386	6.386	6.367
1.0	4.296	4.295	4.278
1.25	3.431	3.431	3.418
1.5	2.839	2.839	2.831
1.75	2.397	2.397	2.392
2.0	2.052	2.052	2.048
3.0	1.188	1.189	1.187
4.0	0.749	0.749	0.749

TABLE 4.4

T300/5208 GRAPHITE EPOXY PLATE

SIMPLY-SUPPORTED ALL EDGES

4-LAYER /45, -45, 45, -45/

A/B = 1 H = 0.022 IN

$\bar{M}(z) = 1.0 + 18.1818z$ (%WT)

A/H (A=B)	$W_{CENTER} \times 10^3$ (IN)		
	LPT	TSD	TSD+TNS
5.0	0.0107	0.0105	0.0104
10.0	0.0430	0.0425	0.0423
15.0	0.0967	0.0962	0.0958
25.0	0.2685	0.2680	0.2669
35.0	0.5263	0.5257	0.5236
50.0	1.074	1.073	1.069
75.0	2.417	2.416	2.406
100.0	4.296	4.295	4.278
200.0	17.18	17.18	17.11
300.0	38.66	38.66	38.50

TABLE 4.5

T300/5208 GRAPHITE EPOXY PLATE

SIMPLY-SUPPORTED ALL EDGES

24-LAYER /45, -45, -45, 45/6s

A/H = 100 H = 0.132 IN

$\bar{M}(z) = 1.0 + 18.1818z$ (%WT)

A/B (A/H=100)	$W_{CENTER} \times 10^1$ (IN)		
	LPT	TSD	TSD+TNS
0.33	3.021	3.022	3.022
0.5	2.298	2.298	2.298
0.67	1.784	1.784	1.784
1.0	1.201	1.200	1.200
1.25	0.9586	0.9585	0.9585
1.5	0.7932	0.7932	0.7932
1.75	0.6705	0.6706	0.6706
2.0	0.5744	0.5746	0.5746
3.0	0.3340	0.3344	0.3344
4.0	0.2110	0.2113	0.2113

TABLE 4.6

T300/5208 GRAPHITE EPOXY PLATE

SIMPLY-SUPPORTED ALL EDGES

24-LAYER /45, -45, -45, 45/6s

A/B = 1   H = 0.132 IN

$\bar{M}(z) = 1.0 + 18.1818z$ (%WT)

A/H (A=B)	$W_{CENTER} \times 10^1$ (IN)		
	LPT	TSP	TSP+TNS
5.0	0.0030	0.0029	0.0029
10.0	0.0120	0.0185	0.0185
15.0	0.0270	0.0268	0.0268
25.0	0.0750	0.0748	0.0748
35.0	0.1471	0.1469	0.1469
50.0	0.3001	0.2999	0.2999
75.0	0.6753	0.6751	0.6751
100.0	1.201	1.200	1.200
200.0	4.802	4.802	4.802
300.0	10.81	10.81	10.81

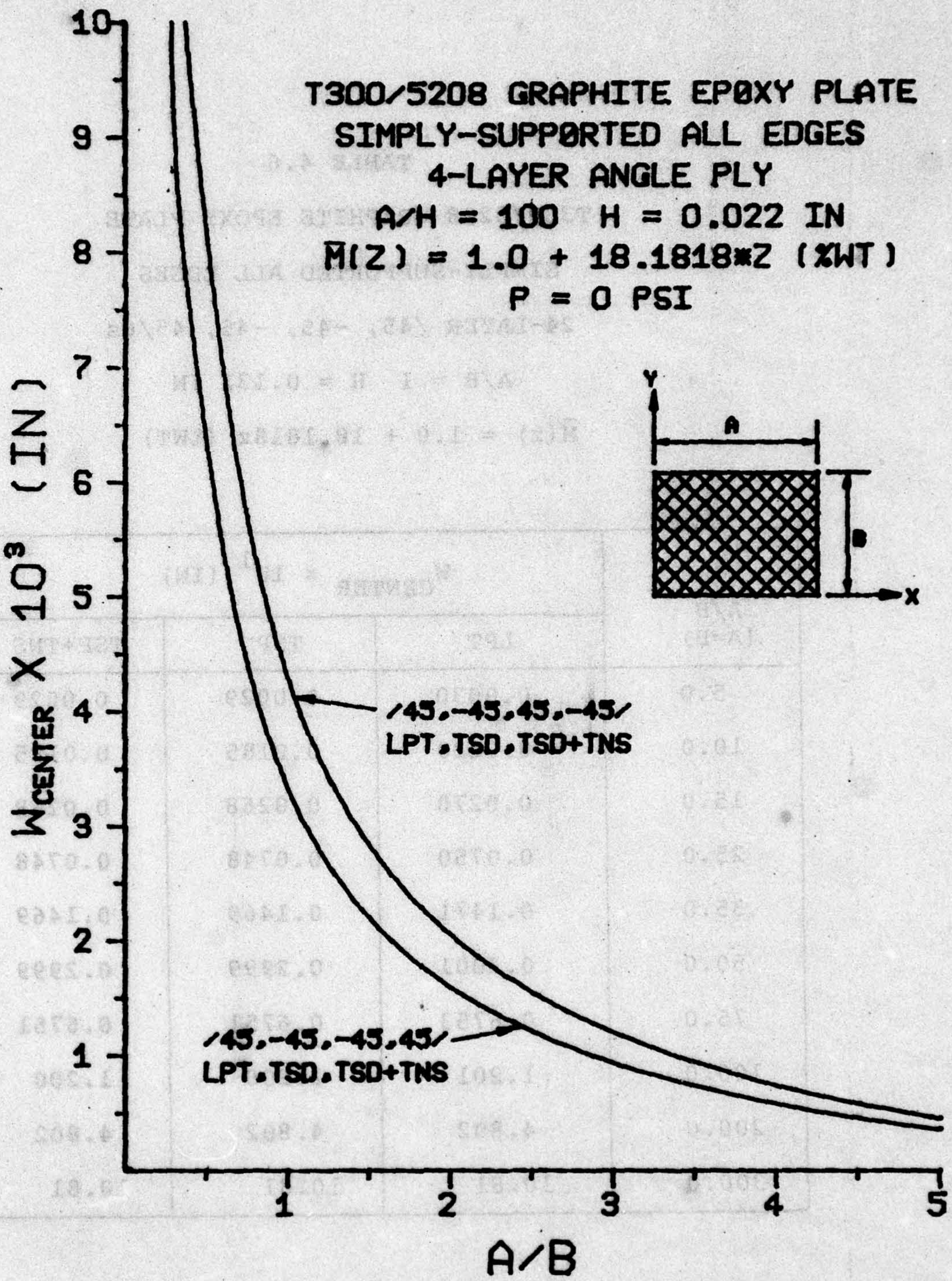
T300/5208 GRAPHITE EPØXY PLATE
SIMPLY-SUPPØRTED ALL EDGES
4-LAYER ANGLE PLY
A/H = 100 H = 0.022 IN
M̄(Z) = 1.0 + 18.1818*Z (%WT)
P = 0 PSI
Y
A
B
X
/45,-45,45,-45/
LPT,TSD,TSD+TNS
/45,-45,-45,45/
LPT,TSD,TSD+TNS
W_{CENTER} X 10^3 (IN)
A/B
10
9
8
7
6
5
4
3
2
1
1
2
3
4
5

Figure 4.1

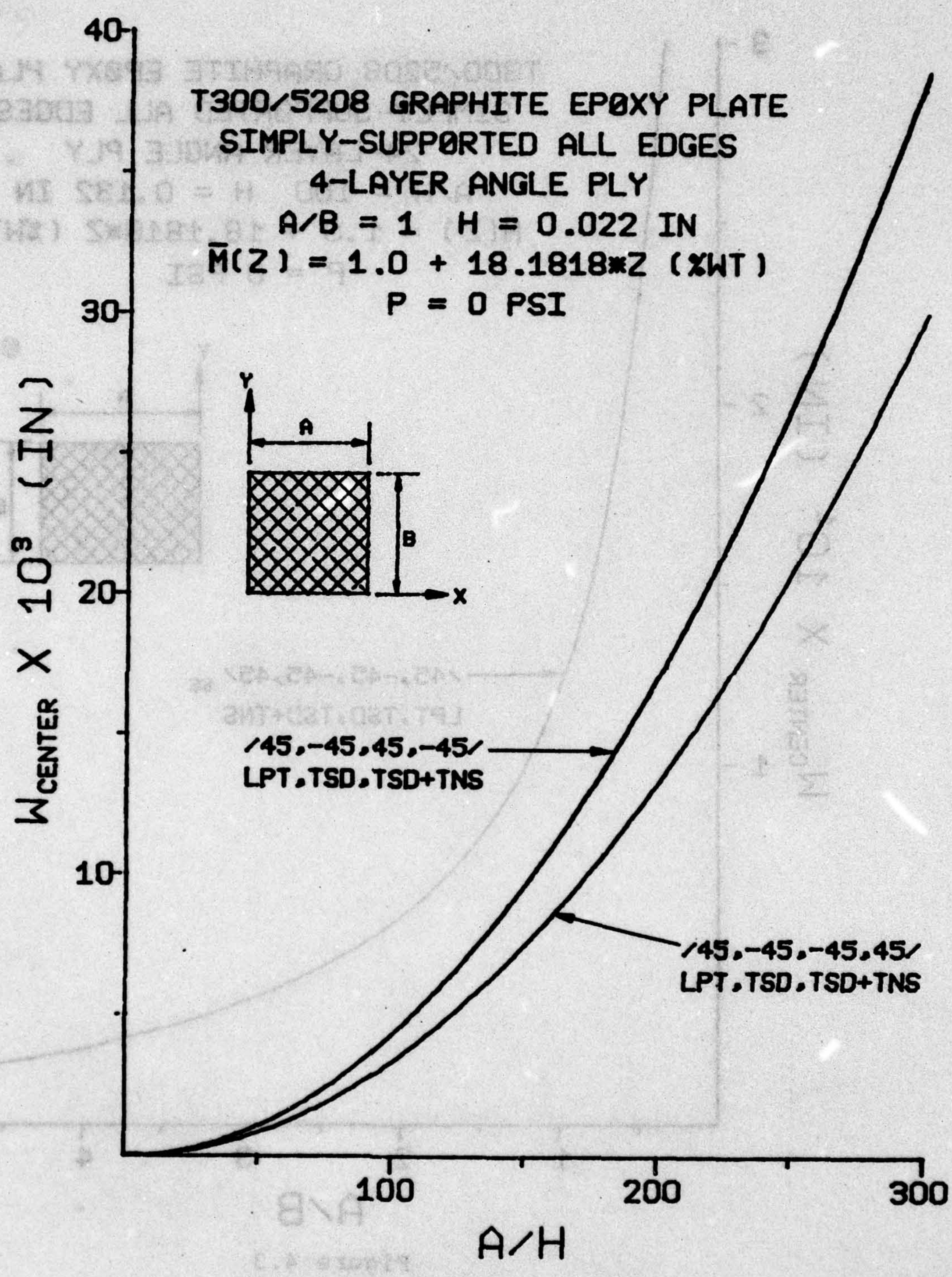
T300/5208 GRAPHITE EPØXY PLATE
SIMPLY-SUPPØRTED ALL EDGES
4-LAYER ANGLE PLY
A/B = 1 H = 0.022 IN
M̄(Z) = 1.0 + 18.1818*Z (%WT)
P = 0 PSI
Y
A
B
X
/45,-45,45,-45/
LPT,TSD,TSD+TNS
/45,-45,-45,45/
LPT,TSD,TSD+TNS
W CENTER X 10³ (IN)
40
30
20
10
100
200
300
A/H

Figure 4.2

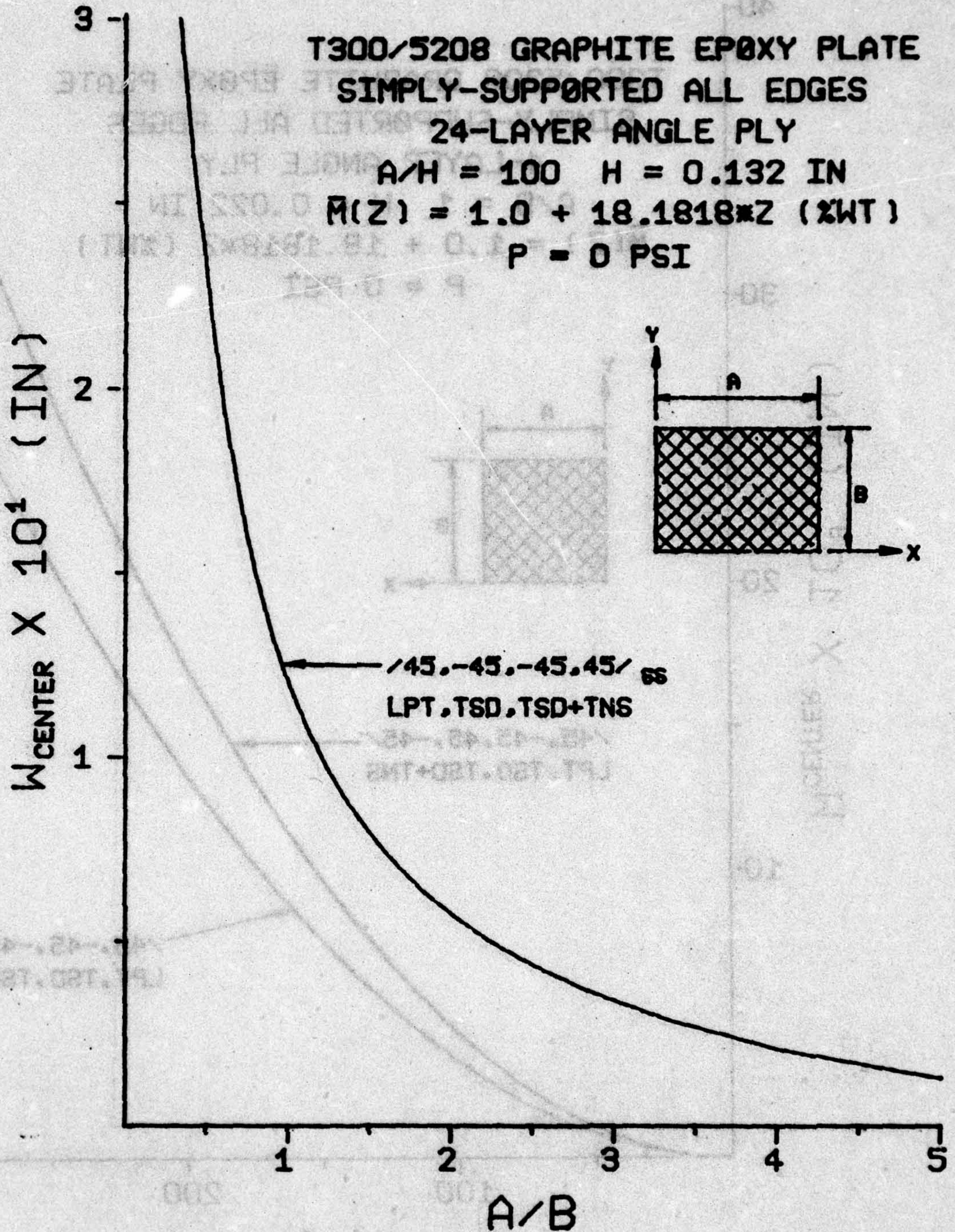
T300/5208 GRAPHITE EPØXY PLATE
SIMPLY-SUPPØRTED ALL EDGES
24-LAYER ANGLE PLY
A/H = 100 H = 0.132 IN
M̄(Z) = 1.0 + 18.1818*Z (%WT)
P = 0 PSI
Y
A
B
X
/45,-45,-45,45/ 6S
LPT,TSD,TSD+TNS
W CENTER X 10¹ (IN)
3
2
1
1
2
3
4
5
A/B

Figure 4.3

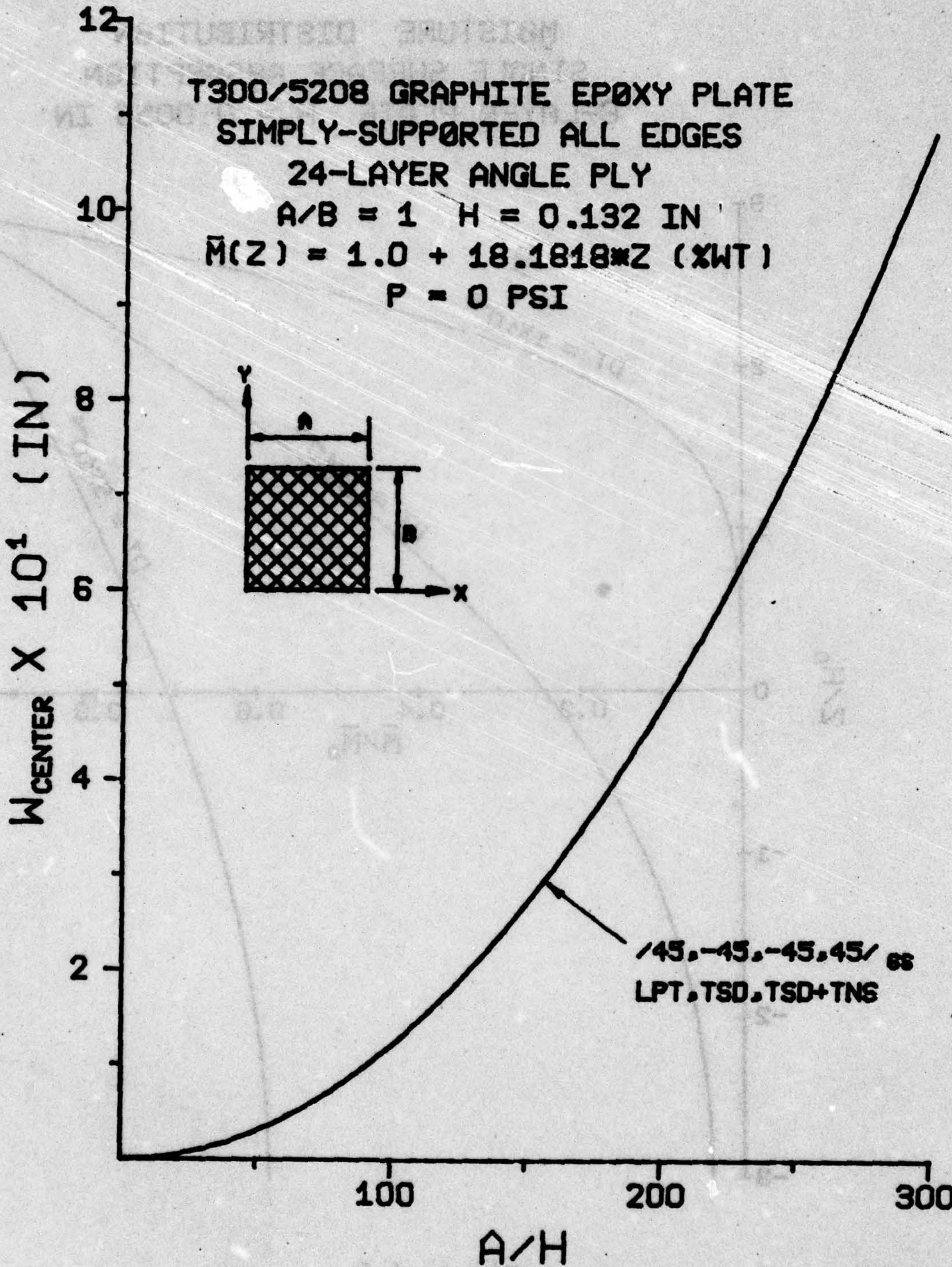
T300/5208 GRAPHITE EPØXY PLATE
SIMPLY-SUPPØRTED ALL EDGES
24-LAYER ANGLE PLY
A/B = 1 H = 0.132 IN
M̃(Z) = 1.0 + 18.1818*Z (%WT)
P = 0 PSI
Y
A
B
X
/45,-45,-45,45/ 6S
LPT,TSD,TSD+TNS
W CENTER X 10^1 (IN)
A/H
12
10
8
6
4
2
100
200
300

Figure 4.4

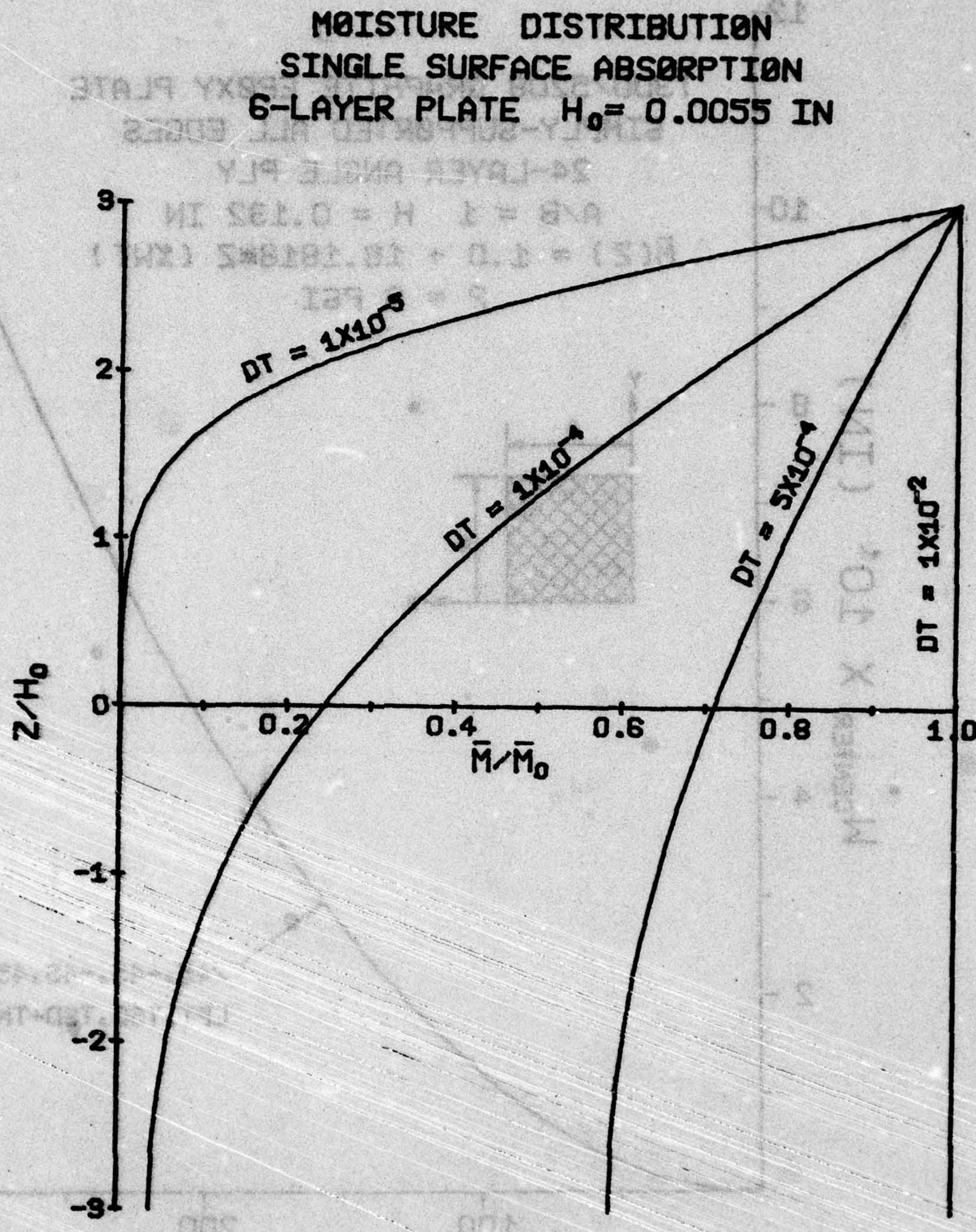
MØISTURE DISTRIBUTIØN
SINGLE SURFACE ABSØRPTIØN
6-LAYER PLATE H_0= 0.0055 IN
DT = 1X10^{-5}
DT = 1X10^{-4}
DT = 5X10^{-4}
DT = 1X10^{-2}
Z/H_0
$\bar{M}/\bar{M}_0$
3
2
1
0
-1
-2
-3
0.2
0.4
0.6
0.8
1.0

Figure 4.5

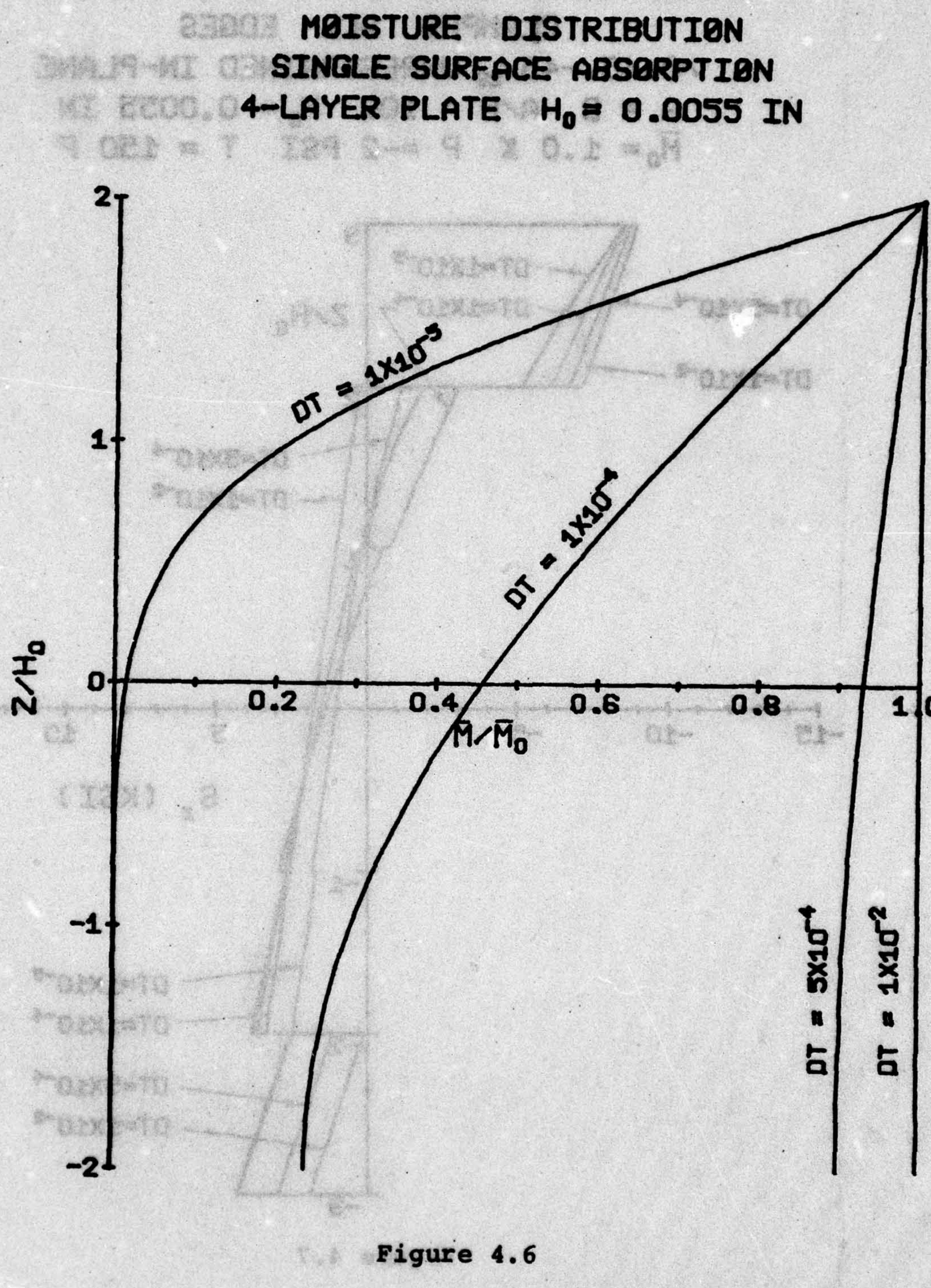
MØISTURE DISTRIBUTIØN
SINGLE SURFACE ABSØRPTIØN
4-LAYER PLATE H0 = 0.0055 IN
DT = 1X10^-5
DT = 1X10^-4
DT = 5X10^-4
DT = 1X10^-2
Z/H0
M̄/M̄0
2
1
0
-1
-2
0.2
0.4
0.6
0.8
1.0

Figure 4.6

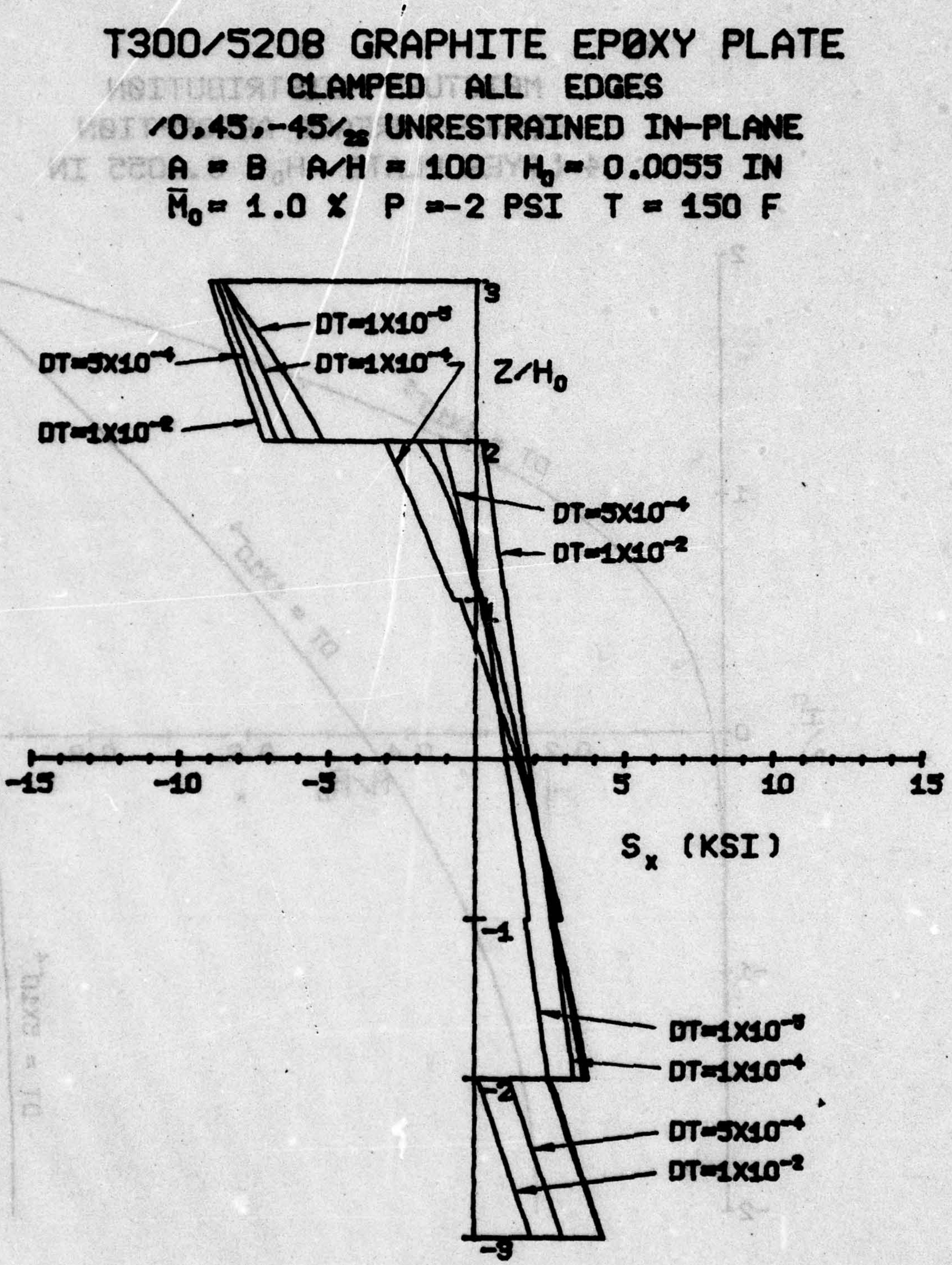
T300/5208 GRAPHITE EPØXY PLATE
CLAMPED ALL EDGES
/0,45,-45/2S UNRESTRAINED IN-PLANE
A = B A/H = 100 H0 = 0.0055 IN
M0 = 1.0 X P = -2 PSI T = 150 F
DT=1X10-3
DT=5X10-4
DT=1X10-4
DT=1X10-2
Z/H0
3
2
1
-1
-2
-3
DT=5X10-4
DT=1X10-2
-15
-10
-5
5
10
15
Sx (KSI)
DT=1X10-3
DT=1X10-4
DT=5X10-4
DT=1X10-2

Figure 4.7

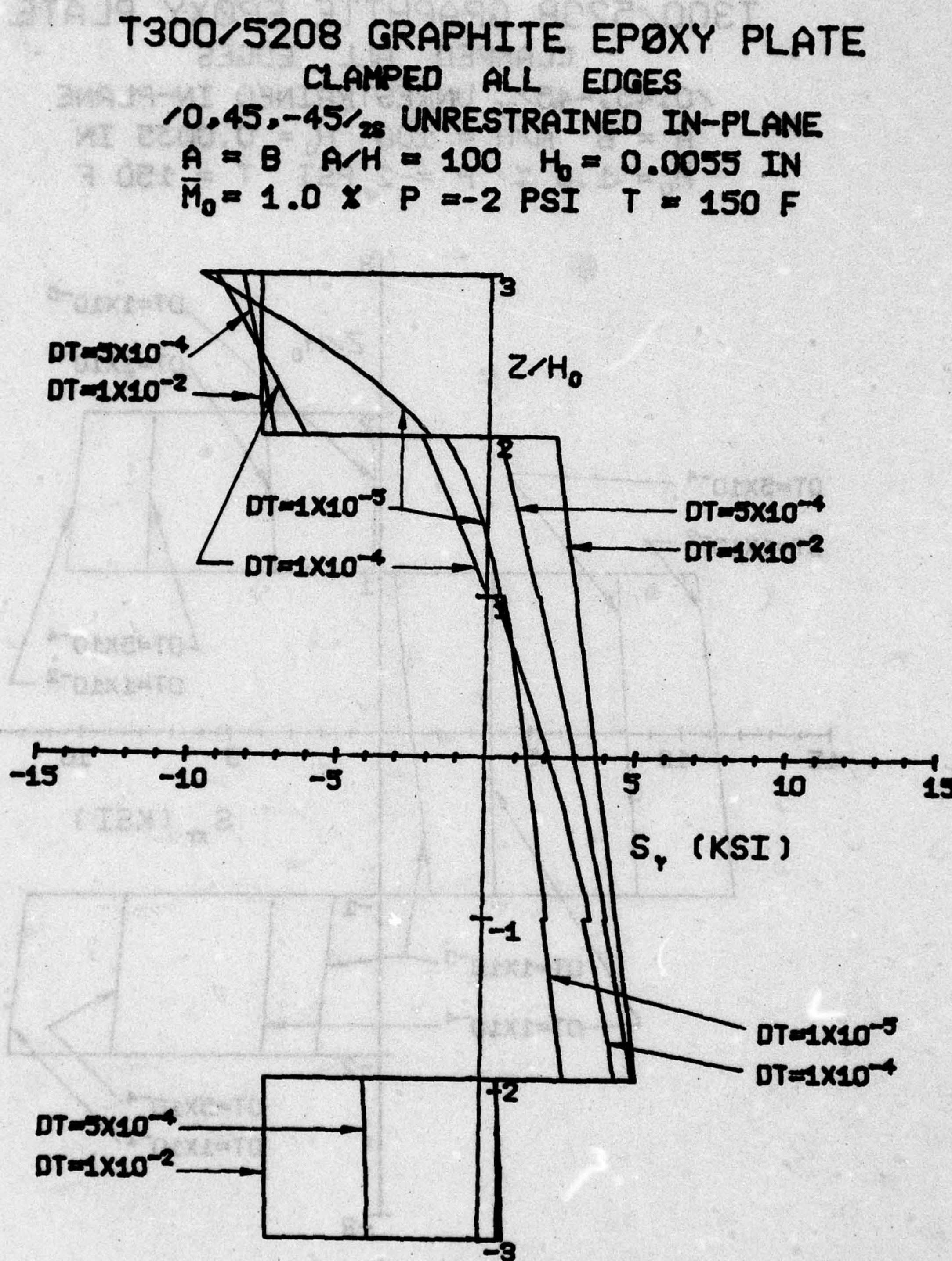
T300/5208 GRAPHITE EPØXY PLATE
CLAMPED ALL EDGES
/0,45,-45/2S UNRESTRAINED IN-PLANE
A = B A/H = 100 H0 = 0.0055 IN
M0 = 1.0 % P =-2 PSI T = 150 F
Z/H0
SY (KSI)
DT=5X10-4
DT=1X10-2
DT=1X10-5
DT=1X10-4
-15
-10
-5
5
10
15
3
2
1
-1
-2
-3

Figure 4.8

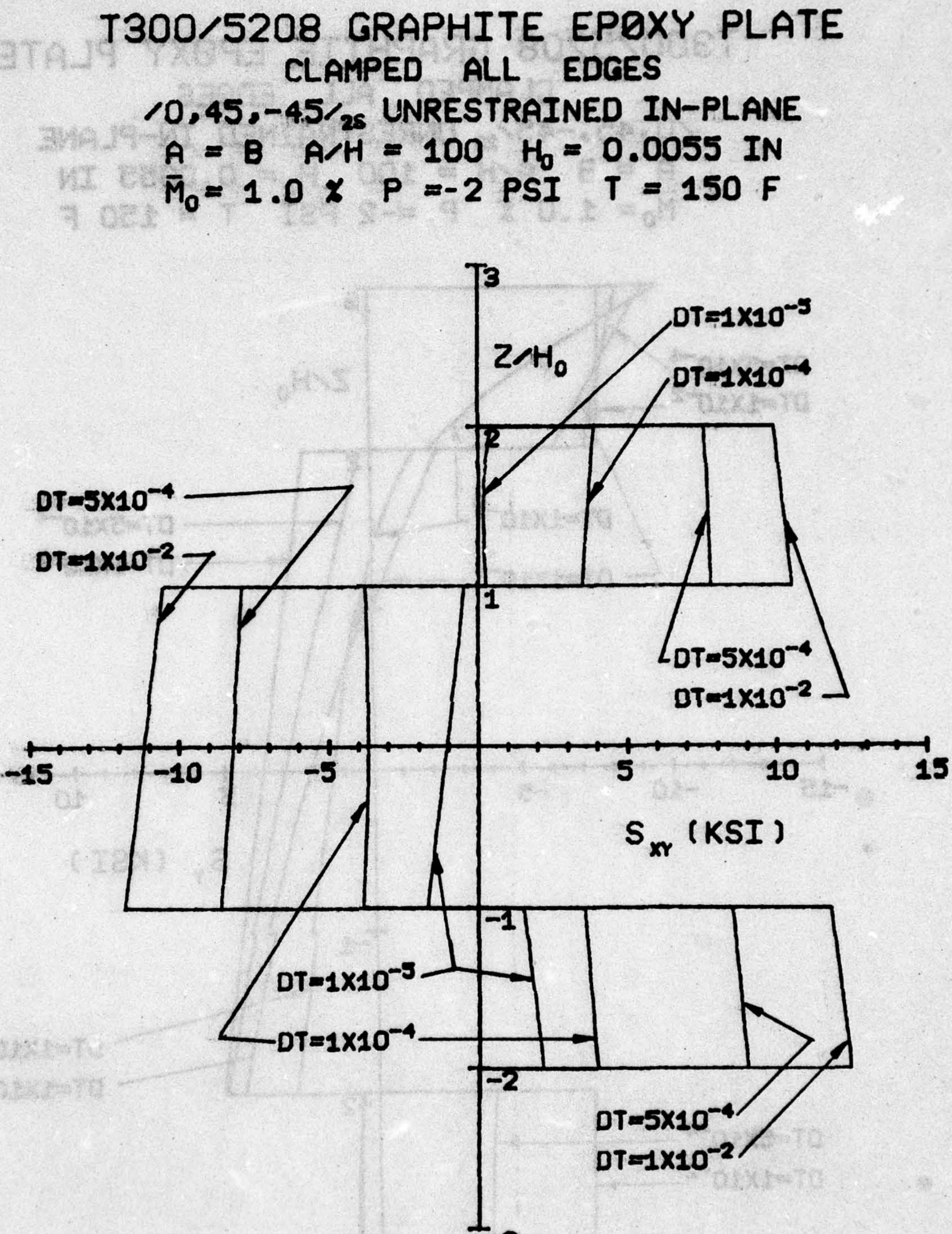
T300/5208 GRAPHITE EPØXY PLATE
CLAMPED ALL EDGES
/0,45,-45/2S UNRESTRAINED IN-PLANE
A = B A/H = 100 H0 = 0.0055 IN
M0 = 1.0 % P =-2 PSI T = 150 F
Z/H0
S XY (KSI)
DT=1X10^-5
DT=1X10^-4
DT=5X10^-4
DT=1X10^-2
3
2
1
-1
-2
-3
-15
-10
-5
5
10
15

Figure 4.9

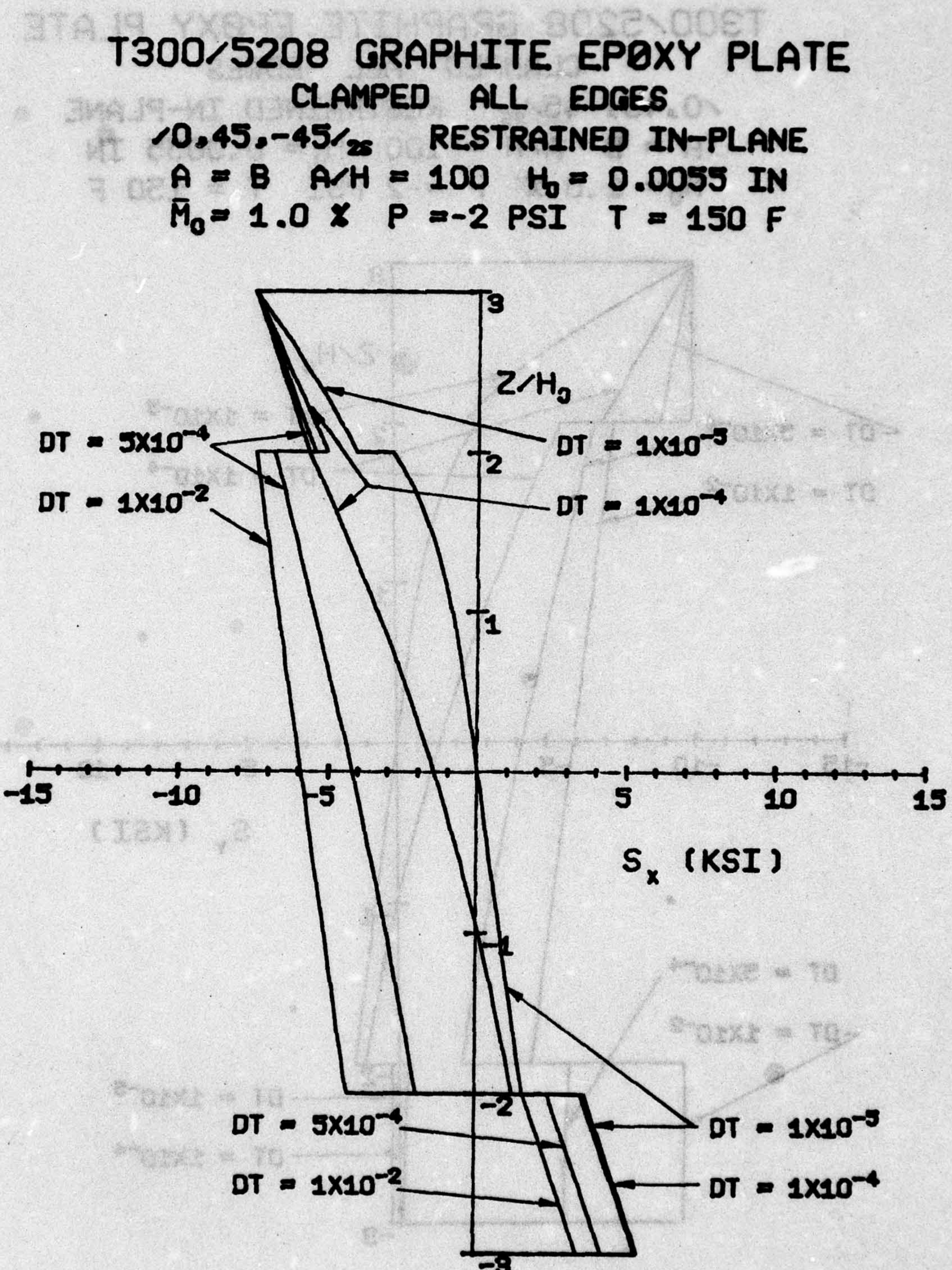
T300/5208 GRAPHITE EPØXY PLATE
CLAMPED ALL EDGES
/0,45,-45/2S RESTRAINED IN-PLANE
A = B A/H = 100 H0 = 0.0055 IN
M0 = 1.0 % P =-2 PSI T = 150 F
Z/H0
DT = 5X10^-4
DT = 1X10^-2
DT = 1X10^-5
DT = 1X10^-4
-15
-10
-5
5
10
15
3
2
1
-1
-2
-3
SX (KSI)

Figure 4.10

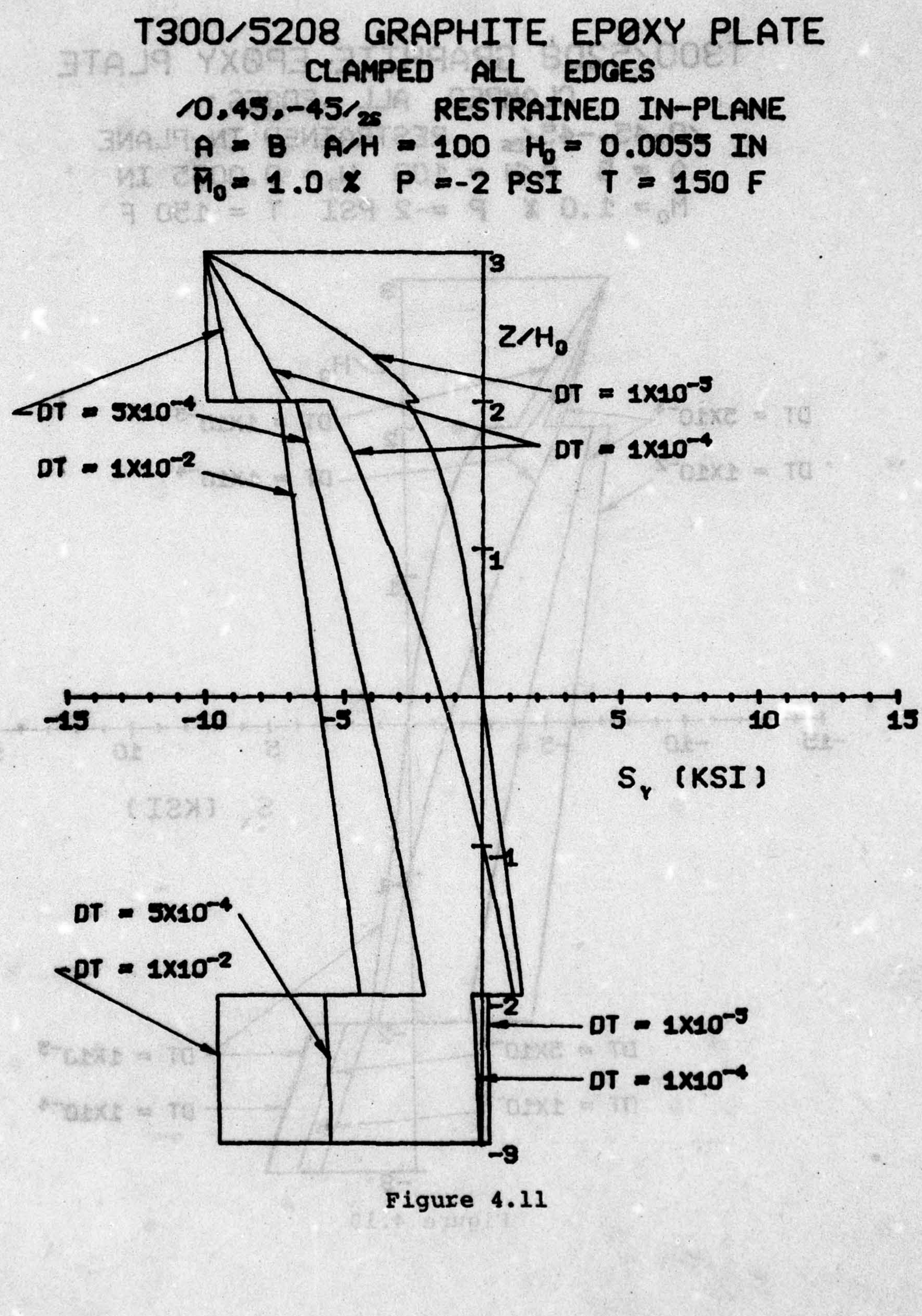

T300/5208 GRAPHITE EPØXY PLATE
CLAMPED ALL EDGES
/0,45,-45/2S RESTRAINED IN-PLANE
A = B A/H = 100 H0 = 0.0055 IN
M0 = 1.0 % P =-2 PSI T = 150 F
Z/H0
DT = 1X10^-5
DT = 5X10^-4
DT = 1X10^-4
DT = 1X10^-2
3
2
1
-1
-2
-3
-15
-10
-5
5
10
15
SY (KSI)
DT = 5X10^-4
DT = 1X10^-2
DT = 1X10^-5
DT = 1X10^-4

Figure 4.11

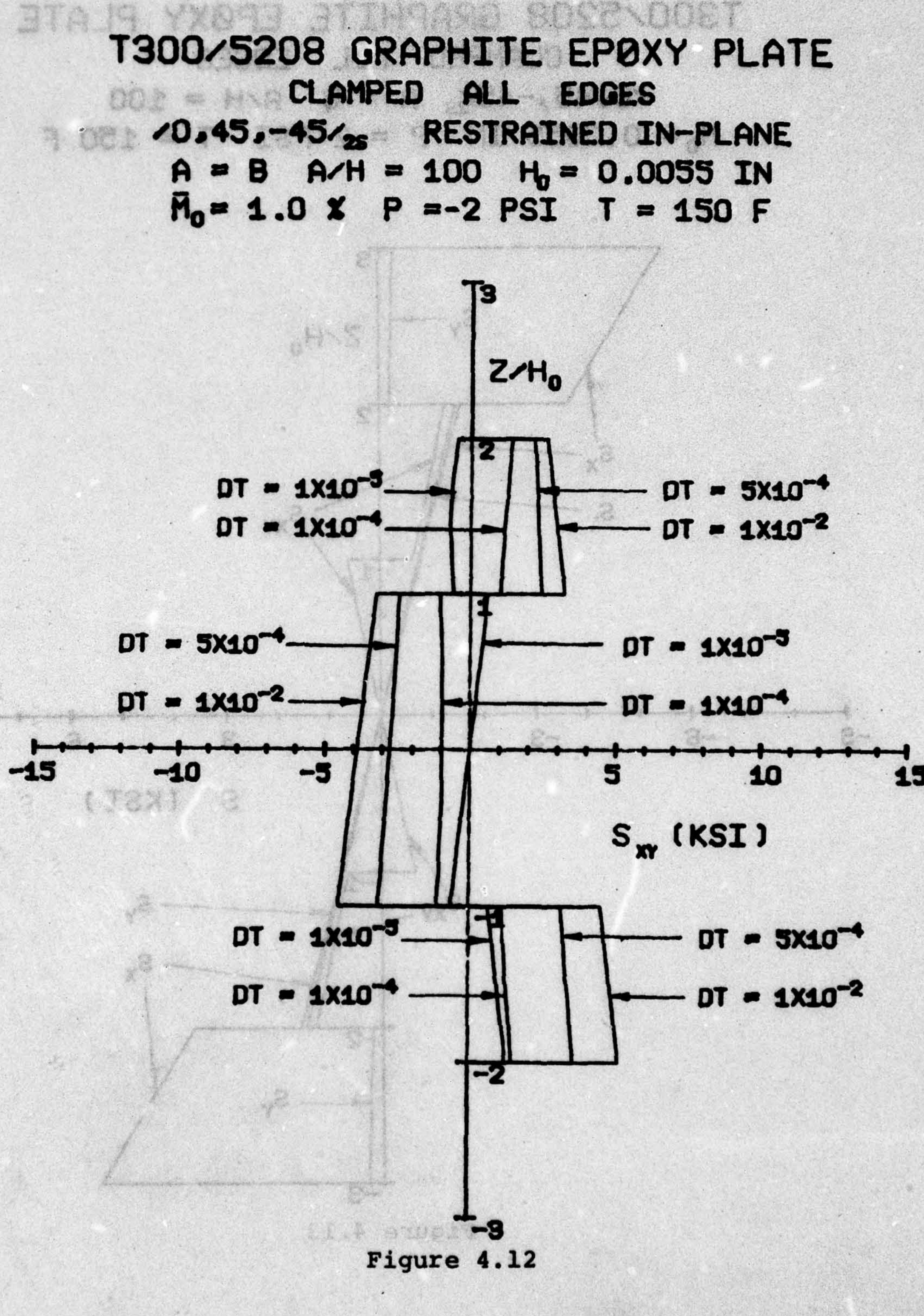

T300/5208 GRAPHITE EPØXY PLATE
CLAMPED ALL EDGES
/0,45,-45/2S RESTRAINED IN-PLANE
A = B A/H = 100 H0 = 0.0055 IN
M0 = 1.0 % P =-2 PSI T = 150 F
Z/H0
DT = 1X10-5
DT = 1X10-4
DT = 5X10-4
DT = 1X10-2
S XY (KSI)

Figure 4.12

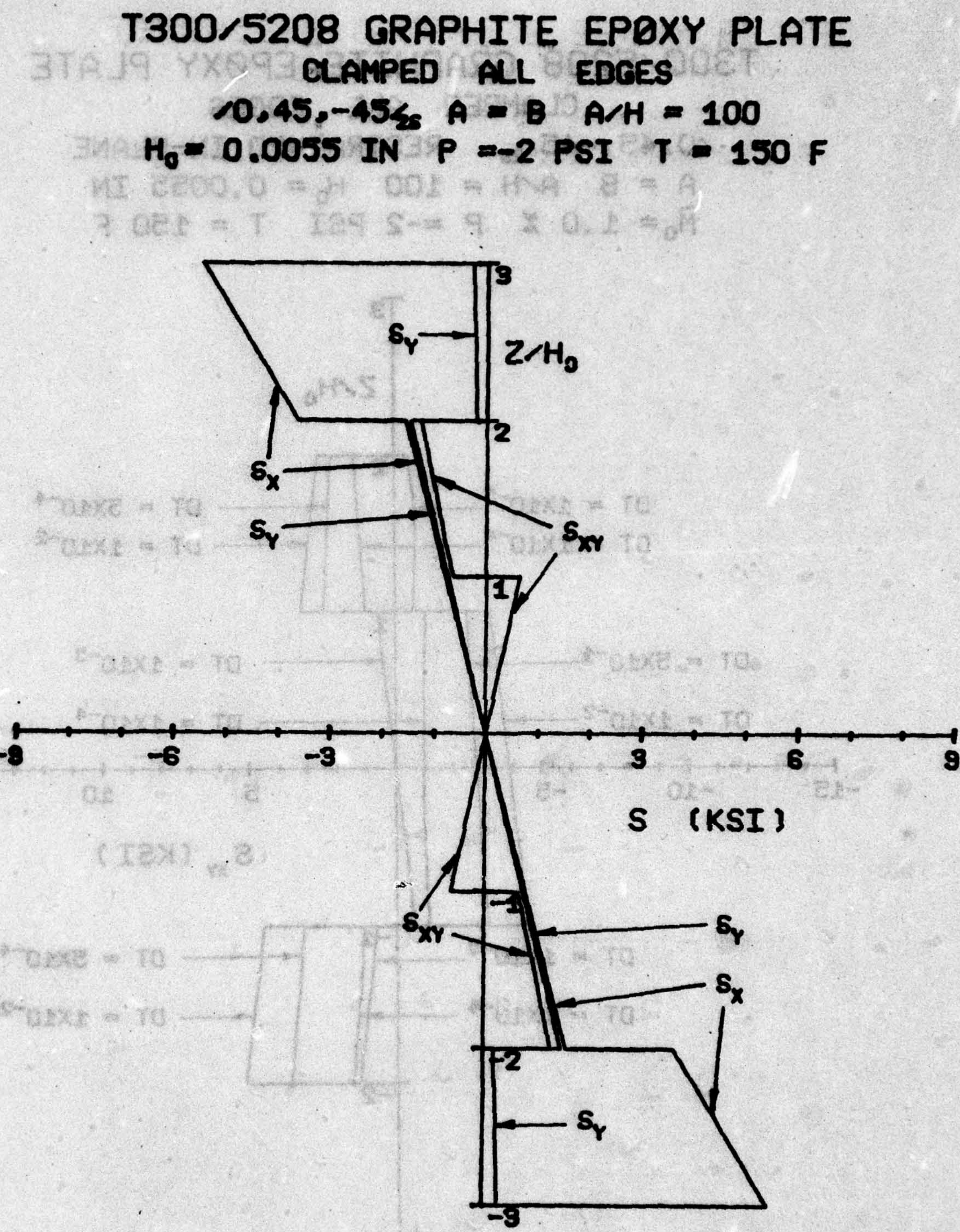
T300/5208 GRAPHITE EPØXY PLATE
CLAMPED ALL EDGES
/0,45,-45/2S A = B A/H = 100
H_0 = 0.0055 IN P =-2 PSI T = 150 F
3
2
1
-1
-2
-3
Z/H_0
S_Y
S_X
S_{XY}
-9
-6
-3
3
6
9
S (KSI)

Figure 4.13

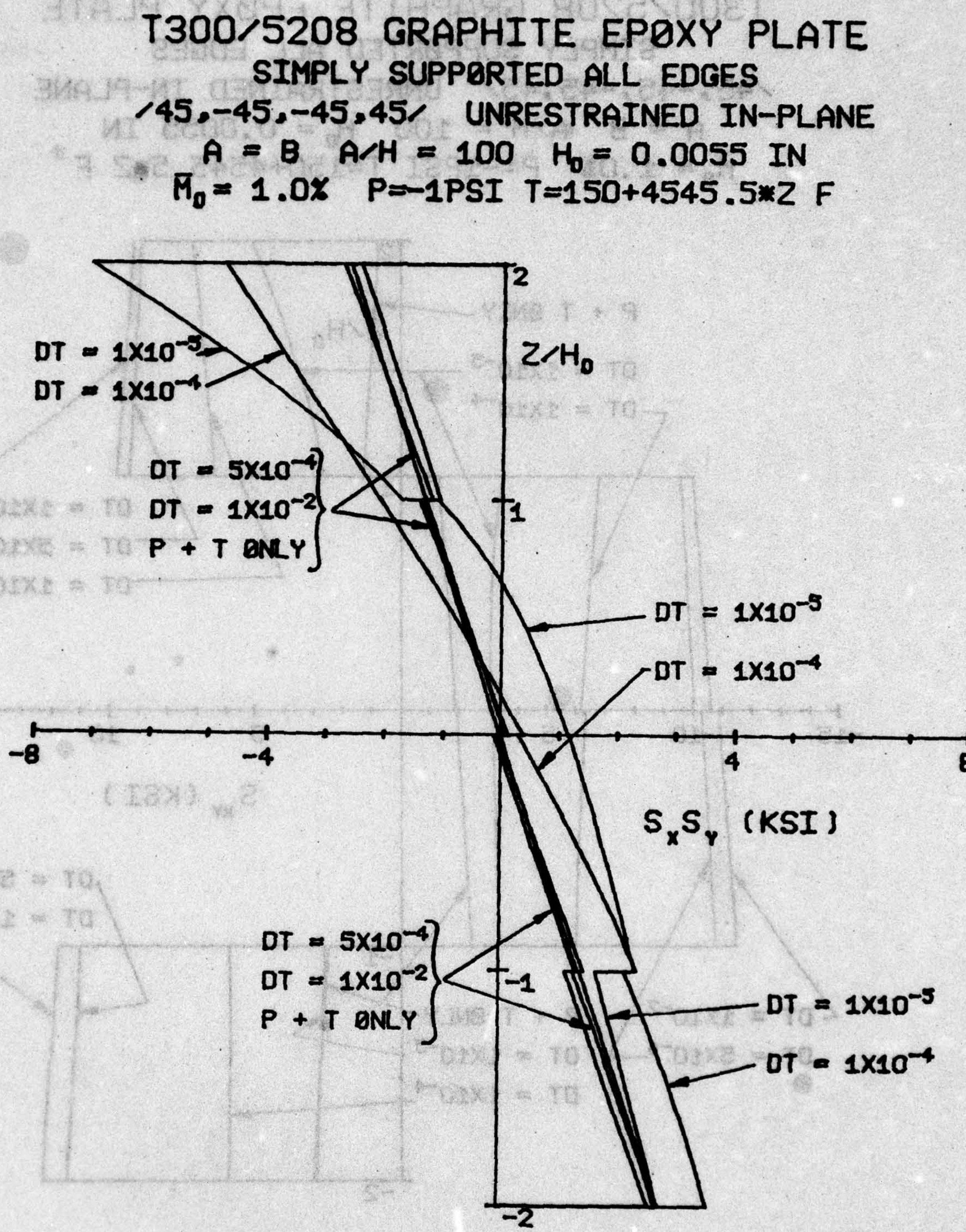
T300/5208 GRAPHITE EPØXY PLATE
SIMPLY SUPPØRTED ALL EDGES
/45,-45,-45,45/ UNRESTRAINED IN-PLANE
A = B A/H = 100 H0 = 0.0055 IN
M0 = 1.0% P=-1PSI T=150+4545.5*Z F
DT = 1X10-5
DT = 1X10-4
DT = 5X10-4
DT = 1X10-2
P + T ØNLY
Z/H0
2
1
-1
-2
-8
-4
4
8
SxSy (KSI)
DT = 1X10-5
DT = 1X10-4
DT = 5X10-4
DT = 1X10-2
P + T ØNLY
DT = 1X10-5
DT = 1X10-4

Figure 4.14

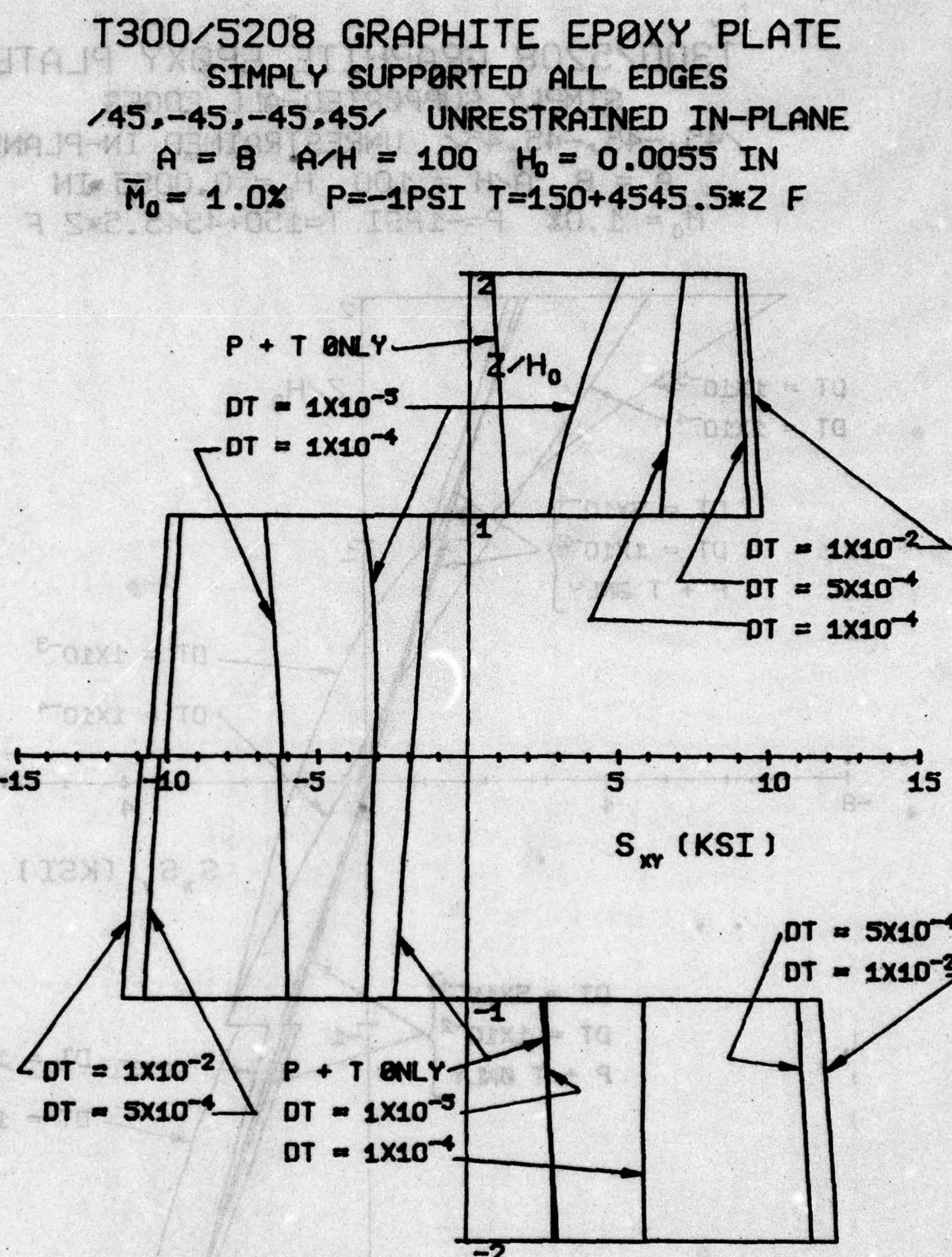
T300/5208 GRAPHITE EPØXY PLATE
SIMPLY SUPPØRTED ALL EDGES
/45,-45,-45,45/ UNRESTRAINED IN-PLANE
A = B A/H = 100 H_0 = 0.0055 IN
$\bar{M}_0$ = 1.0% P=-1PSI T=150+4545.5*Z F
P + T ØNLY
Z/H_0
DT = 1X10^{-5}
DT = 1X10^{-4}
DT = 1X10^{-2}
DT = 5X10^{-4}
DT = 1X10^{-4}
-15
-10
-5
5
10
15
S_{XY} (KSI)
DT = 5X10^{-4}
DT = 1X10^{-2}
DT = 1X10^{-2}
DT = 5X10^{-4}
P + T ØNLY
DT = 1X10^{-5}
DT = 1X10^{-4}
2
1
-1
-2

Figure 4.15

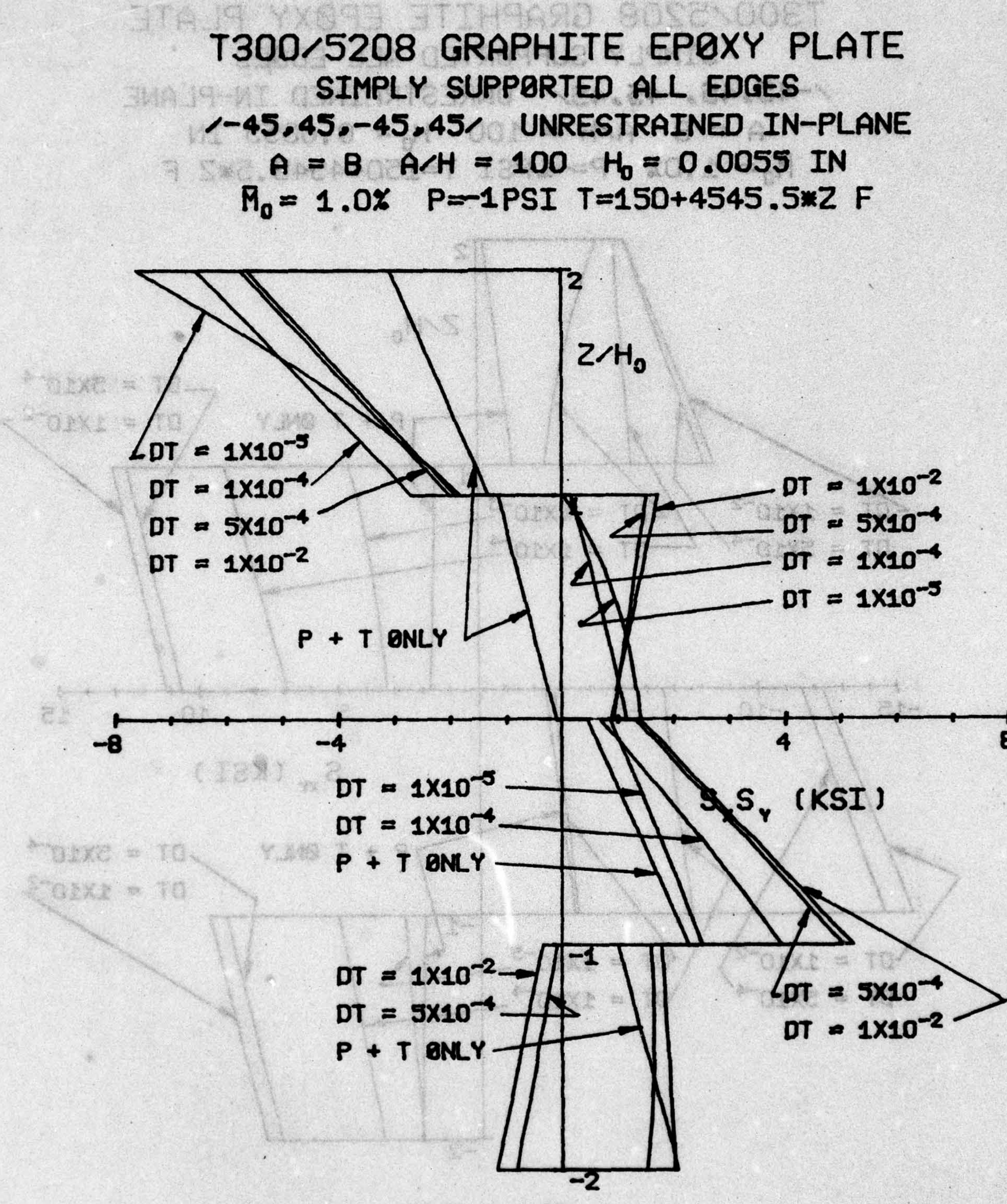
T300/5208 GRAPHITE EPØXY PLATE
SIMPLY SUPPØRTED ALL EDGES
/-45,45,-45,45/ UNRESTRAINED IN-PLANE
A = B A/H = 100 H_0 = 0.0055 IN
$\bar{W}_0$ = 1.0% P=-1PSI T=150+4545.5*Z F
2
Z/H_0
DT = 1X10^{-5}
DT = 1X10^{-4}
DT = 5X10^{-4}
DT = 1X10^{-2}
P + T ØNLY
DT = 1X10^{-2}
DT = 5X10^{-4}
DT = 1X10^{-4}
DT = 1X10^{-5}
1
-8
-4
4
8
S_x,S_y (KSI)
DT = 1X10^{-5}
DT = 1X10^{-4}
P + T ØNLY
DT = 1X10^{-2}
DT = 5X10^{-4}
P + T ØNLY
-1
DT = 5X10^{-4}
DT = 1X10^{-2}
-2

Figure 4.16

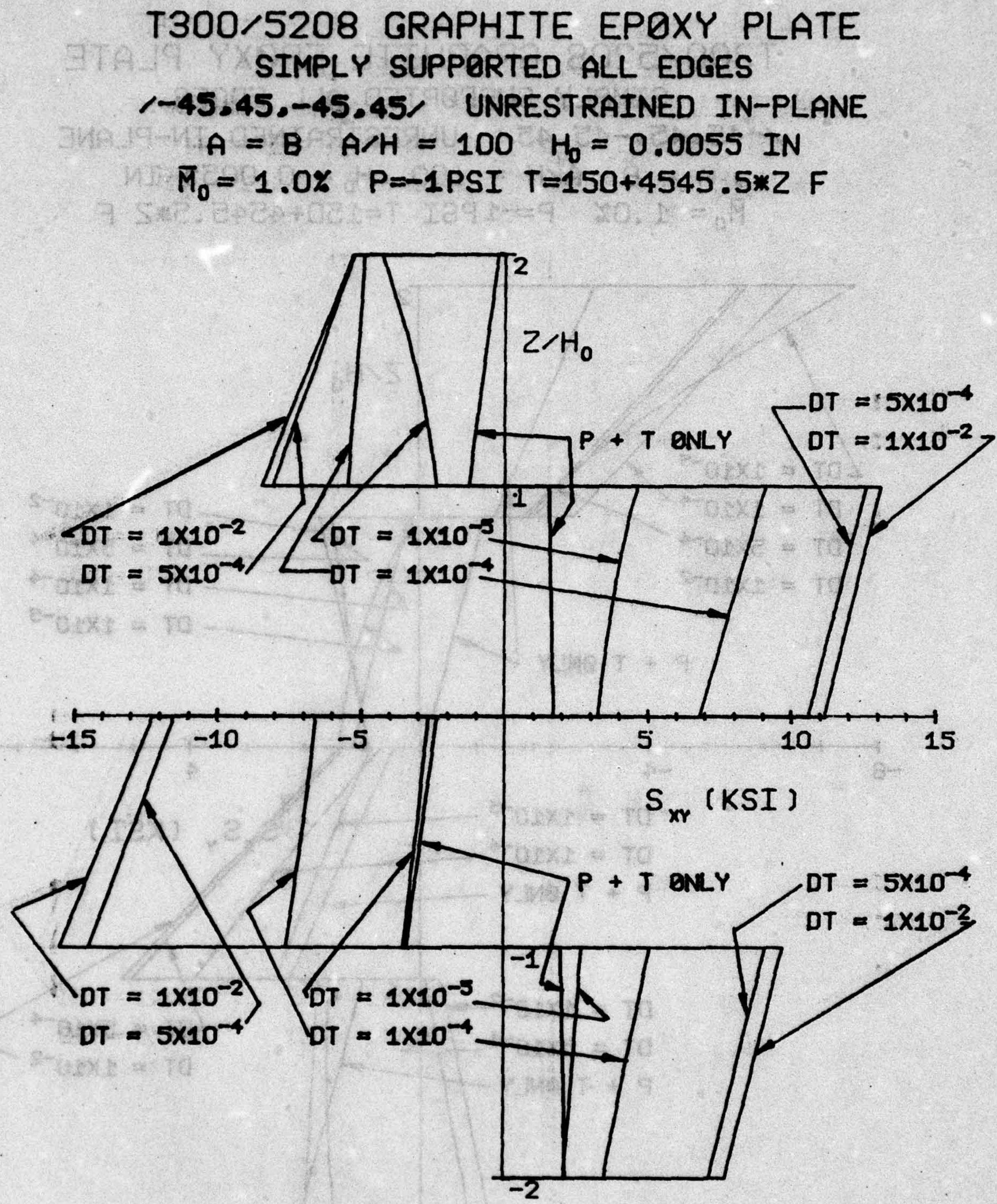
T300/5208 GRAPHITE EPØXY PLATE
SIMPLY SUPPØRTED ALL EDGES
/-45.45.-45.45/ UNRESTRAINED IN-PLANE
A = B A/H = 100 H_0 = 0.0055 IN
$\bar{M}_0$ = 1.0% P=-1PSI T=150+4545.5*Z F
2
Z/H_0
P + T ØNLY
DT = 5X10^{-4}
DT = 1X10^{-2}
1
DT = 1X10^{-2}
DT = 5X10^{-4}
DT = 1X10^{-5}
DT = 1X10^{-4}
-15
-10
-5
5
10
15
S_{XY} (KSI)
P + T ØNLY
DT = 5X10^{-4}
DT = 1X10^{-2}
-1
DT = 1X10^{-2}
DT = 5X10^{-4}
DT = 1X10^{-5}
DT = 1X10^{-4}
-2

Figure 4.17

T300/5208 GRAPHITE EPØXY PLATE
SIMPLY SUPPØRTED ALL EDGES
/0,90,90,0/ UNRESTRAINED IN-PLANE
A = B A/H = 100 H_0 = 0.0055 IN
$\bar{M}_0$ = 1.0% P=-1PSI T=150+4545.5*Z F

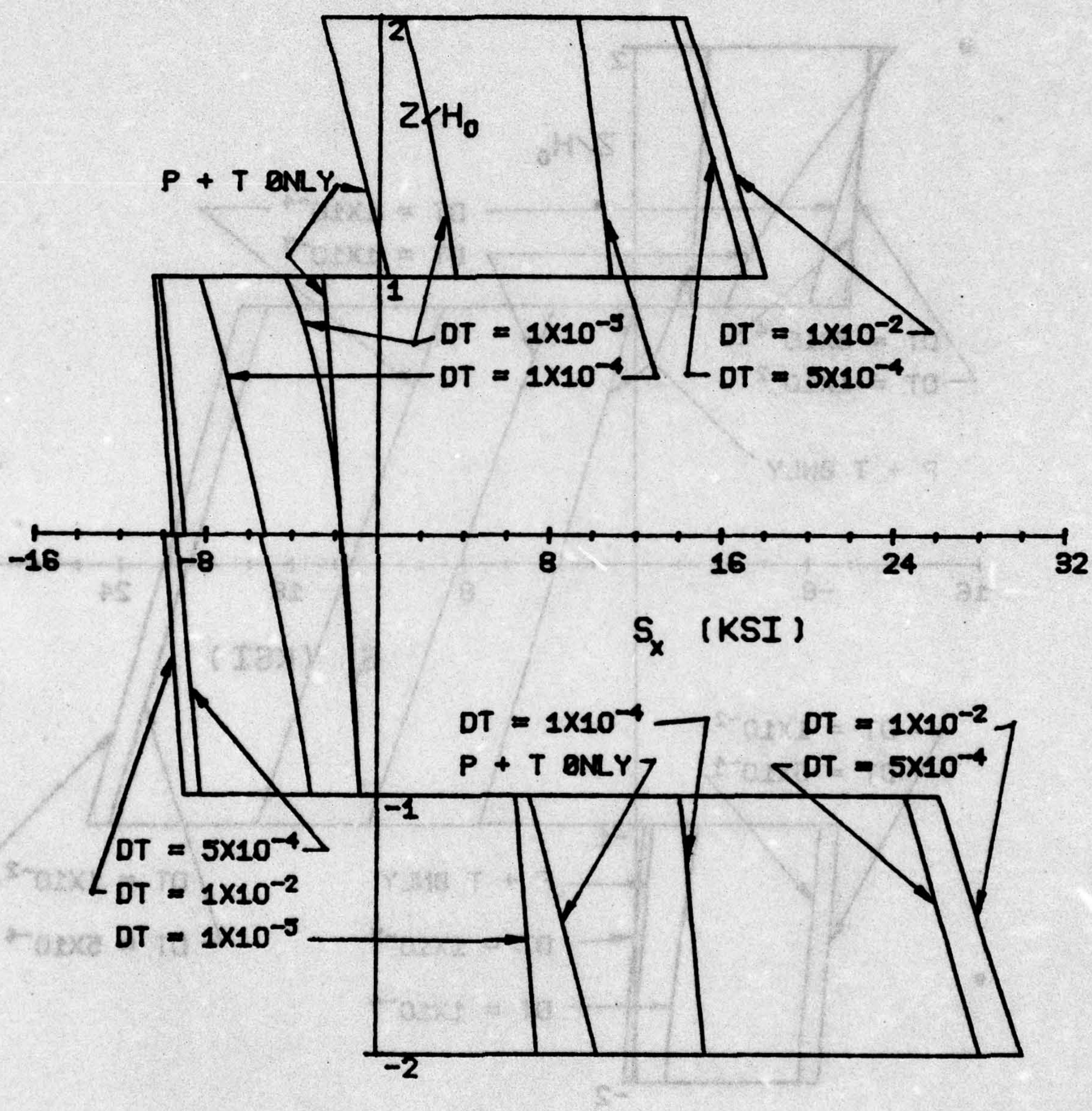

Figure 4.18

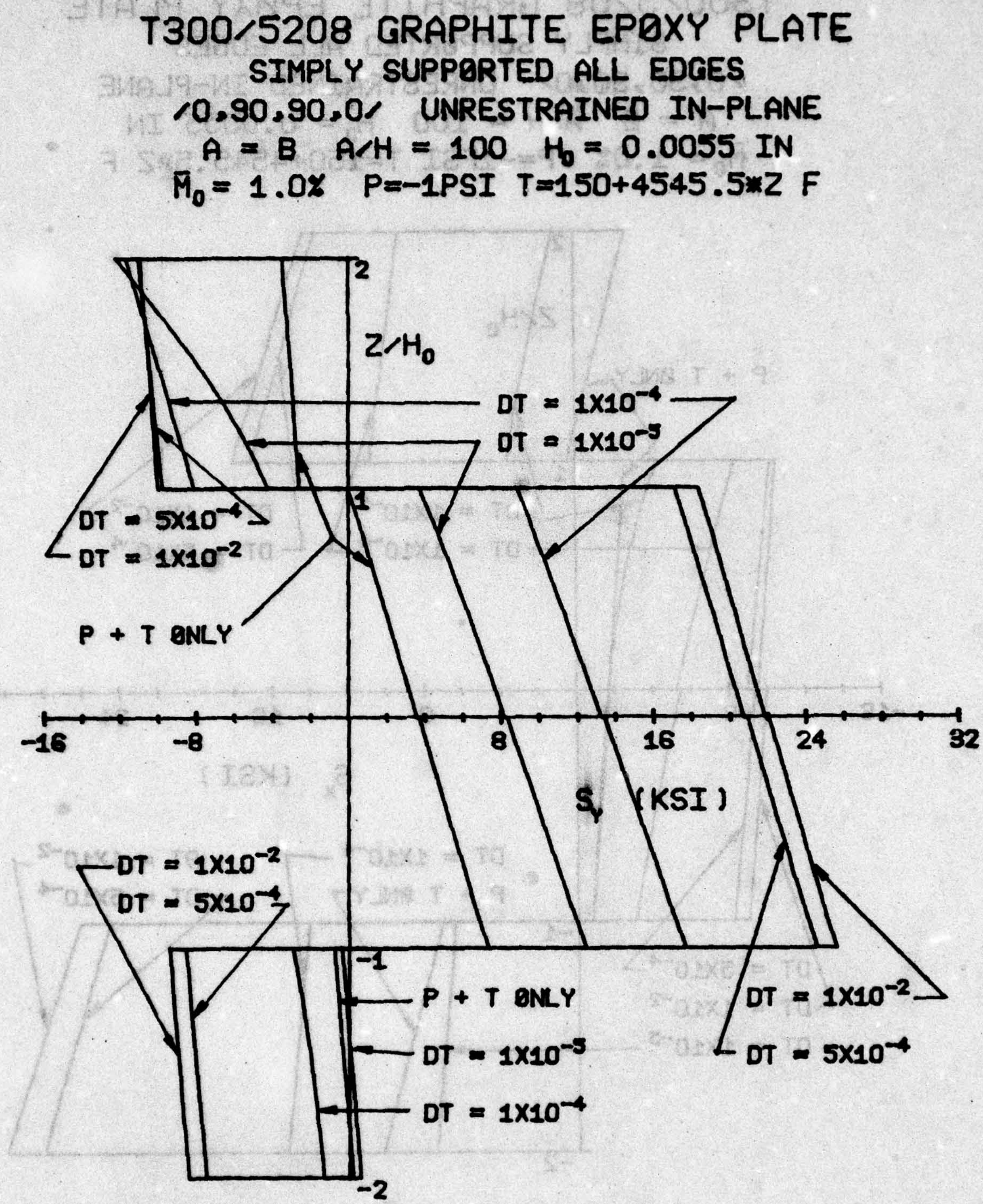
T300/5208 GRAPHITE EPØXY PLATE
SIMPLY SUPPØRTED ALL EDGES
/0,90,90,0/ UNRESTRAINED IN-PLANE
A = B A/H = 100 H0 = 0.0055 IN
M0 = 1.0% P=-1PSI T=150+4545.5*Z F
2
Z/H0
DT = 1X10-4
DT = 1X10-5
1
DT = 5X10-4
DT = 1X10-2
P + T ØNLY
-16
-8
8
16
24
32
Sy (KSI)
DT = 1X10-2
DT = 5X10-4
-1
P + T ØNLY
DT = 1X10-5
DT = 1X10-4
DT = 1X10-2
DT = 5X10-4
-2

Figure 4.19

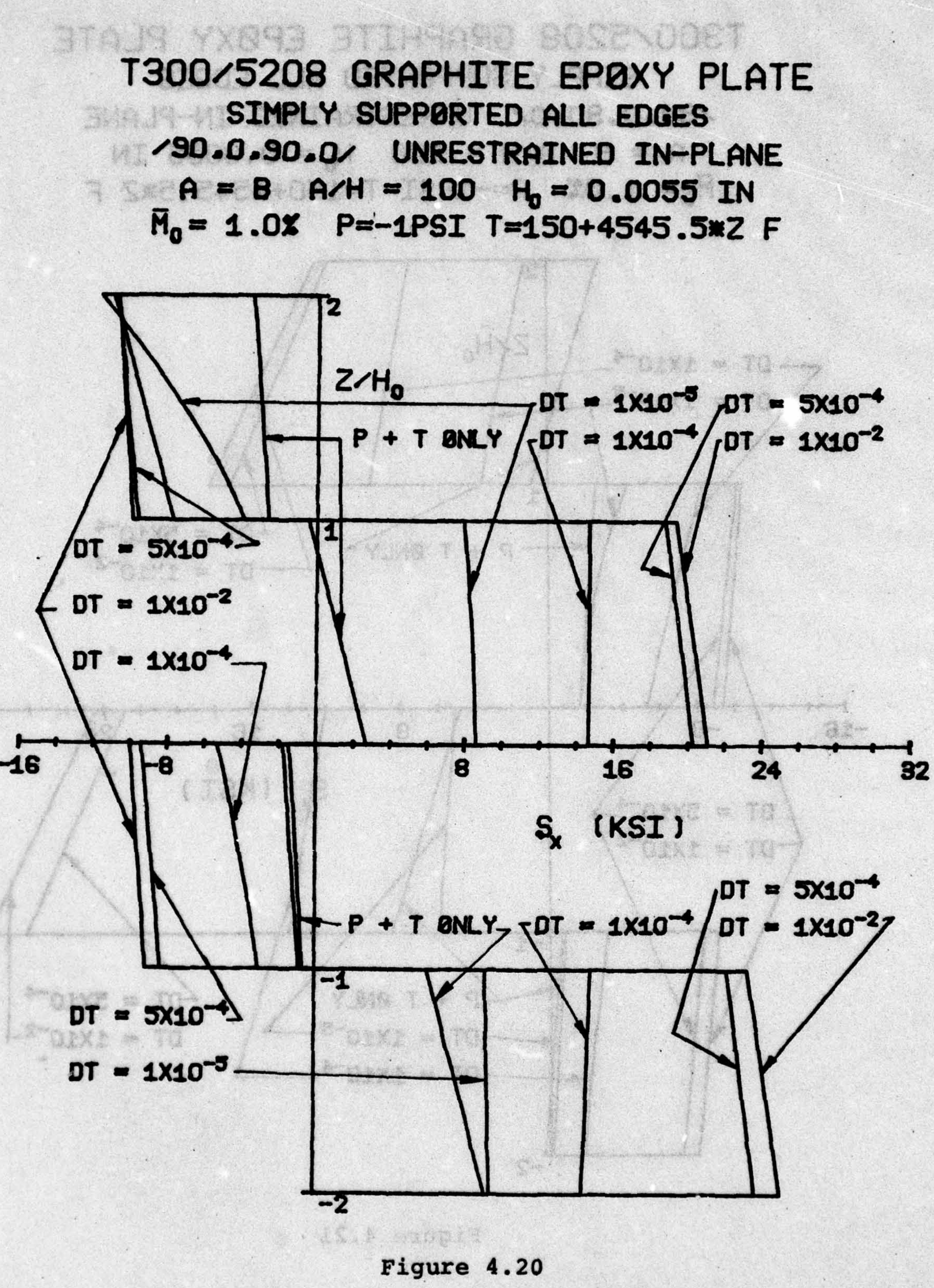
T300/5208 GRAPHITE EPØXY PLATE
SIMPLY SUPPØRTED ALL EDGES
/90.0.90.0/ UNRESTRAINED IN-PLANE
A = B A/H = 100 H0 = 0.0055 IN
M0 = 1.0% P=-1PSI T=150+4545.5*Z F
Z/H0
DT = 1X10-5
DT = 5X10-4
P + T ØNLY
DT = 1X10-4
DT = 1X10-2
DT = 5X10-4
DT = 1X10-2
DT = 1X10-4
2
1
-1
-2
-16
-8
8
16
24
32
Sx (KSI)
DT = 5X10-4
P + T ØNLY
DT = 1X10-4
DT = 1X10-2
DT = 5X10-4
DT = 1X10-5

Figure 4.20

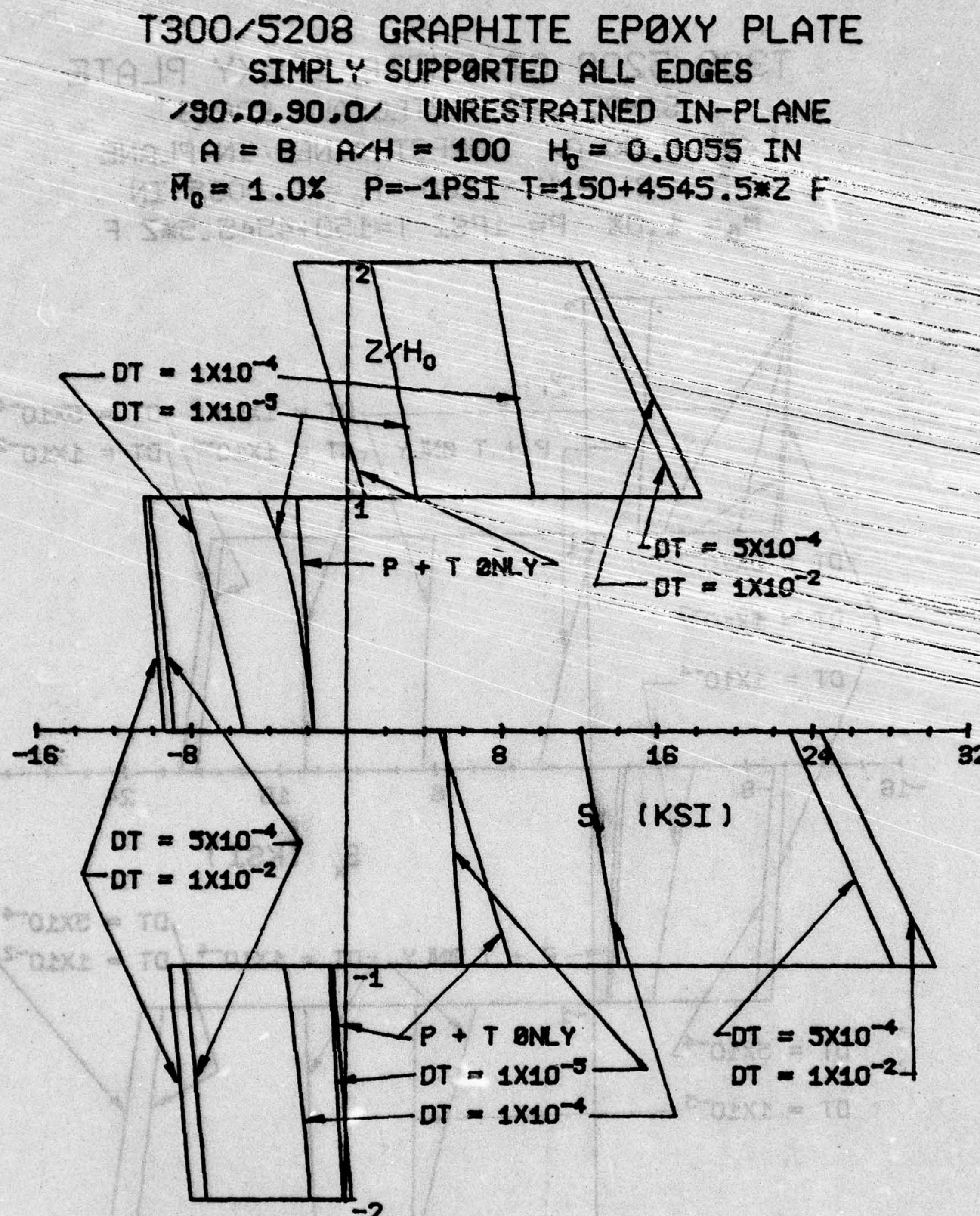
T300/5208 GRAPHITE EPØXY PLATE
SIMPLY SUPPØRTED ALL EDGES
/90,0,90,0/ UNRESTRAINED IN-PLANE
A = B A/H = 100 H0 = 0.0055 IN
M0 = 1.0% P=-1PSI T=150+4545.5*Z F
Z/H0
DT = 1X10-4
DT = 1X10-5
P + T ØNLY
DT = 5X10-4
DT = 1X10-2
-16
-8
8
16
24
32
SY (KSI)
2
1
-1
-2

Figure 4.21

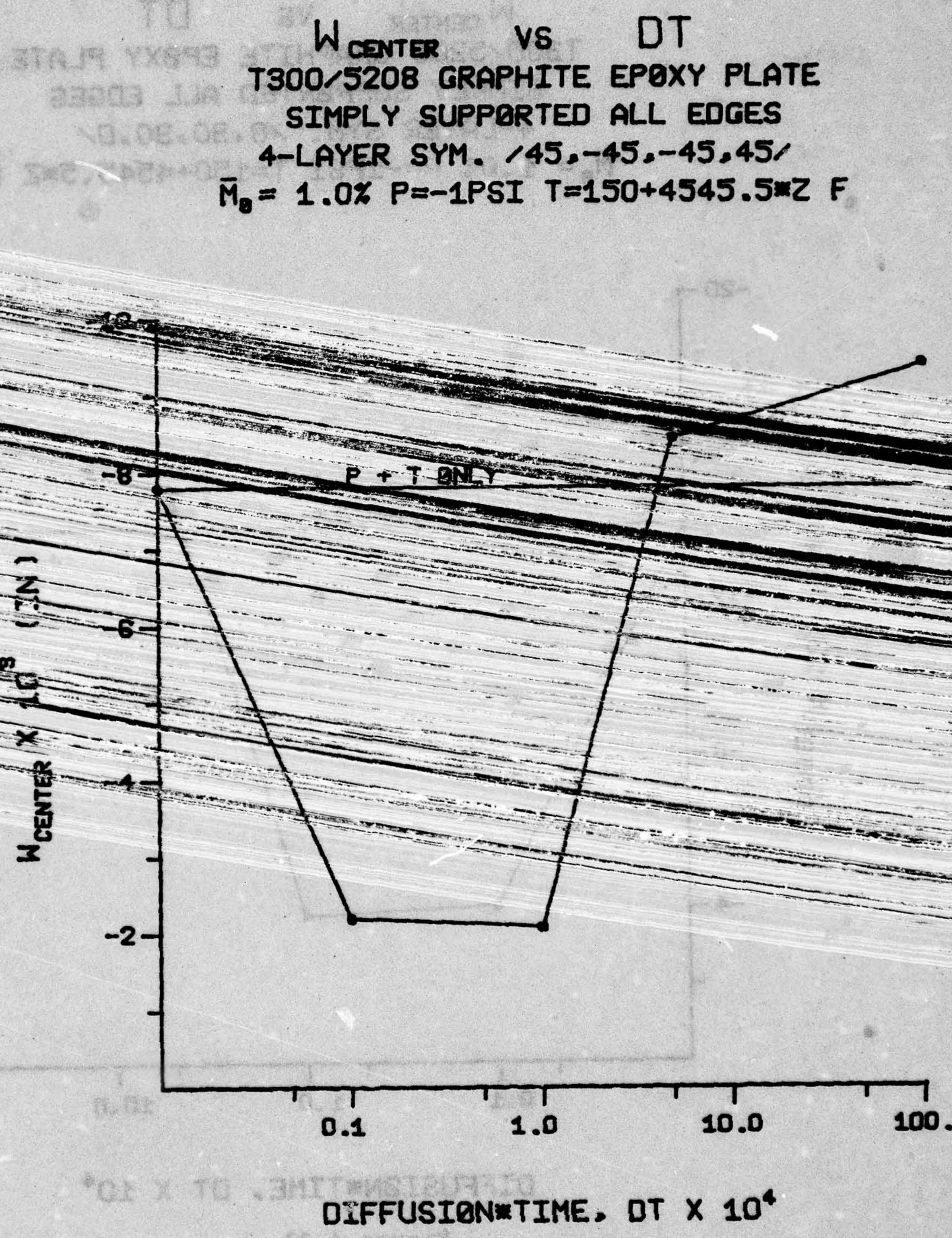

W CENTER VS DT
T300/5208 GRAPHITE EPØXY PLATE
SIMPLY SUPPØRTED ALL EDGES
4-LAYER SYM. /45,-45,-45,45/
$\bar{M}_0$= 1.0% P=-1PSI T=150+4545.5*Z F
-10
-8
-6
-4
-2
P + T ØNLY
W_{CENTER} X 10^3 (IN)
0.1
1.0
10.0
100.0
DIFFUSIØN*TIME, DT X 10^4

Figure 4.22

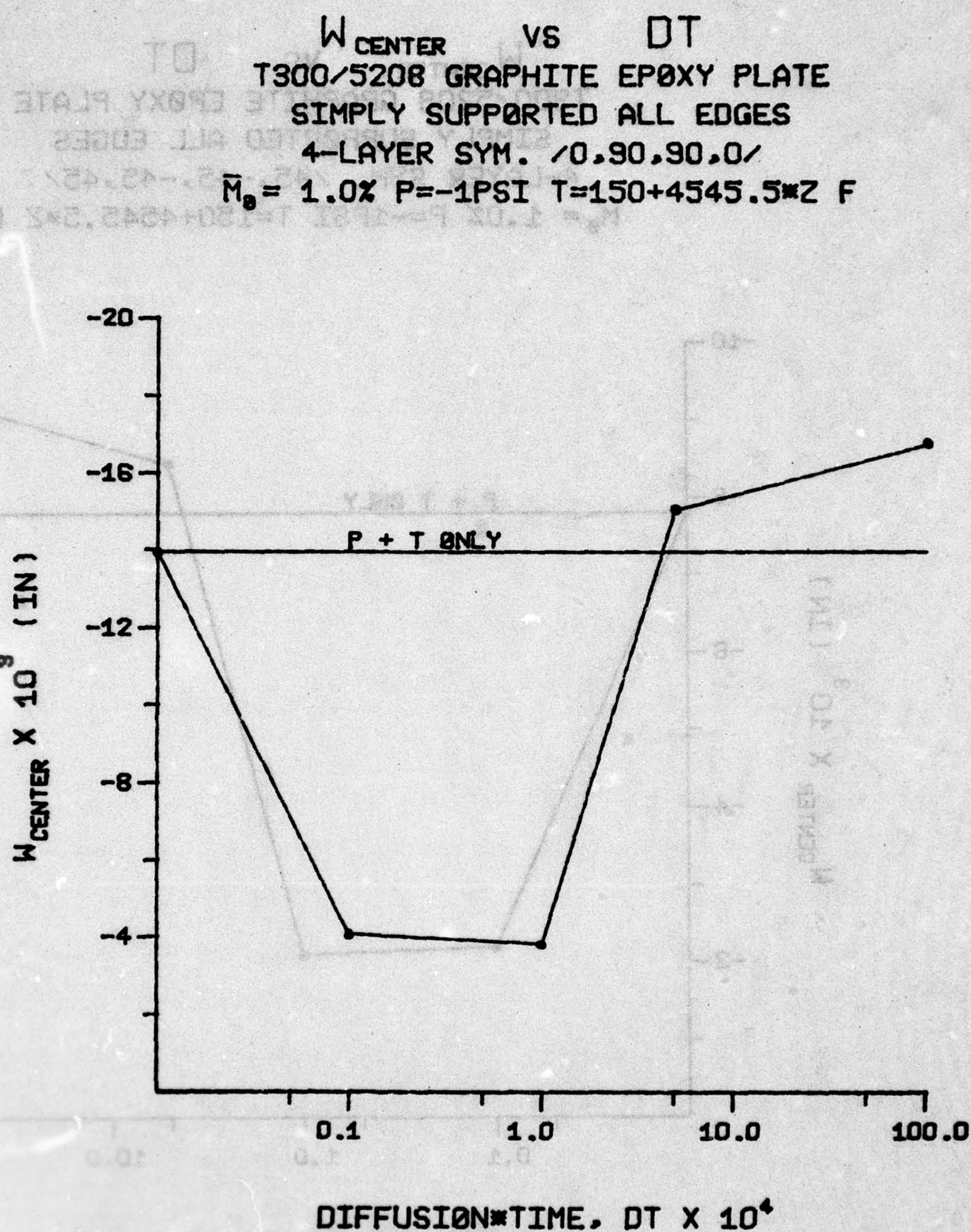

W CENTER VS DT
T300/5208 GRAPHITE EPØXY PLATE
SIMPLY SUPPØRTED ALL EDGES
4-LAYER SYM. /0,90,90,0/
M̄ₒ = 1.0% P=-1PSI T=150+4545.5*Z F
-20
-16
-12
-8
-4
P + T ØNLY
W CENTER X 10^3 (IN)
0.1
1.0
10.0
100.0
DIFFUSIØN*TIME, DT X 10^4

Figure 4.23

CHAPTER FIVE

DISCUSSION OF RESULTS

The results of the numerical examples outlined in Chapter Four will be discussed. The several points of interest will be described in the following two sections under the importance of TNS and the importance of hygrothermal loads in structural analysis.

Importance of TNS

From Figures 4.1 and 4.3 it is evident the effect of both TSD and TSD+TNS on the center deflection, as a function the A/B ratio, is small. In studying these figures, it is important to note that the A/H ratio is held constant at 100. Consequently, only B is varied to obtain various A/B ratios. If the center deflection were non-dimensionalized by dividing by B, the more traditional deflection curve with a peak at A/B = 1, would be obtained. It should also be noted that the deflections of the 4-layer unsymmetric laminate are greater than those of the symmetric laminate, as one would anticipate [11, 12, 13].

The effect on deflection of the width-to-thickness

ratio, A/H, is also small when comparing the three theories for A/H's greater than 100. For A/H ratio's less the 100, Tables 4.2, 4.4 and 4.6 show a slight decrease in the center deflection when including TSD compared to LPT.

The percent decrease in the deflection using TSD as compared to LPT for the three example plates is tabulated below for various A/H ratios.

A/H	% Decrease in W_{CENTER}		
	4-Layer Symmetric	4-Layer Unsymmetric	24-Layer Symmetric
5	3%	3.8%	3%
25	.2	.2	.3
100	0	0	0

It is interesting to note that contrary to what might be expected from previous efforts with uniform lateral loads [5], the magnitude of the plate deflections decrease when including TSD over LPT. The reason for the decrease is the type of loading. For hygrothermal loadings, the dilatational expansions are satisfied by plate curvatures and consequently deflections. However as greatly exaggerated in the following sketches, by including TSD, part of the expansions are accommodated by shear deformations. This reduces the required curvature change and thus deflections, necessary to satisfy

the expansions.

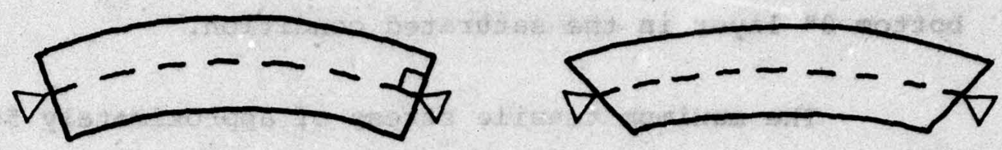

The effect of the TSD+TNS theory appears to be negligible. The slight decrease in the plate deflections for the unsymmetric laminate using the TSD+TNS are less than one percent, and not considered significant.

In comparing the results for the 4 and 24 layer laminates, the effect of laminate thickness is also negligible for the three plate theories.

<u>Importance of Hygrothermal Loads</u>

The stress plots shown in Figures 4.7 through 4.9 are for the 6-layer, /0, 45, -45/2s laminate with clamped boundary conditions. These plots illustrate the stresses generated by pressure acting down on top the plate along with a sudden moisture concentration increase on the top surface.

In examining Figures 4.7 and 4.8, the Sx and Sy on the top, $\theta = 0°$, layer are compressive as expected. The maximum Sx compressive stress of approximately 9 ksi

occurs in the fully saturated condition, while the maximum Sy stress of 10 ksi occurs at early times. Also of interest is the development of compressive stresses in the bottom 0° layer in the saturated condition.

The maximum tensile stress of approximately 5 ksi occurs at late times in the bottom, $\theta = +45°$, layer.

The shear stress, Sxy, increases with increased moisture concentration. The maximum shear stress is approximately 12.5 ksi with large shear stress gradients between the $\pm$ 45° layers. These large stress gradients imply high interlaminar shear stresses as noted in [1].

As a comparison of the hygrothermal environment effects, Figure 4.13 shows the Sx, Sy and Sxy stress distributions for the same plate with all loads except moisture. Note however that the scale for these curves has been expanded when making comparisons. The most obvious differences from Figure 4.13 are the increased Sy stress in the 0° layers and the large increase in Sxy stresses for the results with hygrothermal effects included in the analysis.

Figures 4.10 through 4.12 show the stress distributions for the identical problem as before but with in-plane expansions restrained. The following observations can be made in comparing these curves to those of the previous example.

1. The Sx and Sy stresses in the 45° layers have shifted negative with the maximum compressive stresses occurring at the fully saturated time.

2. The Sx and Sy stresses have not changed in the 0° layers.

3. The Sxy shear stresses have markedly decreased in the middle layers with a maximum stress of only 5 ksi.

The general shift to compressive stresses for Sx and Sy in the middle layers is expected for dilatational in-plane restraints. However, the maximum compressive stress is only slightly higher than before at 7 ksi.

The interesting decrease in shear stresses, to less than half those for the unrestrained case shown in Figure 4.9, is significant. This would indicate an advantage to designing with in-plane restraints to lower the Sxy stresses without materially increasing Sx and Sy . By performing a buckling analysis, such as presented by Flaggs [6], to insure plate stability, the designer could reduce the shear stresses and shear stress gradients by providing in-plane restraints. This would also reduce the possibility of delamination caused by the interlaminar shear stresses.

Table 5.1 illustrates the importance of the hygrothermal loads for these two examples. In this table the max-

TABLE 5.1

COMPARISON OF MAXIMUM STRESSES

WITH AND WITHOUT MOISTURE LOADING

	COMPRESSION		TENSION	
	STRESS RATIO $\frac{S_{HYGRO}\text{(KSI)}}{S_{PRESS}\text{(KSI)}}$	LOCATION z/Ho	STRESS RATIO $\frac{S_{HYGRO}\text{(KSI)}}{S_{PRESS}\text{(KSI)}}$	LOCATION z/Ho
Sx Fig.4.7	$\frac{-8.6}{-5.5} = 1.56$	3.0 (0°Layer)	$\frac{4.4}{5.5} = 0.80$	-3.0 (0°Layer)
Sy Fig.4.8	$\frac{-9.2}{-0.3} = 30.6$	3.0 (0°Layer)	$\frac{5.2}{1.5} = 3.47$	-2.0 (45°Layer)
Sxy Fig.4.9	$\frac{-11.8}{.6} = 19.6$	-1.0 (-45°Layer)	$\frac{12.5}{1.3} = 9.6$	-2.0 (45°Layer)
Sx Fig.4.10	$\frac{-7.5}{-5.5} = 1.36$	3.0 (0°Layer)	$\frac{5.5}{5.5} = 1.0$	-3.0 (0°Layer)
Sy Fig.4.11	$\frac{-10.0}{-\ .3} = 33.3$	3.0 (0°Layer)	$\frac{1.5}{1.5} = 1.0$	-2.0 (45°Layer)
Sxy Fig.4.12	$\frac{-4.5}{-\ .6} = 7.5$	-1.0 (-45°Layer)	$\frac{5.2}{1.3} = 4.0$	-2.0 (45°Layer)

imum compressive and tensile stresses for the analysis including hygrothermal effects are compared to the corresponding maximum stress for the same laminate without hygrothermal loads.

As can be seen in Table 5.1 the Sy compressive stress maximums are grossly underpredicted if hygrothermal loads are not included in the analysis. Another area in which an analysis not including hygrothermal effects underestimates the stresses is in the middle lamina shear stresses, Sxy . Only for the Sx maximum tensile stress for the unrestrained laminate does the analysis not including moisture loading predict a higher stress.

Figures 4.14 through 4.17 show the stress distributions for a simply-supported, 4-layer, angle ply laminate subject to a lateral pressure, a linear temperature gradient, and a moisture gradient. Figure 4.14 and 4.15 represent the case of a symmetric layup pattern. Figures 4.16 and 4.17 are distributions for the unsymmetric layup pattern.

The Sx and Sy stress distributions for the angle ply, $\theta = \pm 45°$, laminates are identical and are therefore plotted together. Also note that for each figure the curve labeled "P+T Only" is the solution for the identical plate under all the same loadings except moisture.

Figure 4.14 for the symmetric plate shows the maximum Sx and Sy stresses occur at initial moisture introduction to the top surface. These maximum stresses then decrease as moisture is absorbed to the P+T only stress values. The shear stress, Sxy , distribution responds in the opposite manner. The early time shear stresses are approximately the same as for the P+T only case. However, the shear stresses increase and reach a maximum as the plate approaches the fully saturated condition. Again note as with the previous example, the large shear stress gradients generated at the lamina boundaries with moisture absorption.

The stress distributions for the unsymmetric laminate, starting with $\theta = -45°$ at the top of the laminate, are shown in Figures 4.16 and 4.17. As a general observation, note the more disjointed pattern of stresses at the lamina boundaries for the unsymmetric plate. Compared to the stress distributions for P+T only, the presence of the moisture gradient exaggerates this condition.

The Sx and Sy stress maximums are generally higher for all layers compared to the symmetric laminate. In addition, observe that the Sx and Sy stresses do not approach the P+T only stresses in the saturated condition, as for the symmetric laminate.

The Sxy shear stress distributions in Figure 4.17

have higher maximums than for the symmetric laminate. Also the stress gradients at the lamina boundaries are larger.

Figures 4.18 through 4.21 show the stress distributions for 4-layer symmetric and unsymmetric cross ply laminates with the same support and load conditions as the previous 4-layer angle ply laminate case. Due to the all cross ply layup pattern, the shear stresses are zero for the loadings considered.

From Figures 4.18 and 4.19 it can be observed that the Sx and Sy stresses reach their maximum values in tension in the saturated moisture condition. For Sx , the maximum occurs in the bottom, $\theta = 0°$, layer at approximately 31.5 ksi. For Sy , the maximum occurs in the next layer up at approximately 25 ksi. It is interesting to note that the maximum stress for the load condition without moisture is less than a third of that with moisture included.

The unsymmetric cross ply laminate stress results with $\theta = 90°$ at the top layer are shown in Figures 4.20 and 4.21. The same general observations made for the angle ply laminate also apply for the cross ply case. The stress magnitudes and gradients are larger for the unsymmetric, compared to the symmetric laminate.

Figures 4.22 and 4.23 are plots of the center deflection of the symmetric angle and cross ply laminates with

respect to time. In these figures the P+T only line represents the deflection caused by the pressure and temperature gradient only and does not vary with time. As would be expected for the single surface moisture absorption the deflections decrease initially due to the moment resultants generated by the moisture gradient. What is interesting is that as the plate reaches the saturated condition, the deflections actual increase beyond those for P+T only. The reason for this reversal is the moment resultant generated by the temperature dependent material properties of the laminate. These properties given in Chapter Four show that the stiffness properties of the composite material vary with the 100°F temperature gradient. By looking at equation (2.26) for the hygrothermal moment resultants, one sees that even though the moisture distribution is constant, the lamina stiffnesses are not. Thus, a residual moment is generated which adds to the deflections for the P+T only condition.

CHAPTER SIX

CONCLUSIONS

An analysis of generally laminated rectangular composite material plates has been presented. Loadings included are hygrothermal gradients and lateral pressures. In developing the analysis the effects of transverse shear and transverse normal deformation have been included. The results presented have shown the importance of including hygroscopic loadings in designing a composite plate structure, as well as, the degree of complexity necessary in the theory used to analyze these structures.

The results of the parametric study of the importance of transverse shear and transverse normal deformation have shown:

1. The effect of transverse normal deformation is negligible.

2. The effect of transverse shear deformation is less pronounced for hygrothermal loads for the material studied than for lateral pressure loads presented by [5].

3. Transverse shear deformation is needed to analyze "thick" (i.e. $A/H<100$) laminated plates which are subjected to hygrothermal and pressure loads.

Stress results presented show that hygrothermal loads are important in a detailed analysis of a composite plate. As demonstrated in the examples given, lamina stresses predicted without including moisture effects may be in error by several hundred percent. Based on the diffusion constants presented in [14] and the plate thickness, the maximum lamina stresses may take two or three years to develop. However, these stresses could cause premature failure if not accounted for in the design analysis.

Hygrothermal loads have also been shown to be important in predicting plate deflections. If plate deflections are critical to a particular design hygrothermal loads must be included in the design analysis.

BIBLIOGRAPHY

1. Pipes, R. B., Vinson, J. R., and Chou, T. W., "On the Hygrothermal Response of Laminated Composite Systems", Journal of Composite Materials, Vol. 10, April 1976.

2. Jones, R. M., Mechanics of Composite Materials, McGraw-Hill, 1975.

3. Vinson, J. R. and Chou, T. W., Composite Materials and Their Use in Structures, Wiley, 1975.

4. Warburton, G. B., "The Vibration of Rectangular Plates", Proceedings of the Institution of Mechanical Engineering, Vol. 168, 1954.

5. Whitney, J. M., "The Effect of Transverse Shear Deformation on the Bending of Laminated Plates", Journal of Composite Materials, Vol. 3, July 1969.

6. Flaggs, D. L., "Elastic Stability of Generally Laminated Composite Plates Including Hygrothermal Effects", Master's Thesis, University of Delaware, June 1978.

7. Smith, A. P., Jr., "The Effect of Transverse Shear Deformation on the Elastic Stability of Orthotropic Plates due to Inplane Loads", MMAE Thesis, University of Delaware, May 1973.

8. Linsenmann, D. R., "Stability of Plates of Composite Materials", MMAE Thesis, University of Delaware, June 1974.

9. Wu, C. I. and Vinson, J. R., "Nonlinear Oscillations of Laminated Specially Orthotropic Plates with Clamped and Simply Supported Edges", Journal of Acoustical Society of America, Vol. 49, No. 5, Pt. 2, May 1971.

10. Benham, P. P. and Hoyle, R., Thermal Stresses, Sir Isaac Pitman & Sons Ltd., 1964.

AD-A062 262 DELAWARE UNIV NEWARK DEPT OF MECHANICAL AND AEROSPA--ETC F/G 11/4
THE BEHAVIOR OF RECTANGULAR COMPOSITE MATERIAL PLATES UNDER LAT--ETC(U)
JUL 78 J G SLOAN, J R VINSON AFOSR-74-2739

UNCLASSIFIED MAE-TR-216 AFOSR-TR-78-1477 NL

2 OF 2
AD
A062262

END
DATE
FILMED
3--79
DDC

11. Whitney, J. M., "Bending-Extensional Coupling in Laminated Plates Under Transverse Loading, Journal of Composite Materials, Vol. 3, January 1969.

12. Whitney, J. M. and Leissa, A. W., "Analysis of a Simply Supported Laminated Anisotropic Rectangular Plate", AIAA Journal, Vol. 8, No. 1, January 1970.

13. Whitney, J. M., "The Effect of Boundary Conditions on the Response of Laminated Composites", Journal of Composite Materials, Vol. 4, April 1970.

14. Shen, C. H. and Springer, G. S., "Moisture Absorption an Desorption of Composite Materials", Journal of Composite Materials, Vol. 10, January 1976.

15. Proceedings of the Air Force Workshop on Durability Characteristics of Resin Matrix Composites, Battelle's Columbus Laboratories, Columbus, Ohio, October 1975.

16. Proceedings of the AFOSR Workshop, "The Influence of Relative Humidity and Elevated Temperature on Composite Materials and Structures", University of Delaware, Newark, Delaware, March 1976.

17. McKaque, E. I., Halkias, J. E., and Reynolds, J. D., "Moisture in Composites: The Effect of Supersonic Service on Diffusion", Journal of Composite Materials, Vol. 9, January 1975.

18. Ishai, O. and Mazor, A., "The Effect of Environmental-Loading History on the Transverse Strength of GRP Laminate", Journal of Composite Materials, Vol. 9, October 1975.

19. Williams, J. G., "The Effects of Tropical Weather on Graphite Epoxy Resins", Composites, Vol. 8, 1977.

20. Augl, J. M. and Berger, A. E., "Moisture Effect on Carbon Fiber Epoxy Composites", 8th National SAMPE Technical Conference, Vol. 8, October 1976.

21. Bergmann, H. W. and Dill, C. W., "Effect of Absorbed Moisture on Strength and Stiffness Properties of Graphite-Epoxy Composites", 8th National SAMPE Technical Conference, Vol. 8, October 1976.

22. Shen, C. and Springer, G. S., "Effects of Moisture and Temperature on the Tensile Strength of Composite Materials", Journal of Composite Materials, Vol. 11,

January 1977.

23. Ashton, J. E. and Waddoups, M. E., "Analysis of Anisotropic Plates", Journal of Composite Materials, Vol. 3, January 1969.

24. Whitney, J. M. and Ashton, J. E., "Effect of Environment of the Elastic Response of Layered Composite Plates", AIAA Journal, Vol. 9, No. 9, 1971.

25. Whitney, J. M. and Leissa, A. W., "Analysis of Heterogeneous Anisotropic Plates", Journal of Applied Mechanics, Vol. 36, No. 2, June 1969.

26. Whitney, J. M., "Stress Analysis of Thick Laminated Composite and Sandwich Plates", Journal of Composite Materials, Vol. 6, October 1972.

27. Hsu, P. W. and Herakovich, C. T., "Edges Effects in Angle-Ply Composite Laminates", Journal of Composite Materials, Vol. 11, October 1977.

28. Pagano, N. J., "On the Calculation of Interlaminar Normal Stress in Composite Laminate", Journal of Composite Materials, Vol. 8, January 1974.

29. Rybicki, E. F., "Approximate Three-Dimensional Solutions for Symmetric Laminates under Inplane Loadings", Journal of Composite Materials, Vol. 5, July 1971.

30. Hahn, H. T. and Pagano, N. J., "Curing Stresses in Composite Laminates", Journal of Composite Materials, Vol. 9, January 1975.

31. Hahn, H. T., "Residual Stresses in Polymer Matrix Composite Laminates", Journal of Composite Materials, Vol. 10, October 1976.

32. Weitsman, Y., "Diffusion with Time-Varying Diffusivity, with Application to Moisture-Sorption in Composites", Journal of Composite Materials, Vol. 10, July 1976.

33. Ashton, J. E., "Anisotropic Plate Analysis-Boundary Conditions", Journal of Composite Materials, Vol. 4, April 1970.

34. Ashton, J. E. and Whitney, J. M., Theory of Laminated Plates, Technomic Publishing Co., Westport, Conn., 1970.

35. Ashton, J. E., Halpin, J. C., and Petit, P. H., Primer on Composite Materials: Analysis, Technomic Publishing Co., Westport, Conn., 1969.

36. Timoshenko, S. and Weinowsky-Krieger, S., Theory of Plates and Shells, 2nd Edition, McGraw-Hill, 1959.

37. Boley, B. A. and Weiner, J. H., Theory of Thermal Stresses, Wiley, 1960.

APPENDIX A

VERIFICATION OF COMPUTER PROGRAM

The computer program given in Appendix D is lengthy and difficult to verify by step-by-step comparisons with hand calculations. Therefore, to verify the accuracy of the program calculations, several example problems were compared against known classical isotropic plate theory solutions and solutions published in the literature for rectangular laminated plates.

Isotropic Plate Solutions

The following solutions for a square steel plate under various load conditions were evaluated using the material properties,

$$E = 30.0 \times 10^{6} \text{ psi}$$
$$\nu = 0.3$$
$$\gamma = 6.6 \times 10^{-6} \text{ in/in °F} ,$$

and dimensions,

$$A = B = 16 \text{ in}$$
$$H = 0.4 \text{ in} .$$

1. Uniform Pressure

For the load condition of a uniform lateral pressure of 1 psi, the center deflection is compared for various boundary conditions.

	Classical Theory [36]	LPT	TSD	TSD + TNS
Simply-Supported, $W_{CTR} \times 10^3$ (in)	1.513	1.507	1.518	1.518
Clamped, $W_{CTR} \times 10^4$ (in)	4.710	4.756	4.790	4.790
Clamped-Simple, $W_{CTR} \times 10^4$ (in)	7.157	7.154	7.197	7.197

2. Linear Temperature Gradient

For the load condition of a linear temperature gradient through the plate thickness of $T(z) = 70 + 1000z$ °F with $T_{REF} = 70$°F , the center deflections for various boundary conditions are as follows. The plate dimensions are $A = B = 100.0$ in and $h = 0.1$ in for this example.

	Classical Theory [37]	LPT	TSD	TSD+TNS
Simply-Supported, W_{CTR} (in)	6.19	6.19	6.18	6.18
Clamped, W_{CTR} (in)	0.0	0.0	0.0	0.0

To verify the stress calculation, the following problems were evaluated using the same material properties but

with dimensions

$$A = B = 100 \text{ in}$$

$$H = 0.1 \text{ in.}$$

1. Uniform Temperature

The stresses developed in a plate subject to a uniform temperature change from $T_{REF} = 70°F$ to $T(z) = 170°F$ with and without in-plane restraints are:

	Classical [37]	Sloan
Unrestrained In-plane (ksi)	0.0	0.0
Restrained In-plane (ksi)	-28.286	-28.286

2. Linear Temperature Gradient

The stress developed in the center, top surface of a plate subject to a temperature distribution of $T(z) = 70 + 1000z$ °F are:

	Classical [37]	Sloan
Simply-supported (ksi)	- 7.519	- 7.519
Clamped (ksi)	-14.143	-14.143

Laminated Plate Solutions

1. Importance of TSD

The center deflections of symmetric cross ply lami-

nated plates were evaluated using LPT and TSD, duplicating the examples presented by Whitney [5]. The following material properties, dimensions and load data were used.

4-layer /0, 90, 90, 0/ $A/B = 1$

$G_{12}/E_{22} = 0.6 \quad G_{23}/E_{22} = 0.5 \quad \nu_{12} = 0.25$

$P(x,y) = P_o \sin \frac{\pi x}{A} \sin \frac{\pi y}{B} \quad P_o = 1$ psi

The deflection results are non-dimensionalized using,

$$W' = \frac{W_{CTR} \, E_{22} \, H^3}{A^4 \, P_o} \times 10^3$$

			Whitney [5] W'	Sloan W'
$E_{11}/E_{22} = 40$				
	$A/H = 10$	LPT	2.8	2.8
		TSD	4.4	4.7
	$A/H = 40$	LPT	2.8	2.8
		TSD	2.9	2.9
$E_{11}/E_{22} = 3$				
	$A/H = 5$	LPT	18	19
		TSD	22	25
	$A/H = 25$	LPT	18	19
		TSD	19	19

2. Symmetric and Unsymmetric Angle Ply Laminates

To verify the program for evaluation of unsymmetric, as well as symmetric laminates, several examples, both simply-supported and clamped, presented by Whitney [12, 13] were duplicated. The load used in the examples is a uniform pressure, $P_o = 1.0$ psi .

The deflection results for the symmetric simply-support plates and the clamped plates were non-dimensionalized using,

$$W' = \frac{W_{CTR} \, E_{22} \, H^3}{A^4 \, P_o} \times 10^2 .$$

The unsymmetric deflection results were also non-dimensionalized and presented as a ratio of the unsymmetric compared to the symmetric deflection.

Simply-Supported:

$G_{12}E_{22} = 0.5$ $\quad {}_{12} = 0.25$ $\quad \theta = \pm 45°$

$H = 0.011$ in $\quad A = B = 10.0$ in

Symmetric Plate		Whitney [12] W'	Sloan W'
4-layer /45, -45, -45, 45/	$E_{11}/E_{22}=40$	0.235	0.235
	$E_{11}/E_{22}=10$	0.875	0.875

Unsymmetric Plate		Whitney [12] W'	Sloan W'
4-layer /45, -45, 45, -45/	$E_{11}/E_{22}=40$	1.2	1.2
	$E_{11}/E_{22}=10$	1.1	1.1
2-layer /45, -45/	$E_{11}/E_{22}=40$	3.1	3.1
	$E_{11}/E_{22}=10$	2.0	2.0

Clamped:

$E_{11}/E_{22} = 40 \quad G_{12}/E_{22} = 0.5 \quad \nu_{12} = 0.25$

$\theta = \pm\ 45° \quad H = 0.011$ in $\quad A = B = 10.0$ in

	Whitney [13] W'	Sloan W'
Symmetric Plate		
4-layer /45, -45, -45, 45/	1.0	1.0
Unsymmetric Plate		
4-layer /45, -45, 45, -45/	1.2	1.2
2-layer /45, -45/	2.8	2.7

3. Symmetric and Unsymmetric Cross Ply Laminates

In the same matter, several cross ply symmetric and unsymmetric laminates were evaluated.

Simply-Supported:

$E_{11}/E_{22} = 40 \quad G_{12}/E_{22} = 1.0 \quad \nu_{12} = 0.25$

$A/B = 3.0 \quad A = 30.0$ in $\quad H = 0.011$ in $\quad \theta = 0{,}90°$

	Whitney [12] W'	Sloan W'
Symmetric Plate		
4-layer /0, 90, 90, 0/	0.811	0.806

	Whitney [12] W'	Sloan W'
Unsymmetric Plate		
4-layer /0, 90, 0, 90/	1.2	1.2
2-layer /0, 90/	3.0	3.0

Clamped:

$E_{11}/E_{22} = 40$ $G_{12}/E_{22} = 0.5$ $\nu_{12} = 0.25$

A = 10.0 in H = 0.011 in $\theta = 0, 90°$

	Whitney [13] W'	Sloan W'
Symmetric 4-layer /0, 90, 90, 0/		
B/A = 1	0.90	0.92
B/A = 2	0.88	0.89
B/A = 4	0.88	0.84
Unsymmetric 4-layer /0, 90, 0, 90/		
B/A = 1	1.2	1.1
B/A = 2	1.9	1.9
B/A = 4	1.8	1.8

APPENDIX B

STRESS PLOTS FOR SINGLE SURFACE ABSORPTION CASE OF REF. [1]

As an aid to those attempting to duplicate the results presented in [1], the correct stress plots for the single surface moisture absorption example are presented. The error described was made in the numerical calculations only. The equations presented in [1] are believed to be correct.

The stresses within each lamina can be calculated according to equation (27) of [1], or

$$\sigma_j^{'k}(z,t) = Q_{ij}^{'k}\left[\epsilon_j^{'o}(t) + z\,\kappa_j(t) - \gamma_j^{T'k}\,T(z,t) - \gamma_j^{M'k}\,\bar{M}(z,t)\right]_{i,j=1,2,6} \qquad \text{(B.1)}$$

The stress computations of [1] omitted the $z\,\kappa_j(t)$ term. This omission only effected the single surface absorption results because of the nonzero curvatures. The other examples presented had symmetric loading and therefore zero curvatures, κ_j .

Another difference between the presented plots and those of [1] is in the sign of the shear stresses. The fol-

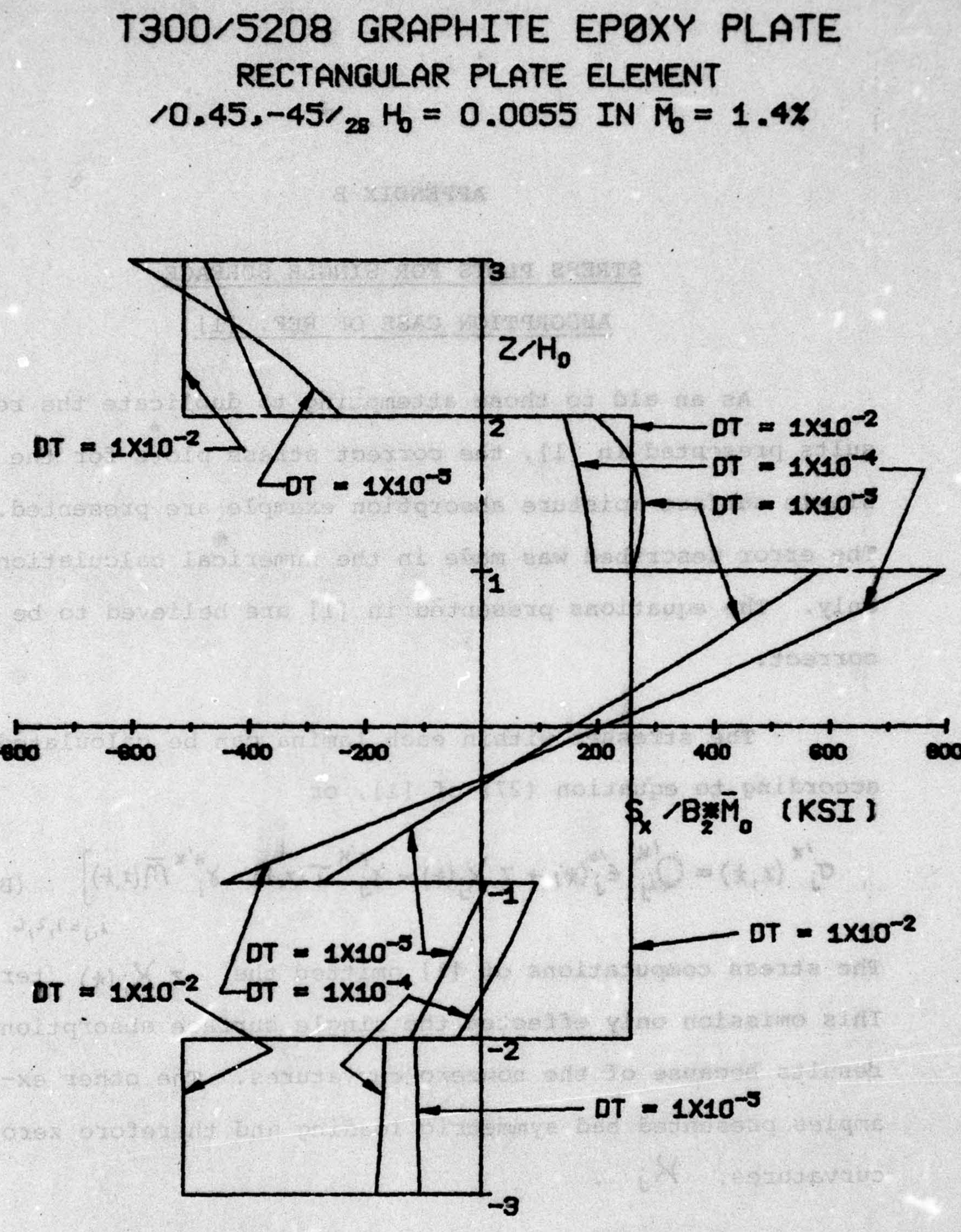
T300/5208 GRAPHITE EPØXY PLATE
RECTANGULAR PLATE ELEMENT
/0,45,-45/$_{2S}$ H_0 = 0.0055 IN $\bar{M}_0$ = 1.4%
Z/H_0
3
2
1
-1
-2
-3
-800
-600
-400
-200
200
400
600
800
S_x /B_2*$\bar{M}_0$ (KSI)
DT = 1X10^{-2}
DT = 1X10^{-5}
DT = 1X10^{-2}
DT = 1X10^{-4}
DT = 1X10^{-3}
DT = 1X10^{-2}
DT = 1X10^{-5}
DT = 1X10^{-2}
DT = 1X10^{-4}
DT = 1X10^{-3}

Figure B.1

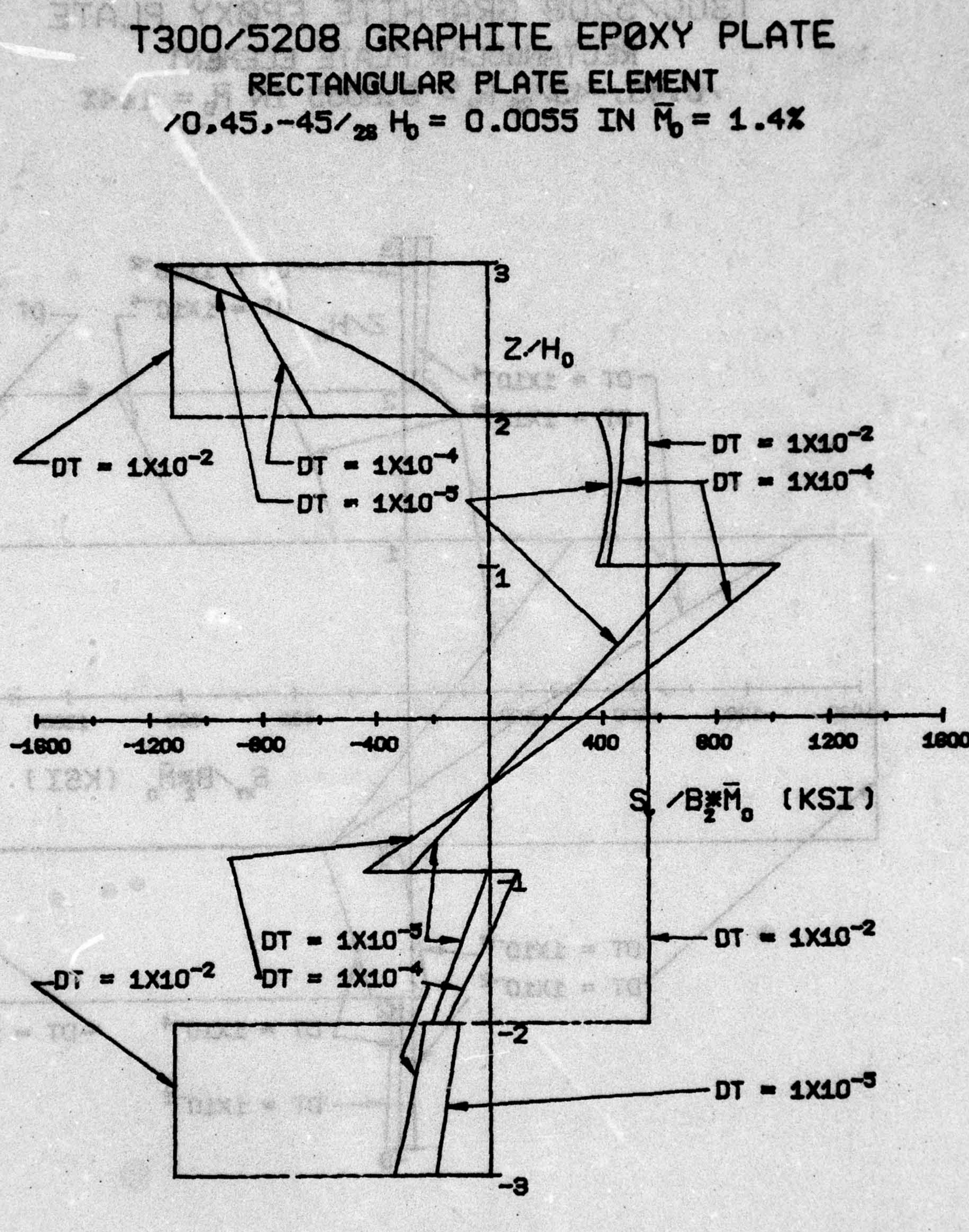
T300/5208 GRAPHITE EPØXY PLATE
RECTANGULAR PLATE ELEMENT
/0,45,-45/28 H0 = 0.0055 IN M0 = 1.4%
Z/H0
3
2
1
-1
-2
-3
DT = 1X10-2
DT = 1X10-4
DT = 1X10-5
-1600
-1200
-800
-400
400
800
1200
1600
S /B2*M0 (KSI)

Figure B.2

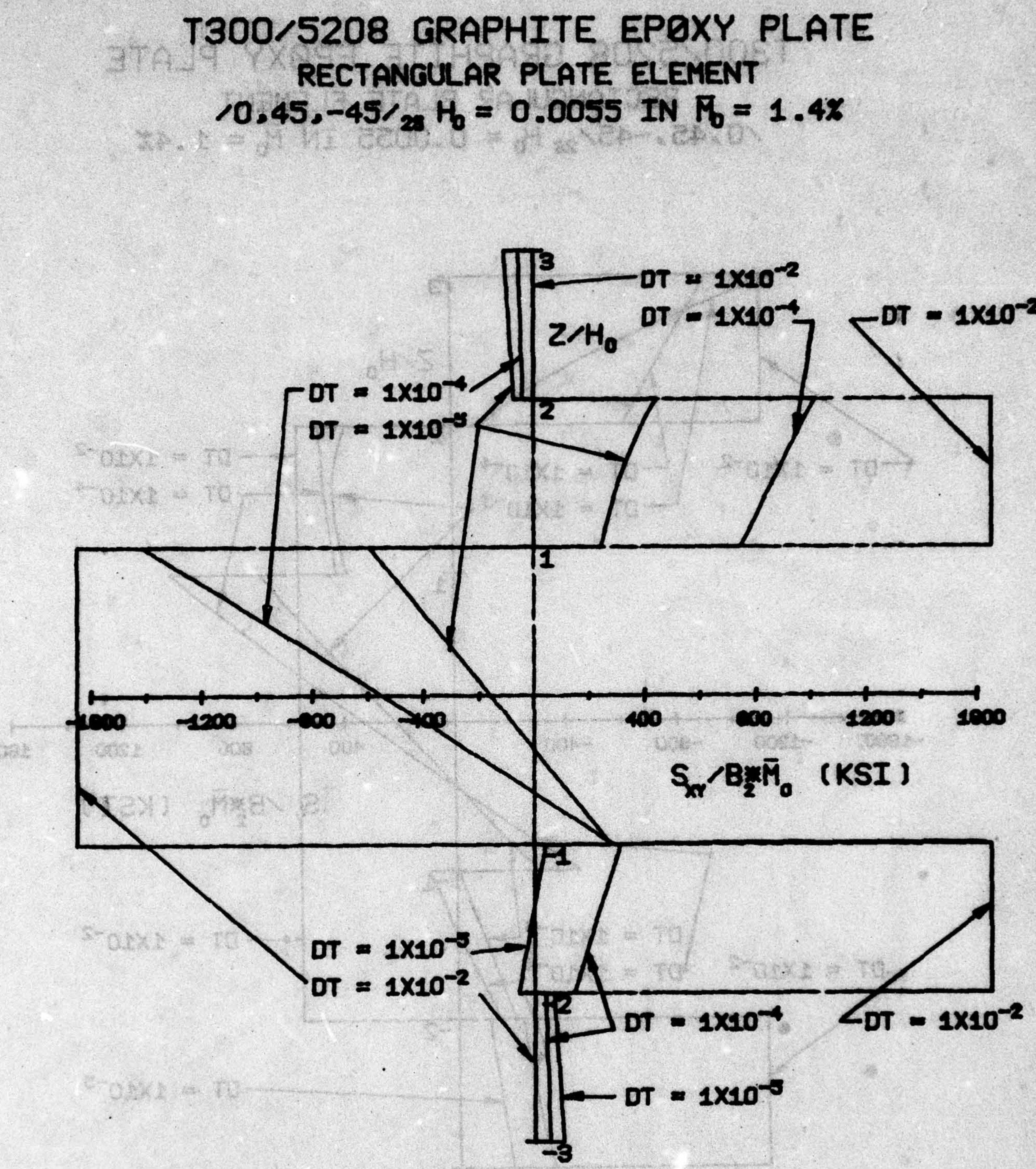
T300/5208 GRAPHITE EPØXY PLATE
RECTANGULAR PLATE ELEMENT
/0,45,-45/2S H0 = 0.0055 IN M0 = 1.4%
Z/H0
3
2
1
-1
-2
-3
DT = 1X10-2
DT = 1X10-4
DT = 1X10-2
DT = 1X10-4
DT = 1X10-5
-1600
-1200
-800
-400
400
800
1200
1600
SXY/B2*M0 (KSI)
DT = 1X10-5
DT = 1X10-2
DT = 1X10-4
DT = 1X10-2
DT = 1X10-5

Figure B.3

lowing stress plots are based on the definition of θ as shown in Figure 2.1. Using this definition the sign of the shear stresses is opposite to that presented in [1].

Figures B.1, B.2 and B.3 show the correct stress distributions for the single surface absorption example. Figures B.1 and B.2 of the x and y stress distributions, respectively, show a much larger stress gradient particularly in the middle layers. The shear stress distributions of Figure B.3 also indicate a more bending type stress gradient through the center layers. It is important to note the shear stress in the $\theta = 0°$ layers is not zero for early times. This nonzero shear is generated by the unsymmetric moisture distribution in the $\pm 45°$ layers even though the layup pattern is symmetric. For the fully saturated condition, $Dt = 1 \times 10^{-2}$, the presented curves match those of [1] except for the sign of the shear stresses.

APPENDIX C

EVALUATION OF THE CHARACTERISTIC BEAM FUNCTION INTEGRALS

The presented evaluation of the general integral forms of the characteristic beam functions are provided to assist those attempting to duplicate this work. The characteristic beam functions used in Chapter Three are expressed in the following shorthand notation.

$$\left.\begin{aligned}
\phi_i(z) &= \cos\mu_i\left(\frac{z}{c}-\frac{1}{2}\right) + \eta_i\cosh\mu_i\left(\frac{z}{c}-\frac{1}{2}\right)\\
\bar{\phi}_i(z) &= \cos\mu_i\left(\frac{z}{c}-\frac{1}{2}\right) - \eta_i\cosh\mu_i\left(\frac{z}{c}-\frac{1}{2}\right)\\
\theta_i(z) &= \sin\mu_i\left(\frac{z}{c}-\frac{1}{2}\right) + \eta_i\sinh\mu_i\left(\frac{z}{c}-\frac{1}{2}\right)\\
\bar{\theta}_i(z) &= \sin\mu_i\left(\frac{z}{c}-\frac{1}{2}\right) - \eta_i\sinh\mu_i\left(\frac{z}{c}-\frac{1}{2}\right)
\end{aligned}\right\} \qquad (C.1)$$

$$\left.\begin{aligned}
CC_i(z) &= \cos\frac{i\pi z}{c}\\
SS_i(z) &= \sin\frac{i\pi z}{c}
\end{aligned}\right\} \qquad (C.2)$$

where z = dummy coordinate direction

c = length of plate along z direction

i = dummy mode index, odd only.

As given in equations 3.11 and 3.12,

$$\eta_i = \frac{\sin(\mu_i/2)}{\sinh(\mu_i/2)}, \tag{C.3}$$

and μ_i are the solutions to

$$\tan(\mu_i/2) + \tanh(\mu_i/2) = 0, \tag{C.4}$$

or

$$\mu_1 = 1.50562\pi, \quad \mu_2 = 2.49975\pi, \quad \mu_i = (i+2)\pi, \quad i \geq 3. \tag{C.5}$$

The following forms of expressions occur often in the evaluations and are abbreviated as

$$AA_i = \sinh\frac{\mu_i}{2}\cos\frac{\mu_i}{2} + \cosh\frac{\mu_i}{2}\sin\frac{\mu_i}{2} \tag{C.6}$$

$$BB_i = \sin\frac{\mu_i}{2}\cosh\frac{\mu_i}{2} - \cos\frac{\mu_i}{2}\sinh\frac{\mu_i}{2} \tag{C.7}$$

$$CC_i = \frac{\sinh\mu_i}{\mu_i} + 1 \tag{C.8}$$

$$DD_i = \frac{\sinh\mu_i}{\mu_i} - 1 \tag{C.9}$$

$$EE_{ij} = \frac{\sin(i\pi - \mu_j)/2}{i\pi - \mu_j} + \frac{\sin(i\pi + \mu_j)/2}{i\pi + \mu_j} \tag{C.10}$$

$$FF_{ij} = \mu_j \cos\frac{i\pi}{2} \sinh\frac{\mu_j}{2} + i\pi \sin\frac{i\pi}{2} \cosh\frac{\mu_j}{2} \tag{C.11}$$

$$GG_{ij} = \mu_j \sin\frac{i\pi}{2} \cosh\frac{\mu_j}{2} - i\pi \cos\frac{i\pi}{2} \sinh\frac{\mu_j}{2} \tag{C.12}$$

$$HH_{ij} = \frac{\sin(\mu_i - \mu_j)/2}{\mu_i - \mu_j} + \frac{\sin(\mu_i + \mu_j)/2}{\mu_i + \mu_j} \tag{C.13}$$

$$KK_{ij} = \frac{\sin(\mu_i - \mu_j)/2}{\mu_i - \mu_j} - \frac{\sin(\mu_i + \mu_j)/2}{\mu_i + \mu_j} \tag{C.14}$$

$$LL_{ij} = \frac{\sinh(\mu_i + \mu_j)/2}{\mu_i + \mu_j} + \frac{\sinh(\mu_i - \mu_j)/2}{\mu_i - \mu_j} \tag{C.15}$$

$$MM_{ij} = \frac{\sinh(\mu_i + \mu_j)/2}{\mu_i + \mu_j} - \frac{\sinh(\mu_i - \mu_j)/2}{\mu_i - \mu_j} \tag{C.16}$$

$$NN_{ij} = \mu_i \cos\frac{\mu_j}{2} \sinh\frac{\mu_i}{2} + \mu_j \sin\frac{\mu_i}{2} \cosh\frac{\mu_i}{2} \tag{C.17}$$

$$PP_{ij} = \mu_i \sin\frac{\mu_j}{2} \cosh\frac{\mu_i}{2} - \mu_j \cos\frac{\mu_i}{2} \sinh\frac{\mu_i}{2} \tag{C.18}$$

$$QQ_{ij} = \frac{\sin(i\pi - \mu_j)/2}{i\pi - \mu_j} - \frac{\sin(i\pi + \mu_j)/2}{i\pi + \mu_j} \tag{C.19}$$

Integrals of the products of the characteristic beam functions across the domain of interest are needed in applying the Rayleigh-Ritz solution technique. Thus, the following general integral forms are useful in evaluating the necessary terms

$$\int_0^c \phi_r \phi_s \, dz = \frac{c}{2} + \frac{2c\eta_r}{\mu_r} AA_r + \frac{c\eta_r^2}{2} CC_r , \quad r=s \tag{C.20}$$

$$= c\,HH_{rs} + \frac{2c}{(\mu_r^2+\mu_s^2)}\left[\eta_r NN_{rs} + \eta_s NN_{sr}\right] +$$

$$\eta_r \eta_s c\, LL_{rs} , \quad r \neq s \tag{C.21}$$

$$\int_0^c \bar{\theta}_r \bar{\theta}_s \, dz = \frac{c}{2} - \frac{2\eta_r c}{\mu_r} BB_r + \frac{c\eta_r^2}{2} DD_r , \quad r=s \tag{C.22}$$

$$= c\,KK_{rs} - \frac{2c}{(\mu_r^2+\mu_s^2)}\left[\eta_r PP_{rs} + \eta_s PP_{sr}\right] +$$

$$\eta_r \eta_s c\, MM_{rs} \quad r \neq s \tag{C.23}$$

$$\int_0^c \bar{\phi}_r \bar{\phi}_s \, dz = \frac{c}{2} - \frac{2c\eta_r}{\mu_r} AA_r + \frac{c\eta_r^2}{2} CC_r , \quad r=s \tag{C.24}$$

$$\int_0^c \Phi_r^- \Phi_s^- \, dz = c\,HH_{rs} - \frac{2c}{(\mu_r^2+\mu_s^2)}\left[\eta_r NN_{rs} + \eta_s NN_{sr}\right] + \eta_r \eta_s c\, LL_{rs}, \qquad r \neq s \quad (C.25)$$

$$\int_0^c \Phi_r^- \Phi_s \, dz = \frac{c}{2} - \frac{c\eta_r^2}{2} CC_r, \qquad r = s \quad (C.26)$$

$$= c\,HH_{rs} - \frac{2c}{(\mu_r^2+\mu_s^2)}\left[\eta_r NN_{rs} + \eta_s NN_{sr}\right] - \eta_r \eta_s c\, LL_{rs}, \qquad r \neq s \quad (C.27)$$

$$\int_0^c SS_r \phi_s \, dz = c \sin\frac{r\pi}{2}\, EE_{rs} + \frac{2c\eta_s \sin\frac{r\pi}{2}}{\mu_s^2 + (r\pi)^2} FF_{rs}, \qquad \begin{matrix} r=s \\ r\neq s \end{matrix} \quad (C.28)$$

$$\int_0^c SS_r \Phi_s^- \, dz = c \sin\frac{r\pi}{2}\, EE_{rs} - \frac{2c\eta_s \sin\frac{r\pi}{2}}{\mu_s^2 + (r\pi)^2} FF_{rs}, \qquad \begin{matrix} r=s \\ r\neq s \end{matrix} \quad (C.29)$$

$$\int_0^c CC_r \Theta_s \, dz = -c \sin\frac{r\pi}{2}\, QQ_{rs} - \frac{2\eta_s c \sin\frac{r\pi}{2}}{\mu_s^2 + (r\pi)^2} GG_{rs}, \qquad \begin{matrix} r=s \\ r\neq s \end{matrix} \quad (C.30)$$

$$\int_0^c CC_r \Theta_s^- \, dz = -c \sin\frac{r\pi}{2}\, QQ_{rs} + \frac{2\eta_s c \sin\frac{r\pi}{2}}{\mu_s^2 + (r\pi)^2} GG_{rs}, \qquad \begin{matrix} r=s \\ r\neq s \end{matrix} \quad (C.31)$$

APPENDIX D

RECTANGULAR COMPOSITE MATERIAL PLATE

COMPUTER PROGRAM

A computer program for the analysis of laminated composite material plates has been written. The program, LAMINATE, performs the numerical computations for analyzing rectangular plates using the solution technique given in Chapter 3. LAMINATE will handle plates with all edges simply-supported, or all edges clamped, or with two opposite edges clamped and the other two edges simply-supported. The program will analyze plates subject to lateral pressures and with temperature and moisture distributions through the thickness. Composite material plates may be up to 32 layers thick of either symmetric or unsymmetric layup patterns.

Description of Input Data

The input data required to run problems using the LAMINATE computer code is assembled as a data card deck. A data card deck consists of a card type A and any number of data card sets (card types B through J). One data card set is included for each case of a run.

The first card of a data card deck must be a type A card, as this card inputs the number of data card sets to be read. After card type A, NCASE, data card sets (card types B through J) must be included.

Not every data card set needs to contain all the card types B through J. Depending on the control options selected, some of the card types may be omitted. These control options allow data which was inputted in the previous case to be omitted from subsequent data cards sets, if desired.

All cards of card types B, C, E, F, G, and H must be included in each data card set. Cards of card types D and I may be omitted if it is desired to use values from the previous case.

In the following section the detailed input instructions for each card type are given. If there is more than one card for a particular card type, the cards are numbered in the order in which they should appear in the data card set (i.e. D1, D2, D3, etc.). The information given for each card of each card type consists of the variable name, the input format, and a description of the input and units of measure required.

All input for an integer (I) format field must be right justified. All input for exponential (E) format must have the exponent right justified in the field.

INPUT DATA

Card Type A (one card) must be included only once for each computer run and be the first card of the data card deck.

Variable	Format	Description
NCASE	I5	Number of B through J data card sets for this run.

Card Type B (one card) must be included in each data card set.

Variable	Format	Description
COM(i)*	18A4	Comment up to 72 characters long; any alphanumeric character except, (;), semicolon.

Card Type C (two cards) must be included each data card set.

Card C1

Variable	Format	Description
IFUNCT	I5	= 1 Simply-supported all edges
		= 2 Clamped all edges
		= 3 Clamped x-edges, simply-supported y-edges
		= 4 Rectangular plate element per [1], no boundary conditions

*Indicates subscripted variable.

Variable	Format	Description
		= 5 Calculate and print the A, B, D matrices only
KTS	I5	= 1 Transverse shear included using the distribution $f(z) = [1-(\frac{z}{H})^2]$
		= 2 Transverse shear included using the distribution $f(z) = \frac{5}{4}[1-(\frac{z}{H})^2]$
		= 3 Transverse shear including without a weighting distribution
		= 4 Simulate the neglect of transverse shear deformation
*KTNS	I5	= 0 Neglect transverse normal strains
		= 1 Include transverse normal strains
*KTEMP	I5	= 0 No temperature dependent material properties
		= 1 Linearly interpolate material properties based on the mean lamina temperature (KMATP must equal 2)
*KDET		Number of points at which a detailed deflection and/or stress printout is desired (number of Card Type J's included in data card set)

Variable	Format	Description
KHYGRO	I5	= 0 Neglect all moisture and temperature loading
		= 1 Polynomial temperature distribution only
		= 2 Polynomial moisture distribution only
		= 3 Both polynomial temperature and moisture distributions
KPRESS	I5	= 1 Uniform lateral pressure
		= 2 Whitney pressure distribution $P(x,y) = P_o \sin \frac{\pi x}{a} \sin \frac{\pi y}{b}$
		= 3 No lateral pressure loadings
KMATP	I5	|KMATP| is the number of material property data sets, card type D's. If KMATP is positive, KMATP is the number of Card Type D sets inputted.
		If KMATP is negative, |KMATP| is the number of Card Type D's used in the previous case, or |KMATP| is the number of laminate layers if in the previous case material properties were linearly interpolated (KTEMP=1).

Variable	Format	Description
ITERMN	I5	Maximum odd index used in the series expansion of the assumed displacement and rotation functions ($ITERMN \leq 9$)
KMOIST	I5	= 0 Moisture distribution not per diffusion equation solution
		= 1 Moisture distribution per diffusion equation solution of [1]. Note KMOIST = 1 will override polynomial moisture distribution
KSYM	I5	= 0 Unsymmetric laminate
		= 1 Symmetric laminate (sets B_{ij} = 0)
KCROSS	I5	= 0 Angle ply or mixed laminate
		= 1 Cross ply laminate

Card C2

Variable	Format	Description
KPRINT	I5	= 0 Print material property data
		= 1 Suppress all material property data printout
KPQ	I5	= 0 Print Q matrix for all layers (see Card Type I to suppress printout for specific layers.)
		= 1 Suppress Q printout for all layers

Variable	Format	Description
KPQB	I5	= 0 Print $\bar{Q}$ matrix for all layers (see Card Type I to suppress printout for specific layers)
		= 1 Suppress $\bar{Q}$ printout for all layers
KCSPR	I5	= 0 Suppress printout of simultaneous equations coefficient and source matrices
		= 1 Print simultaneous equations coefficient and source matrix. (Note number of lines printed is large for ITERMN$\geq$5.)
KINTP	I5	= 0 Suppress integration subroutine check run
		= 1 Perform integration subroutine check

Card Type D (four cards). The Card Type D cards are only required if KMATP $\geq$ 1. If KMATP (card C1) is greater than or equal to one, the KMATP is the number of Card Type D sets (i.e. D1, D2, D3, D4) inputted for in case.

Card D1

Variable	Format	Description
TMAT(i)	F10.3	Temperature (°F) for the material properties in this Card Type D set

Variable	Format	Description
EEI(i,j)	3E10.4	Elastic moduli in E_{11}, E_{22}, E_{33} order (psi)

Card D2

Variable	Format	Description
GGI(i,j)	3E10.4	Shear moduli in G_{12}, G_{13}, G_{23} order (psi)

Card D3

Variable	Format	Description
XNU(i,j)	6F10.3	Poisson ratios for material in order ν_{12}, ν_{21}, ν_{13}, ν_{31}, ν_{23}, ν_{32}

Card D4

Variable	Format	Description
ALPHA(i,j)	3E10.4	Coefficients of thermal expansion in the order γ_{11}, γ_{22}, γ_{33} (in/in °F)
BETA(i,j)	3E10.4	Coefficients of hygroscopic expansion in the order β_{11}, β_{22}, β_{33} (in/in %WT)

Card Type E (one card) must be included in each data card set.

Variable	Format	Description
KLAYER	I10	|KLAYER| is the number of layers in

Variable	Format	Description
		the laminate considered. If KLAYER is negative, the laminate of |KLAYER| layers used in the previous example will be used.
AX	F10.4	Plate length in X-direction (in)
BY	F10.4	Plate length in Y-direction (in)
HTOTAL	F10.4	Total thickness of plate (in)

Card Type F (one card) must be included in each data card set.

Variable	Format	Description
PRESS	F10.4	Lateral pressure (psi), positive acting down on plate
TREF	F10.4	Reference temperature of plate prior to loading (°F)
XMREF	F10.4	Reference moisture concentration of plate prior to loading (%WT)
XMS	F10.4	Moisture concentration for diffusion solution moisture distribution (%WT). Only included if KMOIST > 0 on Card C1.
DT	F10.4	Diffusion time parameter for diffusion equation moisture distributions (in^2). Only included if KMOIST > 0 on Card C1.

Card Type G (one card) must be included in each data card set.

Variable	Format	Description
TD(i)	5E12.3	Coefficients for the temperature distribution through the thickness of the plate in the form, $T(z) = TD(1) + TD(2)*Z + TD(3)*Z^2 + TD(4)*Z^3 + TD(5)*Z^4$

Card Type H (one card) must be included in each data card set.

Variable	Format	Description
HM(i)	5E12.3	Coefficients for the moisture concentration distribution through the plate thickness in the form, $\overline{M}(z) = HM(1) + HM(2)*Z + HM(3)*Z^2 + HM(4)*Z^3 + HM(5)*Z^4$

Card Type I (|KLAYER| cards). Card Type I's are only included if KLAYER on Card Type E is greater than zero. If KLAYER > 0, then KLAYER cards will be inputted, one for each layer in the order of the stacking in the laminate starting at the bottom (z=-HTOTAL/2) of the laminate.

Variable	Format	Description
THETA(i)	F10.4	Angle from the X to 1 axis for this

Variable	Format	Description
		lamina, in degrees
THICK(i)	F10.4	Thickness of this lamina of the laminate (in)
KMAT(i)	I5	Material property (Cards D1 through D4) data set for this lamina. If KTEMP > 0, KMAT must equal the layer number starting with 1 for the bottom layer.
KPROP(i)	I5	= 0 Print material properties for this lamina
		= 1 Suppress material properties printout for this lamina
KPQBL(i)	I5	= 0 Print stiffness properties for this lamina
		= 1 Suppress print of stiffness properties for this lamina

Card Type J (KDET cards). KDET Card Type J's are inputted in each data card set.

Variable	Format	Description
X	F10.3	X-position for evaluation of the deflections and stresses (in)
Y	F10.3	Y-position for evaluation of the deflections and stresses (in)

Variable	Format		Description
KSTRES	I5	= 0	No stress calculation for this position X,Y
		> 0	KSTRES is the number of equally spaced points through the thickness for each lamina
KPRINV	I5	= 0	Suppress printing of the inverted A, B, D matrix
		= 1	Print inverted A, B, D matrix
KPREL	I5	= 0	Suppress printing the plate strains (ε) and curvatures (κ)
		= 1	Print plate strains (ε) and curvatures (κ)
KPREK	I5	= 0	Suppress printing lamina strains
		= 1	Print lamina strains at each stress evaluation location through the lamina
KIPE	I5	= 0	No in-plane dilatational plate restraints
		= 1	Restrain in-plane dilatational strains

Repeat Card Types B through J as required, NCASE-1 times.

Example Problem

The input data required and output printout for the

following example problem is included to illustrate the use of the LAMINATE program.

The example problem will be a 4-layer, angle ply, T300/5208 Graphite Epoxy laminated plate. All edges of the plate will be simply-supported. The plate layup pattern is /45, -45/s. The length in the x and y directions is 10.0 inches. The total plate thickness is 0.022 inches. In-plane dilatational strains will be unrestrained. The plate loading will be a uniform pressure, $P_o = 0.1$ psi , a linear temperature gradient, $T(z) = 150 + 4545.5 * z$ (°F) and a moisture distribution based on the single surface diffusion equation solution with $M_o = 1.0\%$ WT and $Dt = 1 \times 10^{-5} in^2$.

The input data card data for the example is shown in Figure D.1. The printout (10 pages) of the example is included after Figure D.1.